Analysis of Dscam Diversity in Regulating Dendritic Morphology of Lobula Plate Tangential Cells

Jing Shi

München, 28.09.11

Analysis of Dscam Diversity in Regulating Dendritic Morphology of Lobula Plate Tangential Cells

Dissertation

der Fakultät für Biologie

der Ludwig-Maximilians-Universität

München

vorgelegt von

Jing Shi

aus Shanghai

München, 28.09.2011

Erstgutachter: Professor Dr. Alexander Borst

Zweitgutachter: Professor Dr. Hans Straka

Table of Contents

Abbreviations

ASLV-A	Avian Sarcoma Leucosis Virus -A
Bl	Bristle
Btx	Bungarotoxin
Ca2+	Calcium cation
CH cell	Centrifugal horizontal cell
CNS	Central Nervous System
CVS	Rabies virus strain
CyO	Curly of Oyster
Cyto	Cytosolic
DG	Deletion of Glycoprotein
Dlg	Discs large
Dscam	Down syndrome cell adhesion molecule
Dscam +7.6.19.2	Dscam overexpression with isoform 7.6.19.2
Dscam +11.31.25.1	Dscam overexpression with isoform 11.31.25.1
EGFP	Ectopic Green Fluorescent Protein
EM	Electron-Microscope
EnvA	Envelope A
FD cell	Field Detection cell
Flp	Flippase
FRET	Fluorescence Resonance Energy Transfer
FRT	Flippase Recognition Target
G protein	Glycoprotein
GABA	Y-Aminobutyric acid
Gal4	Galactosidase 4
Gal80	Galactosidase 80
HA	Hemagglutinin
HP	High Pass
HS cell	Horizontal Sensitive cell
HSE	Horizontal Sensitive Equatorial

HSN	Horizontal Sensitive Northern
HSS	Horizontal Sensitive Southern
ID	Infrared Detector
IE	Infrared Emitter
IRES	Internal ribosome entry sites
L2	Laminar Monopolarcell 2
L3	Third instar larva
LED	Light Emitting Diode
LP	Low Pass
LPTC	Lobula Plate Tangential Cell
M	Multiplication
M protein	Matrix Protein
MARCM	Mosaic Analysis with a Repressible Cell Marker
MB	Mushroom body
Minus symbol (-)	Subtraction
MKRS	Marker for 3rd Chromosome: stubble
N protein	Nucleocapsisprotein
ND	Null Direction
ORN	Olfactory Receptor Neuron
P protein	Phosphoprotein
P50	Pupa stage 50
PD	Preferred Direction
PN	Projection Neuron
PNS	Peripheral Nervous System
R7/R8	Photoreceptor 7/8
S2 cells	*Drosophila* Schneider 2 cells
SAD	Rabies virus strain
SEM	Scanning Electron Microscope
Sb	Stubble
TM 6	Third Multiple 6

Table of Figures

1 Abstract

In *Drosophila*, *Dscam1* (Down syndrome cell adhesion molecule) encodes neuronal cell recognition proteins of the immunoglobulin superfamily that play a profound role in wiring the fly brain. By alternative splicing of three exon clusters, each encoding half or a complete variable immunoglobulin domain, *Dscam1* generates 19,008 different ectodomains. In this thesis, variable functional Dscam1 experiments have been performed in Horizontal Sensitive (HS) cells, which belong to the group of Lobula Plate Tangential Cells (LPTCs). The HS system comprises three individually identifiable cells—the northern HSN, the equatorial HSE, and the southern HSS cells which are tuned to large-field horizontal motion in a direction-selective way. Their dendritic terminals are located within the lobula plate where they overlap each other up to 90%. These anatomical properties of the HS system make them an excellent model to study the role of Dscam1 in shaping complex branching patterns. Using homologous recombination, Dscam1 loss-of-function animals were generated in which the number of alternative exons is reduced at the endogenous locus within these cells. Reduction of Dscam1 diversity as well as expression of unfunctional protein elicits strong self-crossings of dendritic branches whereas the dendritic fields of neighboring HS cells do not fasciculate, suggesting that heteroneuronal tiling may not depend on Dscam1. Furthermore, *Dscam1* mutant neurons can alter the projections of neighboring wild-type neurons thereby showing a non-cell-autonomous effect of *Dscam1*. In contrast, overexpression of single Dscam1 isoforms leads to reduced branching complexity and significant smaller dendritic fields, assuming that this phenotype is elicited by Dscam mediated repulsive responses. Dscam-elicited gain-of-function phenotype strongly depends on the onset of overexpression during cell development. Both results speak for a cell-autonomous role of *Dscam1* function in self-avoidance. Anatomical findings were complemented with detailed anatomical reconstructions carried out by Friedrich Förstner. Further functional analyses with Dscam gain-of-function and loss-of-function flies were performed by Bettina Schnell and Väinö Haikala.

For further investigations on the function of LPTCs and their role in flight control, a series of genetic tools and protocols was developed. Firstly, RicinA induced ablation of single LPTCs revealed normal development of remaining LPTCs thereby

suggesting independence from neighboring LPTCs during development. Secondly, to identify the neurons presynaptic to LPTCs I started to establish a viral system for retrograde transsynaptic labeling of neurons in collaboration with Conzelmann Lab. At present, we are able to target viral infection to identified and labeled neurons. Third, different transgenic flies were generated for blocking inhibitory and excitatory inputs to the LPTCs and for detailed optical recording of neuronal activity.

2 Introduction

2.1 The scientific career of *Drosophilae*: history and genetics

The fruit fly *Drosophila melanogaster* has been used as a model organism for biological studies since the early 1900´s. Since then Drosophila has been used to study many topics, most notably genetics and development. Although first described by Johann Wilhelm Meigen in 1830 (Meigen 1830) it took more than 70 years until *Drosophila* was discovered for scientific research. Harvard Professor William Ernest Castle was one of the first alongside Charles W. Woodworth to work with the fruit fly.

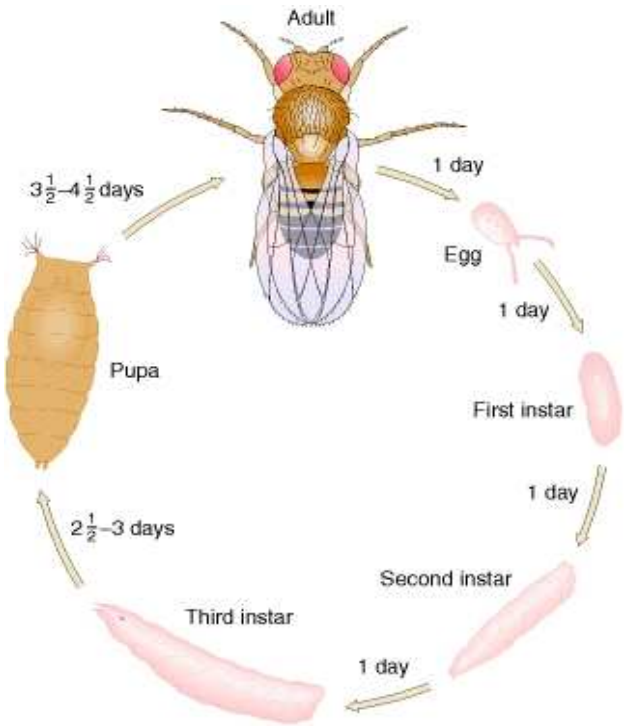

Fig. 1: The life cycle of *Drosophila melanogaster.*
Drosophila, like all flies, is a holometabolous organism. The embryonic stage takes 1 day. Thereafter, the larva hatches out of the egg. The larvae are mobile and undergo molting twice. This larval stage takes around 3 days. The pre-pupal stage, when the larva starts to become a pupa, lasts only one hour. During this time, the larva becomes immobile and develops a solid shell surrounding its body. This shell turns brown and non-transparent when the pupal stage starts. After 4 days, the adult fly hatches out of the pupa. In total, the life cycle takes about 10 days at 25°C. Modified from "An introduction to Genetic Analysis, 7th Edition"

The major advantages of fruit flies are their fast reproduction cycle and high fertility: During 10 days of captivity, flies cycle through all steps of life (Fig. 1) and a single female fly is capable of laying several hundreds of eggs during its life span.
In 1909, Thomas Hunt Morgan discovered a mutation affecting the eye-color of a single fruit fly. The *white* mutant possessed white eyes instead of red ones (Fig. 2 A) and its offspring were expressing this phenotype according to Mendel's law of heredity (Fig. 2 B) (Morgan 1910).

Morgan was also the first who proposed that the material basis of heritage within the fly is conserved in fiber-like structures in the cells, the chromosomes and each chromosome consists of genes, which are reorganized during reproduction.

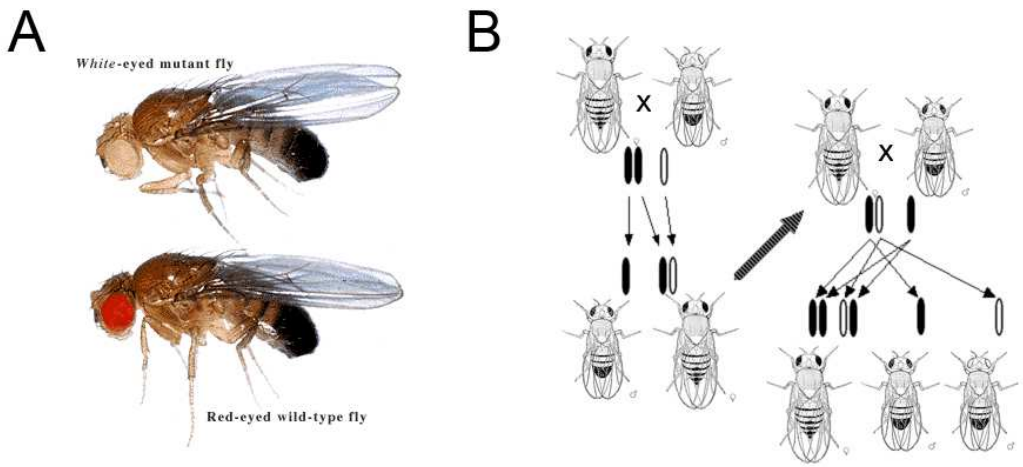

Fig. 2: The white-eyed mutant is a spontaneous recessive mutation on the X chromosome of *Drosophila melanogaster* and therefore sex-linked inherited.

(A) Mutant *white*- flies have a lack of pigment cells in the photoreceptors and therefore possess white eyes instead of red ones. (B) Shows the crossing scheme with which Thomas Hunt Morgan was able to locate the mutation on the X chromosome and demonstrate the recessive, sex-linked inheritance of the according feature. When a *white*+ male is crossed to a wildtype virgin female, then all offspring have normal-colored red eyes, pointing to the recessive heritage. If those progenitors are crossed inter se then the male offspring split up into flies with white eyes and flies with red eyes whereas all female flies are red-eyed. Therefore, Morgan concluded that the mutation must be located on the X-chromosome. Modified from Morgan 1919: "The physical basis heredity", Philadelphia: J.B. Lippincott Company 1919.

In late 1926, Hermann Joseph Muller, a former student of Morgan, obtained critical evidence of the abundant production of gene mutations and chromosome changes by radiation (X-ray mutagenesis). The appearance of *Drosophila* mutants contributed much to the comprehension of the basic rules of heritage.

In 1933, Theodosius Dobzhansky discovered the genetic variability between fly individuals (Dobzhansky 1938) by recording inversion events in the giant polytene chromosomes of the salivary glands. Dobzhansky also discovered that these genetic changes were causing reproduction barriers to other fly population, an observation that has strongly supported Darwin's theory about the origin of species.

In the following years: 1940-1970, research on *Drosophila* put much effort into the comprehension of the hierarchical structure of genes. Here, outstanding studies unraveling the genetic key mechanisms of embryonic development were performed by Edward B. Lewis, Eric Wieschaus and Christiane Nüsslein-Volhard whose work was honored by the Nobel Prize. Within the same period, Seymour Benzer made the first behavior studies on *Drosophila*, showing that fruit flies possess a short term as well as a long-term memory. Further experiments were carried out in *Drosophila* memory mutants by Tim Tully (Benzer 1974; Tully and Quinn 1985). These findings revealed that *Drosophila* is able to show complex behavior patterns. In addition, they demonstrated that genetic mutations could interfere with the behavior of organisms.

In the 1980s, scientists unraveled the function of DNA fragments called transposons. These elements exist within all organisms and are able to jump within the genome of the host species. By doing so, random mutations could appear whenever the transposon hits a gene locus. It was possible to extract a specific transposon called P-element, which was already discovered in the 1950s in a wild population of *Drosophila melanogaster.* With that, they opened up a revolutionary possibility: The incorporation of alien DNA sequences into the native *Drosophila* genome. In 1982, Gerald M. Rubin and Allan C. Spradling pioneered technology to use artificial P elements to insert genes into *Drosophila* by injection into embryos (Spradling and Rubin 1982). This procedure must happen during the syncytial blastoderm stage before the cell membranes are built. With that genetic accessibility the era of genetic manipulations in *Drosophila melanogaster* has started.

2.2 The Gal4/ UAS system

Based on the discovery of P-elements, Andrea Brand und Norbert Perrimon were able to introduce a new genetic method called the Gal4/UAS-System (Brand and Perrimon 1993) for targeted gene expression that is still one of the most used methods to manipulate the *Drosophila* genome (Fig. 3).

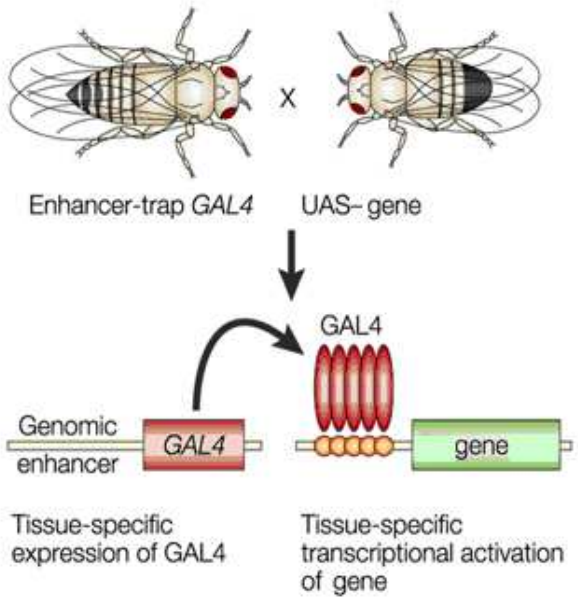

Fig. 3: The Gal4/ UAS-System

The system has two parts: the Gal4 gene, encoding the yeast transcription activator protein Gal4 (Galactosidase 4), and the UAS (Upstream Activation Sequence) sequence, a short section of the promoter region, to which Gal4 specifically binds to activate gene transcription. In this system, expression of the gene of interest, the responder, is controlled by the presence of the UAS element. This only occurs when the responder line is mated to flies that express Gal4 in a particular pattern, termed the driver. The resulting progeny then express the responder in a transcriptional pattern that reflects the Gal4 pattern of the respective driver. Scheme modified from Muqit and Feany 2002.

The transcriptional activator galactosidase 4 (Gal4), together with the upstream activator sequence (UAS) form a two component system which enables a spatial and temporal controlled expression of a certain gene. The Gal4 sequence does not possess a consensus in *Drosophila* as it is originally derived from the yeast genome. Thus, it will not interfere with endogenous cis- active sequences.

The promoter in the P-element is too weak for expressing the Gal4 gene. However, if the insertion happens to be close to an endogenous enhancer region in the

Drosophila genome the Gal4 expression will be controlled and regulated through that enhancer. Due to the “enhancer trap” method, it has been possible to create a large spectrum of Gal4 lines with variable onsets of gene expression.

The reporter gene downstream of the UAS sequence is only transcribed through the binding of the Gal4 protein to the promoter region upstream. The UAS-reporter gene sequence is also included into the genome by P-element insertion. With this method it is possible to do variable genetic manipulations (e.g. overexpression of specific genes or introduce RNAi sequences into the genome for knockdown of gene function). Further methods to specify the Gal4 expression pattern are described in Chapter 2.8 ff.

The establishment of the Gal4/UAS system was a genetic breakthrough in the scientific career of *Drosophila melanogaster* and combined the attributes of temporal and spatial control over gene-expression in a single organism.

2.3 The anatomical basis of the motion detection pathway in flies

Motion vision is a major function of all visual systems. However, only little is known about the underlying neural mechanisms and the identity of the neurons constituting those circuits. In this chapter, I want to outline the most important relay stations in which visual information is processed and the proposed pathways of motion detection.

Just looking at the outer appearance of fly eyes, the differences to those of humans are striking; not only their shape and structure but also their relative proportion to the rest of the body is outstanding, thereby underlining the importance of this sense organ to flies. Each compound eye of the fly consists of around 800 ommatidia.

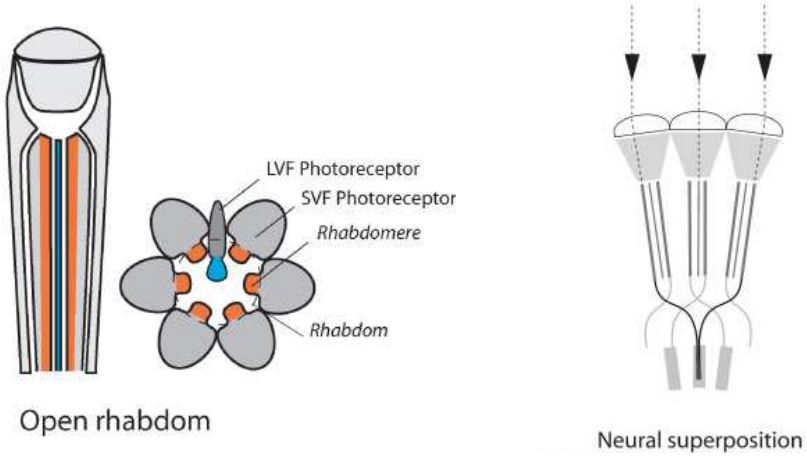

Fig. 4: *Drosophila melanogaster* possesses neural superposition eyes.

The compound eyes of flies are built up of 800 single ommatidia. Each ommatidium possesses a strong refractive lens called cornea, beneath the lens is the crystalline cone. Both bundle the light towards the 8 photoreceptor cells located in the center of each ommatidium. Pigment cells are surrounding each ommatidium, separating them from each other. Flies possess an open rhabdom in which the rhabdomeres of one ommatidium have different optical axes whereas the optical axes of seven rhabdomeres in seven adjacent ommatidia are parallel. The axons of such retinula cells project onto a common cartridge in the first optical ganglion, the lamina. Thus, each lamina cartridge looks at one point in the visual space. This kind of neural superposition eye allows vision under lower light levels. Modified from Moses et al. 2006.

Every ommatidium is a dioptic apparatus with a lens system, pigment and receptor cells (Fig. 4). The light conducting rod structures in arthropods are called rhabdomeres accommodating millions of light receptor molecules required for

efficient photon collection. *Drosophila melanogaster* possess an open rhabdom system, in which the seven rhabdomeres of each ommatidum are optically separated from each other. Therefore, these rhabdomeres function as independent light guides. The central rhabdomere contains two photoreceptors: R7/R8. It is surrounded by six peripheral non-fused rhabdomeres containing photoreceptors R1-R6.

Photoreceptors are signaling components that capture and transform photons into an electrical signal that is conveyed to higher visual brain regions. All outer photoreceptors within one rhabdom possess divergent optical axes. Whereas seven rhabdomeres located in neighbored ommatidia are orientated in parallel and are therefore directed towards the same environmental point. The axons of such retinula cells (except the central R7 and R8, which pass through to the second optic ganglion, the Medulla) converge onto the same cartridge of secondary neurons in the first optic ganglion, the lamina. Thus, each lamina cartridge 'looks at' one point in space. Visual information is thereby processed from the photoreceptors down to all neuropil layers in a strictly retinotopic way (i.e. information from two neighbored spots in the visual field is processed via axons to two neighbored columns in all neuropils). The neuronal superposition eye built by R1-R6 is used at low light intensities and for broad-spectral band motion vision; the other part is built by R7 and R8, is used at high light intensities, and is used for color vision (Hardie and Raghu 2001).

In the Lamina, photoreceptors R1-R6 provide input onto five different Lamina Monopolar cells: L1-L5 via chemical synapses. Two of them, L1 and L2 have been proposed to be the major input lines to the motion detection circuitry (Bausenwein et al. 1992). Based on the co-stratification of columnar neurons (Fig. 5) as well as 2-deoxyglucose the neurons potentially constituting these pathways have been predicted long ago. Recent studies have provided the physiological basis for split motion detection in the fly showing that L1 and L2 are specifically involved in the processing of ON and OFF stimuli (Joesch et al. 2010). In the first pathway, L1 synapses onto medulla intrinsic neuron Mi1 and L2 onto Transmedullar neuron Tm1. Mi1 proposed to contact T4 cells and Tm1 cells are synapsing onto T5 cells (Bausenwein et al. 1992; Bausenwein and Fischbach 1992; Fischbach and Dittrich 1989). The axons of these cells converge on the dendrites of the lobula plate tangential cells (LPTCs) that are part of the optomotor pathways.

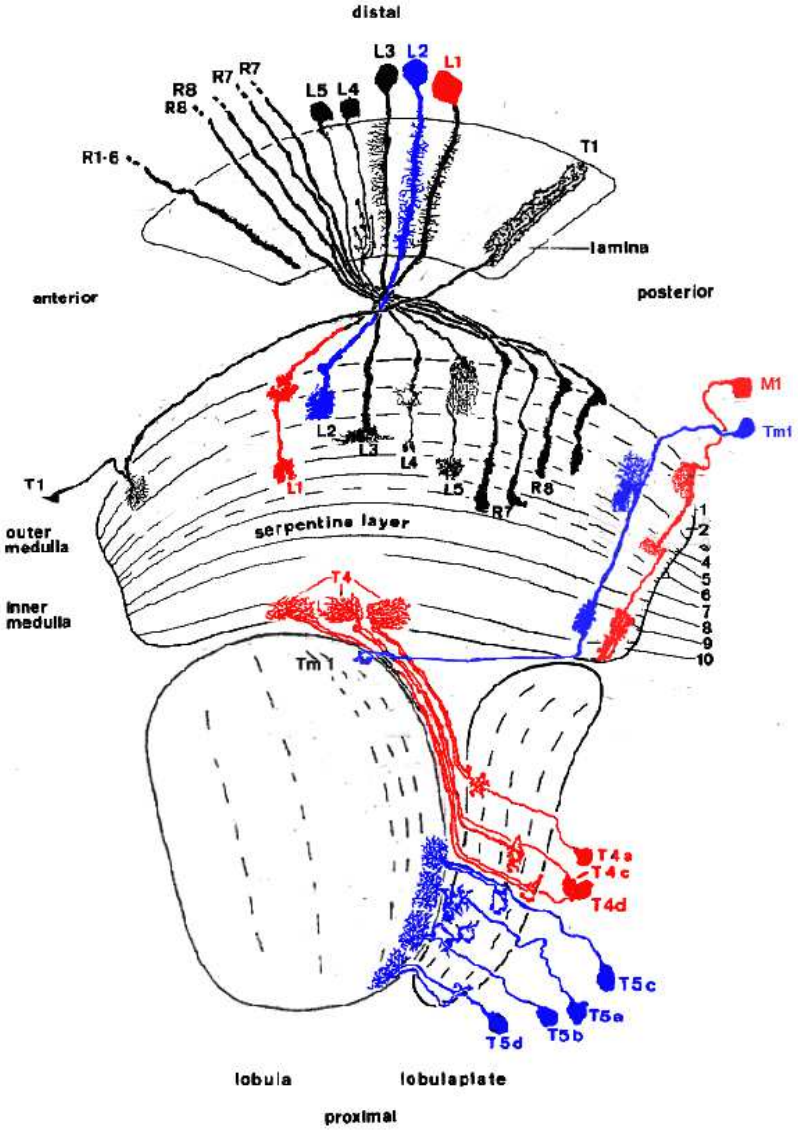

Fig. 5: Two motion pathways in the fly visual system.

Light information captured by the photoreceptors is split into five pathways: L1-L5. L1 and L2 are proposed as the entry points to the motion vision pathways in the fly. Based on co-stratification studies the pathway from L1, labeled in red, continues to M1 which dendrites are co-located with the L1 axon terminals at the Medulla layers 1 and 4. M1 in turn synapse onto T4 cells at the Medulla layer 10. The second pathway is labeled in blue. Here, L2 is supposed to be synaptic connected to Tm1 at the Medulla layer 2. Tm1 contacts T5 cells in the Lobula layer1. Modified from Fischbach and Dittrich 1989.

2.3.1 The Horizontal and Vertical System in *Calliphora*

LPTCs are giant tangential neurons which can be grouped into horizontal (HS) and vertical (VS) systems (Pierantoni 1976).

The HS system consists of three neurons, which dendritic ramifications extend over the entire innermost layer of the lobula plate. The dendrites are distributed along the dorsal-ventral axis where HSN is the dorsal horizontal neuron, HSE the equatorial, and HSS the ventral horizontal neuron. HSN and HSE give rise to many branches over the lateral border of the lobula plate and overlap widely at the para-equatorial level. HSS, on the other hand, occupies space at the lowermost region in the lobula plate and does overlap with HSE (Fig. 6).

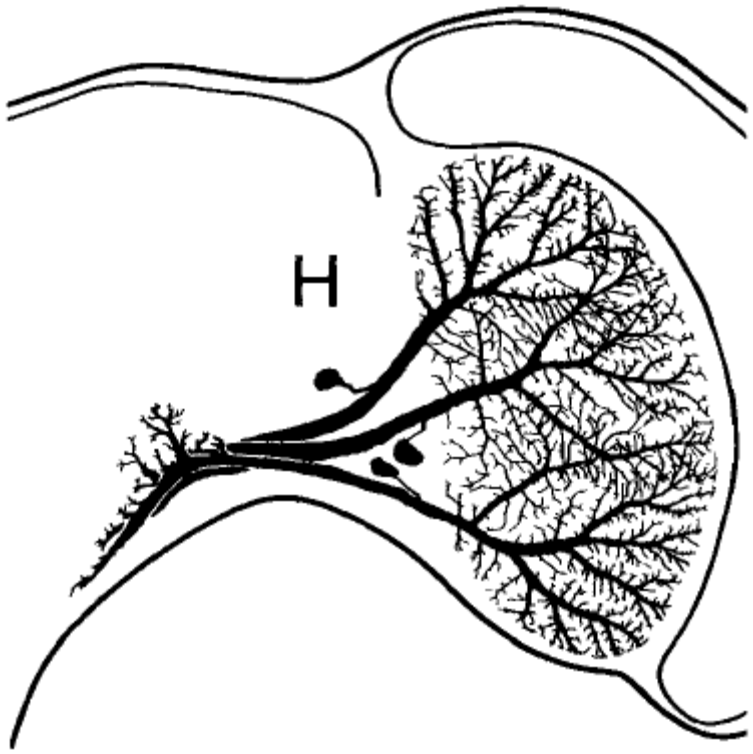

Fig. 6: The HS system in *Calliphora.*

Frontal view of the 3 horizontal cells of the right lobula plate. The cobalt diffusion technique allows simultaneous impregnation of all three horizontal cells, thus resolving not only their complete arborization patterns, but also the relative positions of their dendritic fields and the degree of overlap between them. Modified from Hausen et al. 1980.

Electron microscopy has revealed that all fibers in the lobula plate are post-synaptic possessing a high concentration of synapses and receptors (Pierantoni, 1976; Hausen et al. 1980). The number of such spines increases with distance from the main stem and reaches its maximum at the lateral border of the lobula plate. A rule proposed by Pierantoni says that the synaptic density is inversely proportional to the local radius of the curvature of the membrane. Despite the high density of ramifications, the fibers of the HS never synapse with one another. Furthermore, it has been proposed that not only the arborization density, but also the number of spines and hence the density of input synapses in each horizontal cell increases from the proximal to the lateral margin of the lobula plate, which represents the frontal part of the visual field (Hausen et al. 1980). Much is known about the anatomical aspects of HS dendrites however, the pre-synaptic elements have yet to be identified.
Within the lobula plate, the fibers of the three HS cells are running independently from each other. Around 200 µm from the lobula plate, they converge to a large and very long branch descending towards the ipsilateral posterior slope of the central brain. Their endings are located near the external face of the connective and below the esophagus. During their way, the fibers are additionally connected to three other large units, which descend along the esophageal connective. The HS fibers are ipsilateral and do not enter the contra-lateral connective. At the level of the branching in the mid-brain, the HS fibers are simultaneously pre- and post-synaptic; at their endings, in the periesophageal region, the fibers of the HS show a pre-synaptic nature. The cell bodies of the HS neurons are located at between the ventral medial edge of the lobula plate and the bundle of the VS fibers (Dvorak et al. 1975).

The vertical system of *Calliphora* consists of eleven neurons, which have vertically oriented dendrites in the most posterior layer of the lobula plate (Hengstenberg et al. 1982). The dendritic fibers in the lobula plate are T-shaped. They enter the lobula plate dorsally and their main dendrite turns ventrally. Therefore, the main arbors are covering lateral parts of the retinotopic map and the smaller arbors located at the most anterior layer of the lobula plate covering a dorso-frontal retinotopic area. The branching points of all fibers follow the equator of the lobula plate. Like in HS cells, the main branches give rise to a large number of secondary ones that in turn give origin to tertiary endings; the terminals always found postsynaptic. The distribution of secondary branches is highly asymmetric: almost all of them are oriented towards the

lateral edge of the lobula plate and largely overlap with the following main fiber. However, The VS fibers never synapse with one another or with HS fibers. Postsynaptic sites comparable to those in the horizontal cell collaterals were found also at the axon terminals (Hausen et al. 1980). The fibers of the VS gather in a bundle at the equatorial level along the medial edge of lobula plate. Approximately 200 µm after the emergence from the lobula plate, the fibers give rise to long and tiny branches. The terminals are located slightly above the esophagus and remain ipsilateral to the neuropil from which they originated (Pierantoni 1976).

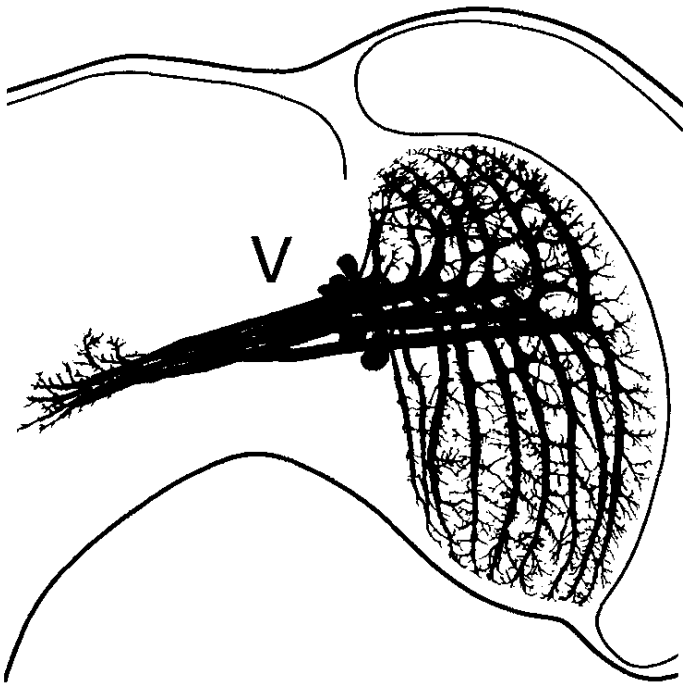

Fig. 7: The VS system in *Calliphora*.
The dendritic fibers of VS neurons are distributed over the proximal-distal axis of the lobula plate. Their axonal terminals are located at the periesophageal region. Modified from Hausen et al. 1980.

The somata of the VS cells are located in close proximity to the cell bodies of HS cells. The dendritic fibers of HS as well as VS neurons do not follow the plane axis straight but bended. In this way, the fibers run along the curved shape of the lobula plate.

2.3.2 The Horizontal and Vertical System in *Drosophila*

The general architecture of the lobula plate is quite similar to that of big flies. All the big fibers join into a horizontal bundle running towards the protocerebral slope close to the esophagus (Heisenberg et al. 1978).

There are 3 cells contributing to the horizontal motion detection. Their fibers, which lie on the frontal surface along the dorsal-ventral axis of the lobula plate, can be distinguished from each other by the domains of their arborizations: north, equatorial, south. In *Drosophila* these overlap considerably (Heisenberg et al. 1978).

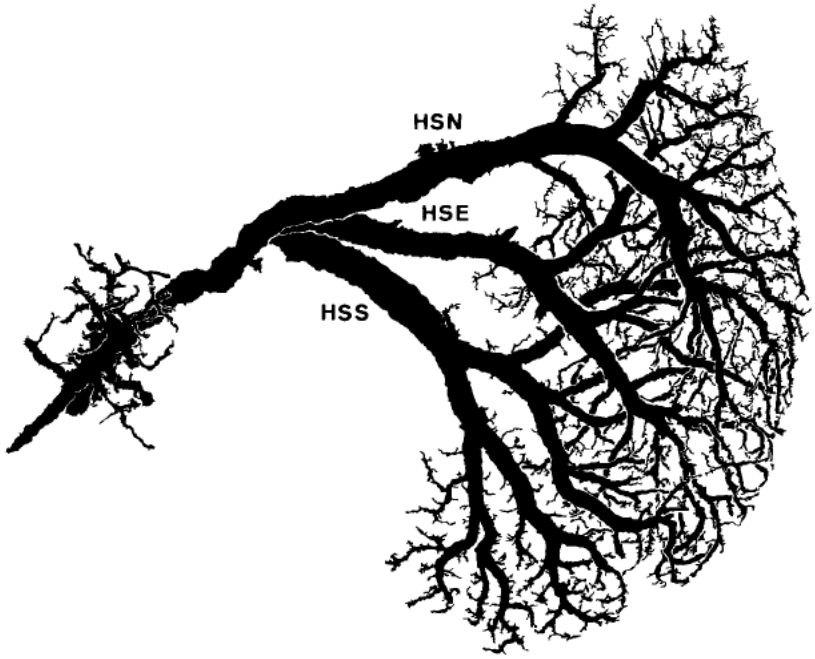

Fig. 8: Camera lucida drawing of the horizontal system in *Drosophila melanogaster.*
The dendritic fibers of HSN cover the dorsal part of the lobula plate whereas HSE ramifies at the equatorial part and HSS in the ventral region. The axonal region is located in the periesophageal region of the central brain. Modified from Fischbach and Dittrich 1989.

In the Lobula plate, their ramifications are slightly tilted in respect to the surface of the plate and are staggered like tiles on a roof. There, the HS cells possess a very rich ramification pattern appearing more complex then in big flies. Golgi stainings have revealed a large number of terminal spines along the secondary and tertiary branches (Hausen 1976; Heisenberg et al. 1978). The north and equatorial fibers join the horizontal bundle where they leave the plate; the south fiber joins it just laterally

to the retractor muscle of the proboscis. Immediately medially to the retractor, the 3 HS cells leave the bundle, bend downward and split each into two branches, one going further down along the posterior slope, the other turning forward into the depth of the brain.

The most significant difference to the larger flies is found in the set of VS cells at the caudal surface of the lobula plate. It is not clear yet how many of these cells there are. Six of them have been identified based on the expression patterns given by Gal4 lines. The general shape of VS cells is comparable to those in big flies (Heisenberg et al. 1978).

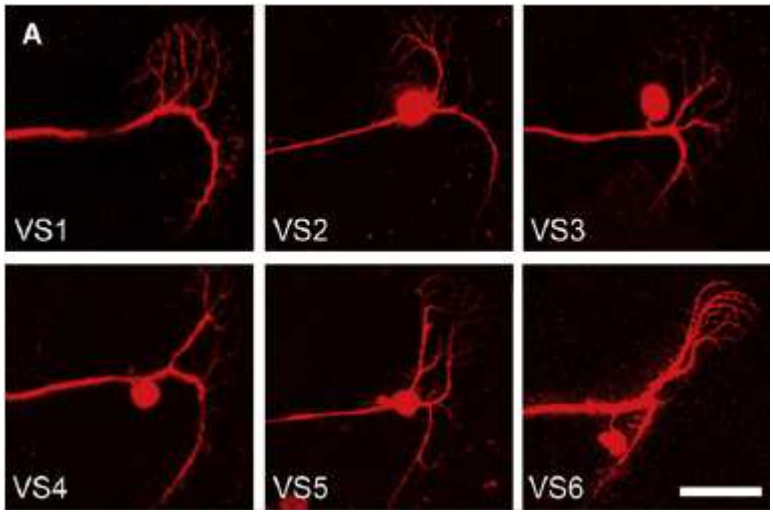

Fig. 9: Identified VS cells in *Drosophila melanogaster*.

VS cells loaded via the patch pipette with Alexa-568. VS cells have vertically oriented dendrites in the most posterior layer of the plate. The VS neurons enter the lobula plate dorsally and their main dendrite turns ventrally. A smaller dendrite branches to the most anterior layer of the lobula plate (Fischbach and Dittrich 1989). Picture from Joesch et al. 2008.

The giant fiber bundle of VS cells enters the lobula plate high up. Around 3/4 of the height of the plate is covered by the prominent branches of VS1 and VS2. All branches run parallel to each other, those of cells VS1 and VS4 and VS5 being closer together than the others are. The branches of VS1, VS2, and VS3 are accompanied by satellite fibers. The upward extending branches are much smaller and less well oriented. What distinguishes the VS cells of *Drosophila* from those of big flies is that several of these collaterals run parallel to the columns of the lobula plate to the frontal surface where they have arborizations in the plane of the HS cells.

These branches end in a part of the lobula plate, which presumably corresponds to the upper frontal part of the visual field. A large branch of cell VS2 enters the middle plane of the plate and fills the upper frontal part of the projection of the visual field. The VS cells have long horizontal extensions to the upper posterior slope. Close to the esophagus, they split into an ascending and a descending branch and end in a region where they meet some of the ocellar giant fibers and a branch of a huge fiber of the cervical connective (Heisenberg et al. 1978).

A detailed analysis of presynaptic release and postsynaptic inhibitory and excitatory sites in LPTCs has been carried out by Raghu SV et al. (2007, 2009). HS as well as VS cells express in their dendritic regions within the lobula plate both gamma-aminobutyric acid (GABA) receptors and Dalpha7-type nAChR subunits. Specifically on higher-order dendritic branches, the density of receptors are increased. These findings underline the postsynaptic nature of HS and VS cell neurites in the lobula plate and shed light on their presynaptic columnar partners, which provide inhibitory and excitatory inputs to these cells. Moreover, presence of these receptors supports a model in which directional selectivity of LPTCs is achieved by the dendritic integration of excitatory, cholinergic, and inhibitory GABAergic input from local motion detectors with opposite preferred direction (Raghu et al. 2009).

The terminals of LPTC neurites in the protocerebrum express synaptobrevin, suggesting the presence of presynaptic specializations there. HS-cell and VS-cell terminals additionally show evidence of postsynaptic GABAergic input.

2.3.3 The Reichardt detector model.

Despite the anatomy-based prediction of the motion detection pathways, columnar neurons in the Medulla have so far escaped electrophysiological analysis because of their small sizes. Here, the so-called Reichardt detector model predicts the key mechanisms of elementary motion detectors downstream of the Lamina. Photoreceptors only provide information on time-dependent variations of local light intensity. For motion detection, at least two input channels are necessary, as motion is a vector in the spatiotemporal domain that needs two points for its representation.

Fig. 10: The Reichardt detector model.
The Reichardt detector model represents a simple principle mechanism of how motion can be extracted from incoming signals of neighboring photoreceptors. This model includes two essential steps, which are firstly, asymmetric temporal filtering through a high-pass (HP), a low-pass (LP) filter, and secondly, nonlinear integration in which the filtered information is multiplied. This composition makes the detector sensitive to motion direction of the motion as well as the stimulus pattern and velocity of movement. At each image location, at least two of these units in orthogonal orientation are needed. Scheme adapted from Borst et al. 2003.

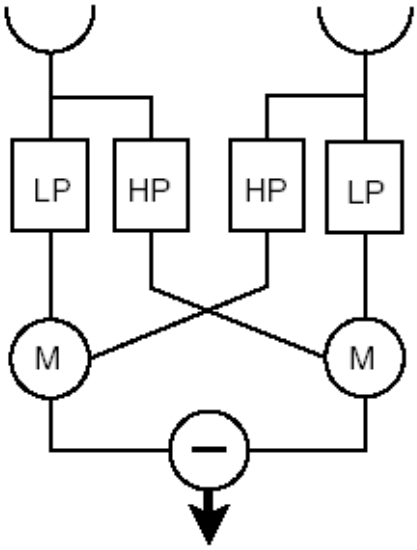

The interaction between both input channels must be non-linear in order to preserve the information about temporal order of the incoming signals and with that, the direction information of the motion. The movement detector must be asymmetrical in order to allow a different response to the direction of motion from that to the opposite direction. In case of the correlation-type motion detector, multiplication-like interactions at each photoreceptor integrate the direct, delayed input signal from the first photoreceptor pathway with the high-pass filtered signal from the second photoreceptor. Output signals from both half-detectors are then subtracted from each other (Borst and Haag 2002).

Many studies of the mechanisms underlying direction selectivity have been first performed on the visual system in large flies, where motion-sensitive LPTCs do spatially pool the output signals on their dendrites from many thousands of

directionally selective neurons. Two fields of Reichardt detectors are supposed to provide input from columnar neurons, one inhibitory, and the other excitatory. Spatially integrated arrays of motion detectors exhibit a velocity optimum beyond which the responses decline. In addition, the responses also depend on the structure of the moving pattern, i.e. high contrast elicits greater responses than lower contrast despite the same moving velocity. Moreover, the optimum velocity depends on the spatial pattern wavelength leading to an invariant temporal frequency optimum (Reichardt 1986; Borst and Haag 2002).

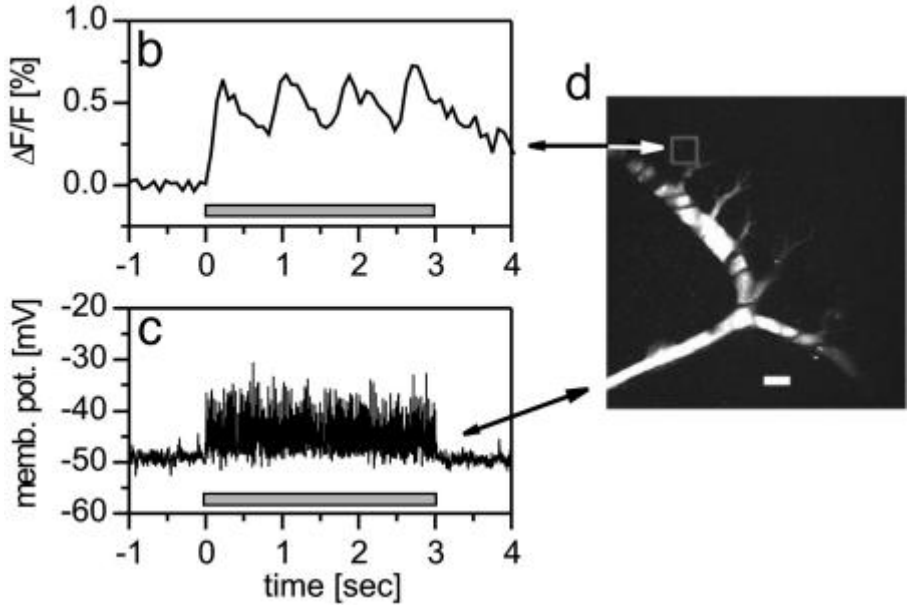

Fig. 11: Sample recording from VS2 cell in a blowfly.

The signal of a fluorescent calcium indicator is shown during motion along the preferred direction of the cell. Measurements were taken from the VS2 cell shown in d within the indicated area (box). (c) Membrane potential is recorded simultaneously from the axon of the cell. Unlike the local dendritic signal, no modulation is visible because of spatial integration over many periodic signals, which are phase-shifted with respect to each other in different dendritic areas. (d) Projected 2-Photon image stack. Modified from Haag et al. 2004.

The axonal signals of these neurons represent the global detector signal in the fly visual system. Using optical recordings of free cytosolic calcium (Fig. 11) revealed that stimulation by uniformly moving gratings elicited local modulations in the dendritic tips of integrating motion-sensitive neurons like LPTCs (Singer and Borst 1998). These modulations were synchronous with the temporal frequency of the

moving pattern and phase-shifted with respect to each other in different parts of the dendrite, thus providing clear evidence in favor of Reichardt-type motion processing in the fly visual system (Haag et al. 2004).

All these predictions have been recently shown to be also true for LPTCs in *Drosophila* (Jösch et al. 2008; Schnell et al. 2010).

2.3.4 The physiological properties of LPTCs in *Drosophila*

Electrophysiology studies have shed light on many intrinsic properties of LPTCs. The 3 HS cells are distributed along the dorsal-ventral axis. The preferred direction (PD) of a presented moving sine grating is from front to back and the null direction (ND) is from back to front (Schnell et al. 2010). The 6 VS cells are distributed along the distal-lateral axis and respond to vertical motion.

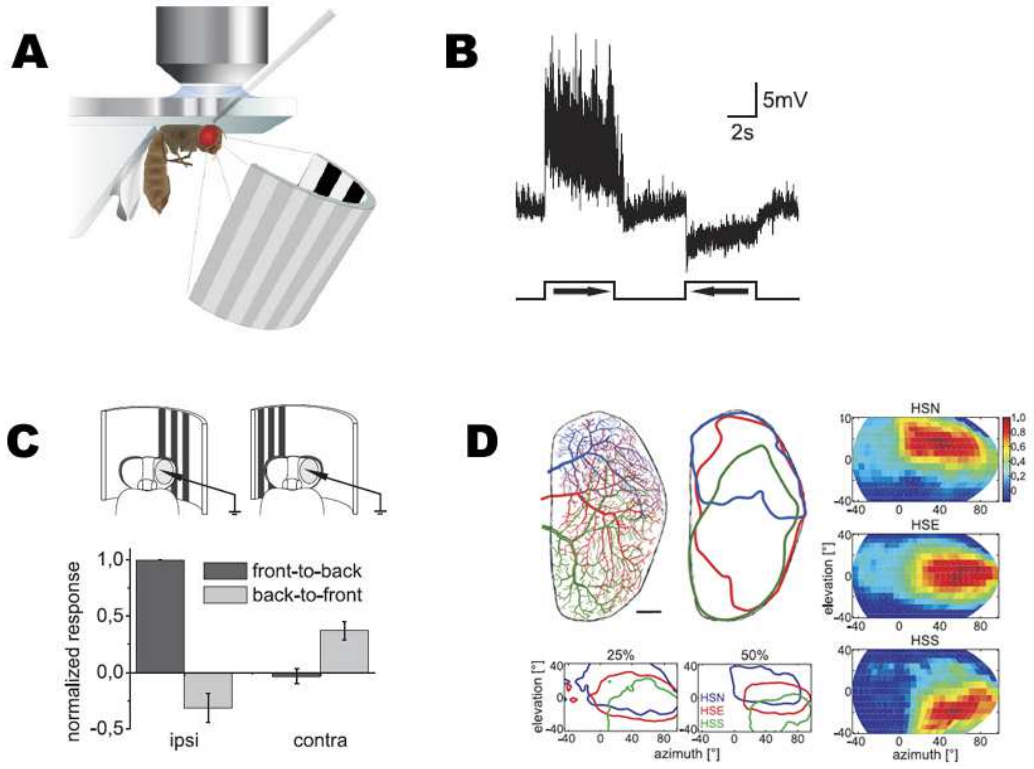

Fig. 12: Anatomical and physiological characteristics of HS cells in *Drosophila melanogaster*.
The recording setup and fly preparation are schematically shown (A). A vertical sine grating moving horizontally is presented to the fly while HS neurons are recorded by whole cell patch clamp. The canonical response of an HSN cell is directionally selective, i.e. the neuron depolarizes to 'front to back motion', whereas the preferred direction (PD) hyperpolarizes to 'back to front motion', the null direction motion (ND). (B) HS neurons are also sensitive to contralateral stimulation. A weak depolarization is visible when the contralateral side is stimulated with 'back to front motion'(C).

Although the dendritic fields of HSN, HSE and HSS strongly overlap, the receptive fields of these cells show that they are most responsive to stimulation in those areas which are covered by their dendrites in the lobula plate (D). Modified from Schnell et al.2010.

The PD of the stimulus is downwards whereas the ND is upwards. Whole cell recordings revealed that stimuli in PD elicit excitatory responses in both LPTC groups in the form of a graded depolarization with superimposed spikelets, while presenting stimuli in ND cause an inhibitory hyperpolarisation response. Response properties also depend on the velocity and contrast of the sine-grating stimulus as predicted from the Reichardt detector model. The receptive field of each HS or VS cell consists of those regions in the visual field in which the presence of a stimulus alters the firing of that neuron (Fig. 12).

2.3.5 The suggested role of LPTCs in behavior

Flies respond to moving visual stimuli with various behavioral actions depending on the specific circumstances. The so-called optomotor responses elicited by rotation of the visual surround serves to reduce the velocity of the pattern movement on the fly's retina. This is important for stabilization of the head and locomotion course, thereby minimizing involuntary, rotatory displacements during flight (Pflugfelder and Heisenberg 1995). One possibility of monitoring optomotor responses is to tether the fly at the dorsal thorax to a torque meter. Presenting a visual stimulus in a drum thus functions as a flight simulator. In flight, under the same conditions, the moving stimulus will elicit the same behavior in tethered flies as in untethered ones (Götz 1964; Heisenberg and Wolf 1984). For example, with a vertical moving grating, passive turns around the fly's vertical body axis can be simulated which are then achieved by an opposing optomotor response. In this case, the yaw torque is exercised through a change of the wing beat amplitude between the left and the right wing. The wing beat analyzer has been used for measuring those wing beat kinematics in real time (Götz 1987; Dickinson et al. 1993). The method implements an infrared light source above the fly in order to cast a shadow of the wings onto photodetectors positioned below. Above each photo detector is a crescent-shaped aperture, which traces out a section of the stroke envelope of the wings. The relative position of the wings can be determined through the monotonic increase of the aperture width from top to bottom that leads to a proportional increase of light-

blocking when the wing is moving through the ventral point of the wing beat. The magnitude of the peak shadow during each wing beat provides a signal that is roughly proportional to the stroke amplitude.

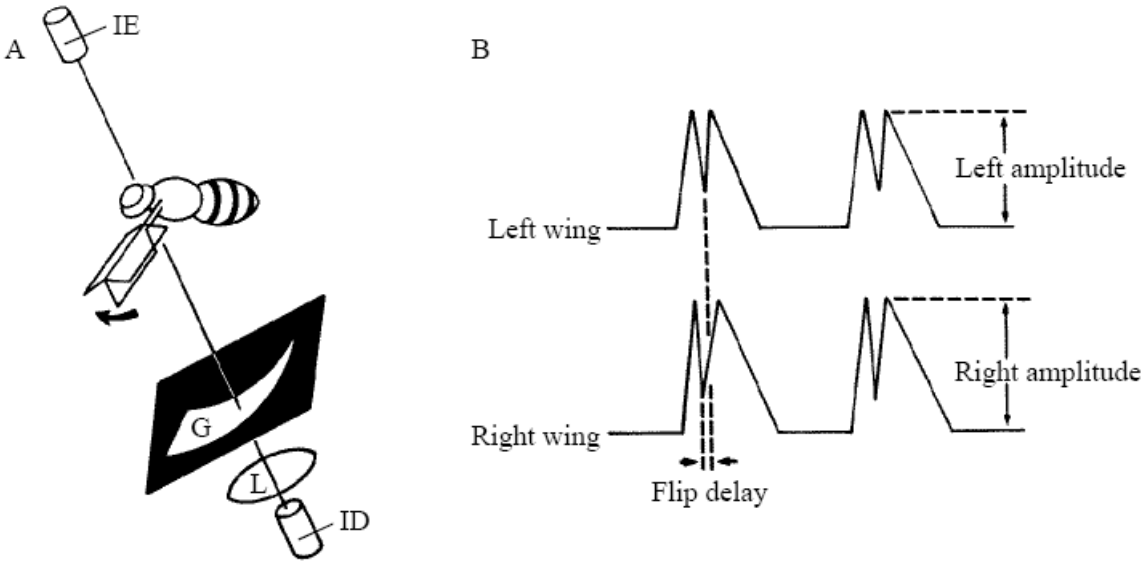

Fig. 13: The wing beat analyzer monitors the wing beat kinematics in real time.
(A) An infrared detector (ID) and a lens (L) are used to track the shadows cast by the wings when they move through the light of the infrared emitter (IE). The crescent-shaped aperture possesses a monotonically increasing width of grating (G) so that maximum occlusion occurs during down stroke. (B) A sharp transmission peak is produced during ventral flip of the wing when the wing becomes aligned with the incident light. Information of the photodectors is used to calculate relative wing beat amplitude and ventral flip delay. Modified from Dickinson et al.1993.

The HS neurons of the lobula plate are most probably part of the optomotor pathways. This has been shown anatomically and electrophysiologically in *Calliphoridae* (Hausen 1989), the blowfly. In support of this evidence, the optomotor responses of the *Drosophila* mutants: optomotor blind omb^{H31} (an omb allele) and lobula plate-less (lop) are strongly interrupted (Heisenberg and Wolf 1984). The omb mutant lacks the HS neurons while in *lop* these neurons are depleted of their suggested input neurons T4 and T5 (Fischbach 1983; Fischbach and Dittrich 1989).
For instance, in omb^{H31} flies (an omb mutant) the yaw torque response to a vertical moving grating is reduced by 30% of the wildtype value. The residual response properties are, however, different from wildtype torque. In wildtype animals, unilateral large field stimulation in front-to-back and back-to-front motion elicits syndirectional-turning tendencies and gratings in frontolateral and caudolateral positions elicit

responses of similar strength. However, in omb^{H31} flies, front to back motion evokes a syndirectional response of only half the wildtype strength and visual stimuli from back-to-front evokes zero or even antidirectional yaw torque (Brunner et al. 1992). However, when presenting individual stripes, omb^{H31} flies show nearly wildtype behavior. Here, movement from front-to-back in the frontolateral visual field elicits syndirectional torque response whereas the fly does not react to back-to-front movements. These results reveal that in omb^{H31} flies the object response is still functional whereas large field response is impaired. Anatomical analysis of omb^{H31} flies revealed the conspicuous absence of HS and VS cells. These results give a strong argument that HS and VS cells are involved in optomotor large field responses.

2.4 The role of *Drosophila* Down-syndrome-cell-adhesion-molecules (Dscams) in neuronal wiring

In *Drosophila,* information in the visual system is processed in a strict retinotopic way. In case of LPTCs, the dendritic branches in the lobula plate are spatially pooling the output signals from many thousands of directionally selective columnar neurons. Therefore, space filling and correct dendritic ramification are crucial for cell function. However, no guidance molecule has yet been identified to date.

One of the most discussed candidates involved in the establishment of neuronal patterning during neuronal development is *Drosophila* Dscam1. In total, there are four *Dscam* paralogs in *Drosophila* (*Dscam1-4*). However, the generated diversity through alternative splicing is unique to Dscam1. This gene locus encodes several thousands of cell surface proteins through alternative splicing. The resulting isoforms are shown to mediate the correct formation of branching patterns via homophilic repulsion between Dscam proteins expressed on opposing cell surfaces, thereby resulting in self-avoidance. Each individual Dscam1 isoform exhibits isoform-specific binding that mediates homophilic recognition (Wojtowicz et al. 2004, 2007, Matthews et al. 2007). This provides the molecular basis for self-recognition in the nervous system.

Although the gene locus is highly conserved throughout arthropods, vertebrate DSCAMs are not diversified. All Dscam isoforms share identical extracellular domain structure with 10 Ig domains and 6 fribronectin type III domains (Schmucker et al. 2000; Yamakawa et al. 1998). However, in *Drosophila* the extracellular part possesses three alternatively spliced hypervariable immunoglobulin domains that contribute to Dscam1 interaction specificity. 12 alternative exons encode for the first half of Ig2, 48 alternative exons encode the first half of Ig3, 33 alternative exons encode Ig7 and finally, 2 exons encode the transmembrane domain. Together, *Dscam1* gives rise to 38,016 different Isoforms and 19,008 different ectodomains, respectively (Fig. 14 a) (review: Hattori et al. 2008, 2009).

Quantitative RT-PCRs of photoreceptor cells as well as mushroom body neurons provided evidence of a stochastic yet biased expression of different Dscam isoforms in neighboring cells (Neves et al. 2004; Zhan et al. 2004). Moreover, RT-PCR of single photoreceptors showed that even neurons of the same type differ in the sets of expressed Dscam isoforms. However, directly neighboring photoreceptors express

between 15-50 distinct mRNAs and thereby possess a unique Dscam cell surface code.

Homophilic binding of Dscam1 isoforms is mediated by matching of all three hypervariable domains, i.e. only self-binding of all three domains initiates a repulsion mechanism between opposing cell surfaces. This requirement of a direct Dscam-Dscam interaction has been demonstrated by a series of biochemical experiments in which it was shown that, from a randomly chosen set of 11 Dscam isoforms, each one binds to itself but not to others (Hughes et al. 2007) (Fig. 14 b). However, rare exceptions exist if differing domain-pairs exhibit high amino acid identity, then heterophilic binding does also occur. Nevertheless, heterophilic binding is always weaker than homophilic binding.

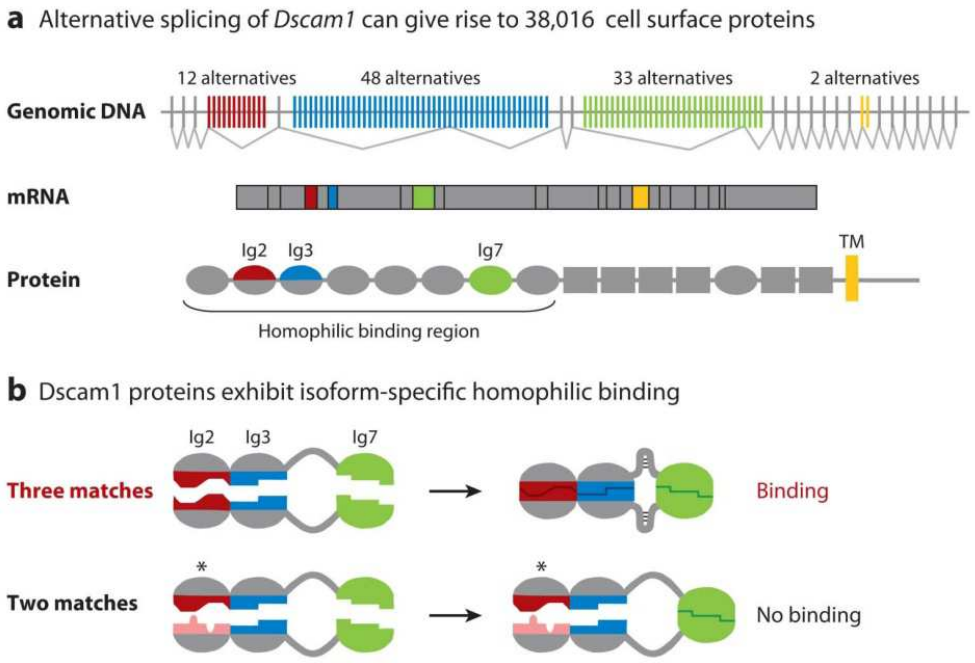

Fig. 14: Alternative splicing of Dscam1 can give rise to 38,016 different cell surface proteins that exhibit isoform-specific homophilic binding.

The *Dscam1* gene locus encodes for four blocks of alternative exons that encode 12 different variants for the N-terminal half of Ig2 (*red*), 48 different variants for the N-terminal half of Ig3 (*blue*), 33 different variants for Ig7 (*green*), and two different variants for the transmembrane domain (TM) (*yellow*). In total, this variable incorporation of alternative exons leads to 19,008 different ectodomains and hence 38,016 different Dscam1 isoforms (a). Despite this vast number of isoforms most of these proteins exhibit isoform-specific binding, i.e. only if all three variable Ig domains match opposing structures will binding occur (b). Figure adapted from Hattori et al. 2008.

The homophilic binding structure and mechanism behind the Dscam-Dscam interaction were extensively studied. Results strongly suggest that the N- terminal eight Ig domains comprise a region sufficient for homophilic binding in vivo. During the binding procedure, each of the three variable domains binds to its identical counterpart in an antiparallel fashion. In crystal structure, the ectodomains fold into S shapes, which position the variable domains on that side of the molecule at which interactions to counterparts of the opposing molecule occur (Meijers et al. 2007). These interactions give rise to a double-S homophilic dimer, formed by two homophilic bound monomers. This homophilic dimer buries the homophilic binding area, more than half of which is made up of variable Ig domains. Therefore, small differences between the Ig domains lead to loss of that variable domain surface. These molecular findings illuminate the molecular basis for the all-or-none binding mechanism of Dscam1 isoforms.

Dendrites distinguish between sister branches and those of other cells. Self-recognition can often lead to repulsion, a process termed 'self-avoidance.' Da-neurons associate closely with the epidermis as they extend across the body wall; their dendrites thus create a two-dimensional meshwork in which developing branches frequently encounter other dendrites. Self-avoidance in *Drosophila* da sensory neurons has been demonstrated to be dependent on cell-recognition molecules encoded by the Dscam locus. For example, da-neurons that were deficient in Dscam function do not recognize sister branches and failed to initiate repulsion, leading to a breakdown in self-avoidance. Furthermore, individual branches of Dscam mutant cells often failed to disperse evenly across their territory. However, processes from specific da neurons still gathered at discrete target sites within their territory. This observation leads to the assumption that Dscams are not involved in heteroneural tiling, a process in which inhibitory interactions with nearby neurons control the size of dendritic fields in such a way as to achieve a complete but nonredundant innervation of a receptive area by functionally uniform groups of neurons (Hughes et al. 2007). Expression of chimeric Dscam1-GFP, in which the cytoplasmic domain was substituted with GFP, elicited an extensive fasciculation of sister branches (Matthews et al. 2007). In In contrast thereto, overexpression of the same Dscam isoforms in two overlapping da neurons forced a spatial segregation of the two fields. This underlines the hypothesis that dendritic branches of da neurons use isoform-specific homophilic interactions to ensure minimal overlap (Fig. 15).

Homophilic binding of the highly diverse extracellular domains of Dscam may therefore limit the use of the same 'core' repulsion mechanism to cell-intrinsic interactions without interfering with heteroneuronal interactions (Hughes et al. 2007). Taken together these experiments revealed that sister dendrites are expressing the same Dscam isoforms in order to mediate self-avoidance in a cell-autonomous fashion and with that correct spacing of dendrites. Thereby, the cytoplasmic tail of Dscam converts homophilic interactions of the ectodomain to dendrite repulsion. By contrast, Dscam diversity ensures that inappropriate repulsive interactions between dendrites sharing the same receptive field do not occur.

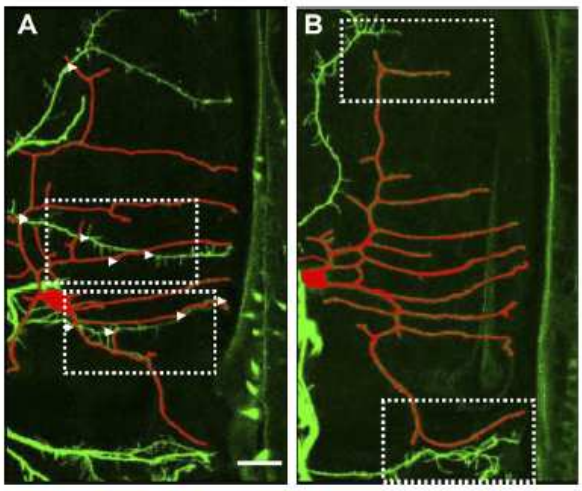

Fig. 15: Overexpression of a single Dscam1 isoform elicits inappropriate repulsion between two da neurons with overlapping dendritic fields.
(A) Da-neurons of different classes (ddaE in red and ddaF/A in green) extensively overlap in wildtype animals. (B) Overexpression of the same Dscam isoform in two da neurons prohibits them from sharing the same region of the hemisegment. Neurons were labeled with GPP. DdaE was pseudocolored in red. Modified from Hughes et al. 2008.

Dscams have the same role in bifurcating mushroom body (MB) axons and in pathway finding of projection neurons (PN) in the olfactory system.
In the MB, the olfactory learning and memory center of insects (Heisenberg et al. 1985), growth cone bifurcation and guidance to the different lobes are very important during development (Grotewiel et al. 1998). *Dscam* deletion mutants revealed defects in the divergent segregation of sister branches (Wang et al. 2002). Instead of two branches that project away from each other, *Dscam* mutant axons gave rise to multiple branches through repeated bifurcation. In addition, *Dscam* mutant axons

altered the projections of wild-type axons within the same MB. The non-cell-autonomous effect of *Dscam* provides the evidence that the first-born alpha'/ß' neurons play a crucial role in shaping the projection patterns of all later-born MB neurons. Overexpression experiments of single Dscam1 isoforms caused multiple core fibers and disorganization within the peduncle and lobes (Hattori et al. 2007). These dominant phenotypes were only seen when large cell populations were involved but not in small or single cell clones, suggesting that the Dscam gain-of-function phenotype is a non-cell-autonomous effect.

In the olfactory system of *Drosophila melanogaster*, axons of olfactory receptor neurons (ORNs) and dendrites of second-order PNS typically target 1 of ~50 glomeruli. Dscams control the formation of dendritic fields in PNs. The removal of Dscam selectively from these neurons leads to dendritic agglomerations and major reduction in their dendritic field size. Overexpression of Dscam in PNs causes dendrites to be more diffuse during development and shifts their relative position in adulthood. Nevertheless, the positional shift of projection neuron dendrites causes a corresponding shift of its partner ORN axons, thus maintaining the connection specificity. This observation provides evidence for a pre- and post-synaptic matching mechanism independent of precise glomerular positioning (Zhu et al. 2006).

Taken together, Dscams are playing a pivotal role in self-avoidance and target finding during the construction of neural circuits in *Drosophila*. Whether these molecules are necessary for the establishment of the motion detection circuitry is unknown and, if so, manipulation of the endogenous Dscam code should have a severe influence on the morphology of LPTCs.

2.5 Methods for functional dissection of the visual circuitry

In *Drosophila melanogaster*, a broad spectrum of genetic techniques is available which allows the dissection of neural circuits. Different approaches based on the Gal4/UAS system have been developed over the last decades, which allow the restriction of individual Gal4 expression patterns from small cell patches down to single cells. On the other hand, the UAS promoter can be used to modulate the expression of any target genes, which can be used to visualize cells, as well as enhancing and removing molecules of interest.

2.5.1 Intersectional strategies

Despite the enormous diversity of available tissue-specific lines, GAL4 expression patterns are rarely restrictive enough to map key elements of neural circuitry (Bohm et al. 2010). However, GAL4 expression can be made more specific by means of intersectional strategies. These can combine two different GAL4 linesin such a way that GAL4 is only expressed in the cells that are in one line but not in the other one, or those that are in both lines. When combined with intrinsically sparse GAL4 lines, this offers very specific selection, often limited to a single cell type. In the following section, I will introduce some basic techniques.

2.5.1.1 Gal4 inhibition via Gal80 expression.

One way to create GAL4 expression in the cells that are only expressed in one line requires line A to be made to express GAL4, and line B made to express GAL80, a repressor protein that blocks Gal4 by binding to its transcriptional activation domain (Lue et al. 1987) (Fig. 16 a). Therefore, only the cells that are in the Gal4 expression pattern but not expressing Gal80 will have active GAL4, which can then drive the reporter gene. A temporal regulation of the Gasl4/UAS system can be additionally achieved by using a temperature sensitive allele of Gal80. At restrictive temperature, the temperature sensitive protein would not splice, hence no functional Gal80 can be produced and Gal4 protein remains fully active (Zeidler et al. 2004).

To express GAL4 in only the cells contained in both lines, a technique called split-GAL4 can be used (Luan et al. 2006). Here the first line is made to express half of

the GAL4 protein, which is inactive by itself. Similarly, the second line is made to express the other half of GAL4, also inactive by itself. Only the cells that are in both lines make both halves, which self-assemble into GAL4 and activate the reporter gene.

2.5.1.2 FRT/FLP mosaic technique

Another mosaic technique uses targeted DNA recombination at FLPase recombination targets (FRTs), which can be driven in flies by the FLP recombinase (FLPase) (Golic and Lindquist, 1989). If a fly has two FRTs in identical positions on homologous chromosomes, heat shock-induced expression of FLPase (hs-FLP) can cause recombination between the FRT sites. With that technique, a random restriction can be achieved by using patches of expression of the recombinase Flippase (FLP) to catalyze removal of sequences between a tandem pair of FLP recognition target sequences (Bohm et al. 2006). The basic FLPout construct contains a strong, ubiquitously active promoter (often that of actin or tubulin) coupled to an FRT, a marker gene, a transcription termination signal, a second FRT and finally, the coding sequence to be misexpressed. In such constructs, the promoter is blocked from driving the expression of the downstream coding sequence by the termination signal.

Another use of FRTs is to remove stretches of DNA and to induce the misexpression of selected genes and constructs in clones of cells via the so-called FLPout technique (Struhl and Basler, 1993). FRTs are removed by FLPase-induced recombination (‘FLPout’), both the marker gene and the termination signals are lost, and the downstream coding sequence is expressed. In most applications of this technique, recombination is driven by hs-FLPase with which the timing of the FLPout and the percentage of cells undergoing recombination depend on the timing and levels of heat shock. Here, the activation of the FLPout does not require mitosis, and can thus be used to drive gene expression in post mitotic tissues.

2.5.1.3 MARCM technique

In the MARCM (mosaic analysis with a repressible cell marker) technique, the tub-Gal80 is removed using FRT mediated mitotic recombination (Lee and Luo, 1999)

(Fig. 16 b). The advantage of this technique over FLPouts is that it simultaneously generates a mitotic recombinant clone. This can be used, for example, to generate a clone of homozygous mutant neurons that also express a membrane-associated GFP, thus marking the mutant axons; in fact, this technique can be used in all cases where one needs to mark homozygous mutant clones. Moreover, this technique can also be used to generate clones that are not only homozygous for a given mutation, but also simultaneously express any chosen UAS construct.

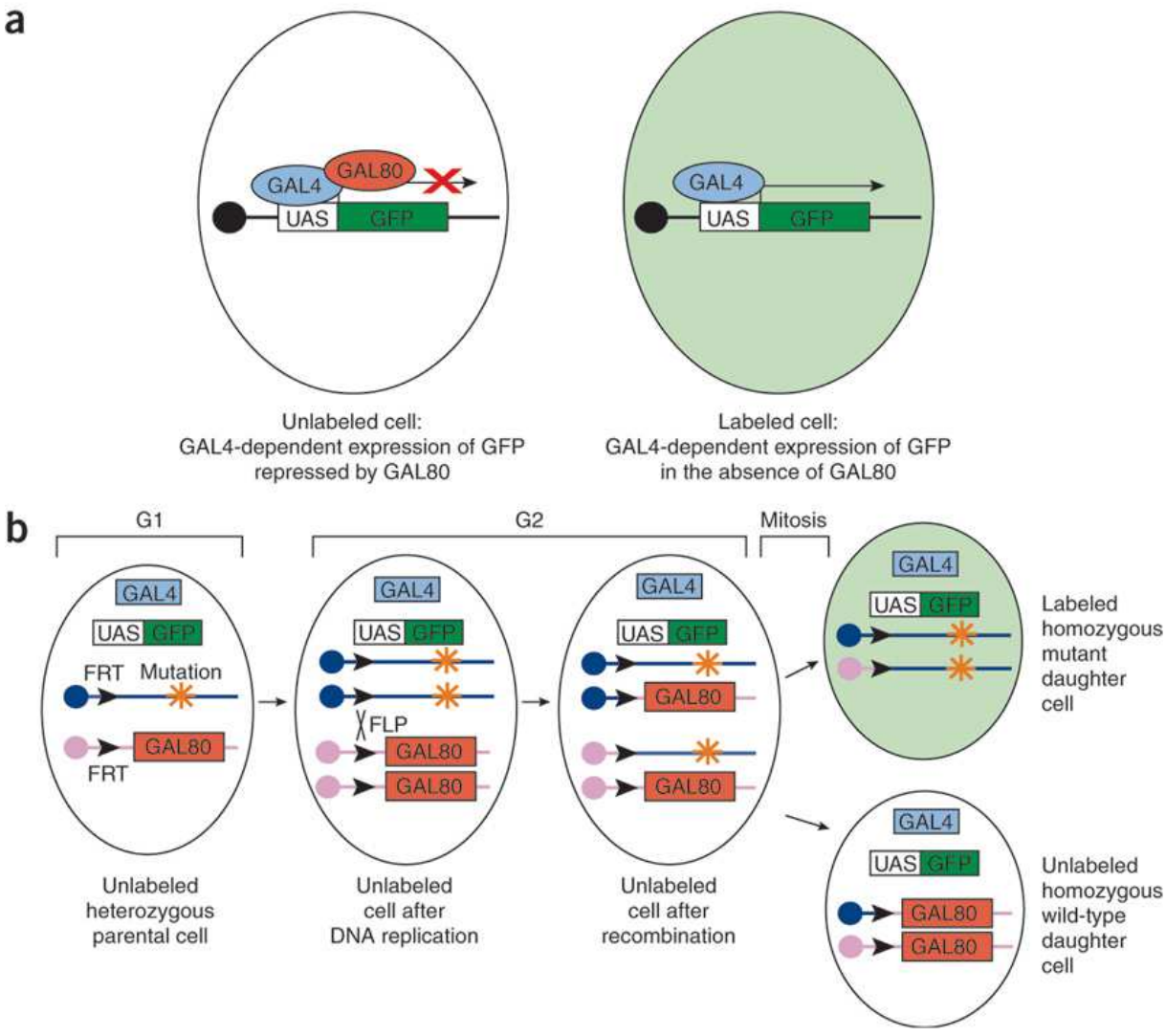

Fig. 16: Restriction of the expression pattern with Gal80 and MARCM

(a) In cells containing the GAL80 protein, GAL4-dependent expression of a UAS–gene (GFP) is repressed. By contrast, cells containing GAL4 but lacking GAL80 will express the UAS–gene (GFP). In this schematic, genes are denoted by colored boxes whereas proteins are denoted by colored ovals. (b) MARCM requires two FRT sites located at the same position on homologous chromosomes. GAL

80 is located distally to one of the FRT sites. The FLP recombinase is located anywhere in the genome. GAL4 is located anywhere in the genome except distally to the FRT site, on the FRT, GAL80 recombinant chromosome arm. The UAS–marker is located anywhere in the genome except distal to the FRT site on the FRT, GAL80 recombinant chromosome arm. Optionally, there is a mutation distal to the FRT in *trans* but not on the FRT, GAL80 recombinant chromosome arm. Site-specific mitotic recombination at FRT sites (black arrowheads) gives rise to two daughter cells, each of which is homozygous for the chromosome arm distal to the FRT sites. Ubiquitous expression of GAL80 represses GAL4-dependent expression of a UAS–marker (GFP) gene. Loss of GAL80 expression in homozygous mutant cells results in specific expression of GFP. Modified from Wu and Luo 2006.

2.5.1.4 Calcium imaging using GECIs

Optical methods have proved helpful in the analysis of the neuronal principles underlying visual motion processing in flies, which allows physiological investigation under in vivo conditions. Many aspects of dendritic processing in large-field motion-sensitive neurons of *Calliphora* have been investigated by calcium imaging. The main advantage in *Drosophila melanogaster* compensating the tiny size of its neurons is the possibility to introduce genetically encoded Calcium indicators (GECIs), such as TN-XXL, via the Gal4/UAS system (Mank et al. 2008). One recently published 2-Photon imaging study (Reiff et al. 2010) demonstrated how these indicators can be used to do functional studies in lamina monopolar neurons. In that study, L2 terminals were expressing the genetically encoded Ca2+ TN-XXL. Visually evoked changes of intracellular Ca2+ in single neurons were recorded optically. The results revealed that Ca2+ in single terminals of L2 neurons in the medulla carried no information about the direction of motion. However, brightness decrements (light OFF) induced a strong increase in intracellular Ca2+ and whereas, brightness increments (light ON) induced only small changes, suggesting that half-wave rectification of the input signal occurs.

Unraveling the function of neurons with that method is elegant, but utilizing the Gal4/UAS system is limited by the expression specificity of the Gal4 promoter. Especially LPTCs with their rich ramifications and overlapping areas are difficult to trace. In addition, there are no Gal4 lines, which express single cells in the lobula plate. The established expression pattern therefore needs to be refined by intersectional expression methods.

2.5.2 Single cell ablation using RicinA

A powerful technique to dissect the motion-vision circuit is by ablating cells genetically, mechanically or with laser (Nässel et al. 1983; Bausenwein et al. 1986; Hausen and Wehrhahn 1989; Warzecha et al. 1992; Farrow et al. 2008, 2009). By selective ablation, the role of individual neurons within synaptic networks can be clarified as the function of a network strongly depends on the appropriate connectivity between its components. Regarding motion detection there are three steps of information flow at the level of LPTCs: the first is the integration of information at the dendritic ramifications, the second is the interchange of information between LPTCs and the last one is the axonal propagation of information to motor neurons. One way of unravelling the function of a single LPTC for motion detection is to monitor the optomotor response of a fly missing that specific neuron. Organic toxins are poisonous molecules, peptides, or proteins produced by living cells or organisms. They are capable of causing cell death on contact with or absorption by body tissues through the interaction with biological macromolecules, such as enzymes or cellular receptors. Here again, the genetic accessibility of *Drosophila* allows the integration of various toxins into the fly genome under the control of the Gal4/UAS system.

Ricin is organically found in the castor bean (Ricinus communis). In nature, the protein is a heterodimeric glycoprotein consisting of an A-chain, which displays a ribosome-inactivating function connected by disulfide bond to a B-chain that is catalytically inactive but serves to mediate entry of the AB-protein complex into the cytosol. In order to display the cytotoxic function the disulfide bond must be reductively cleaved (Fig. 17). In vitro assays demonstrated that the concentration of approximately 5x10^-10 M is toxic to retinoblastoma cells (Merriam et al. 1984). Since 1992, RicinA is used as a genetically encoded toxin for targeted cell ablation in *Drosophila* (Moffat et al. 1992).

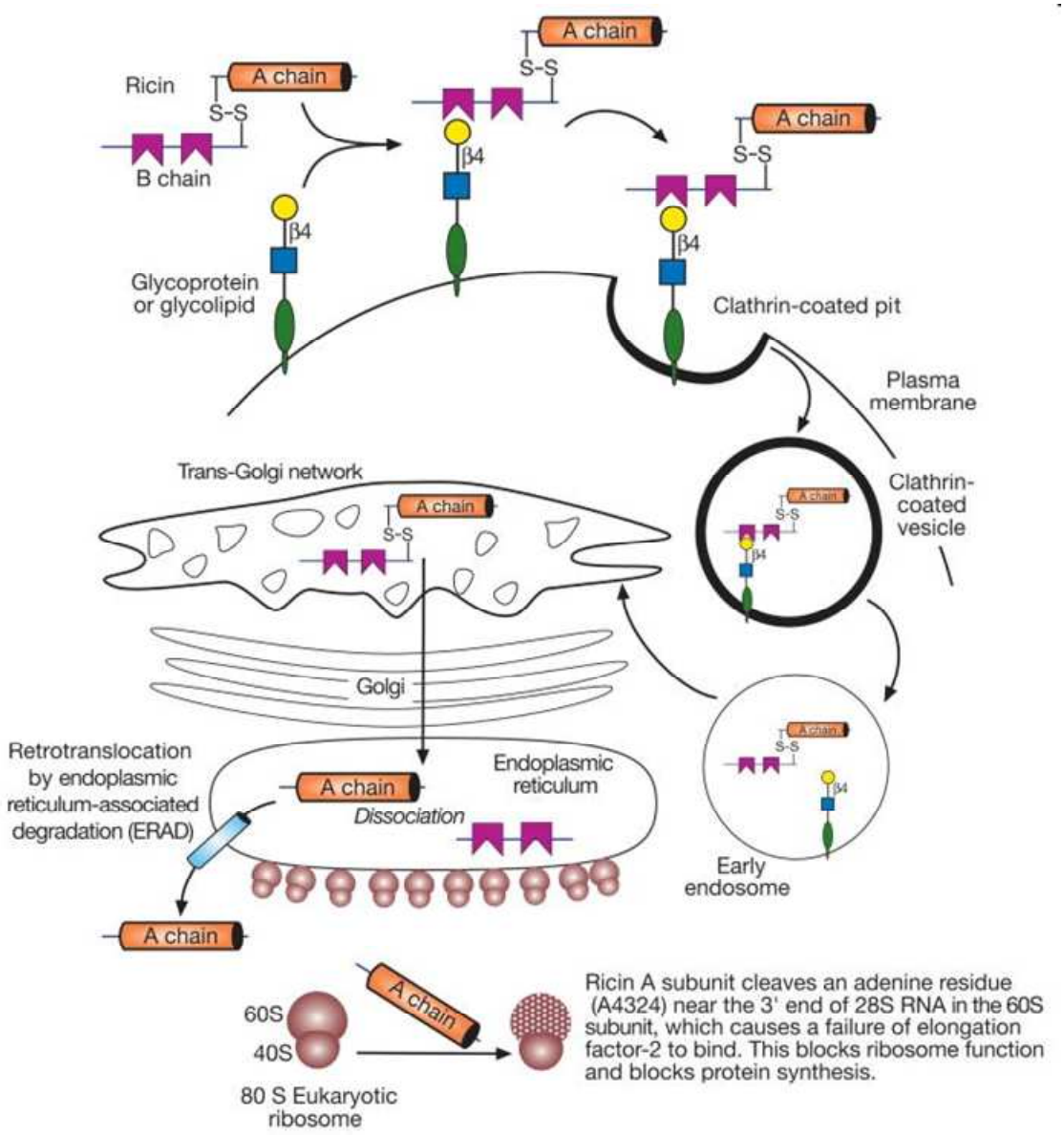

Fig. 17: Synthesis and function of RicinA.

Ricin is cleaved to RicinA in the cell cytosol. Ricin is derived from the castor bean and consists of 2 chains, A- and B chain which are connected by a disulfide bond (S-S). The B-chain is needed for cytosol entrance and binds to glycoproteins or glycolipids present at cell surface. Once bound, the Ricin-Glycoprotein-complex undergoes endocytosis and Clathrin-coating. The vesicle is transported to the Trans-Golgi network, where the coat is removed, and reaches the Endoplasmic Reticulum. There, the A chain dissociates from the B-chain via cleavage. The RicinA (A-chain alone) is the efficient toxin that blocks protein synthesis in the Endoplasmatic Reticulum by cleaving an adenine residue near the 3' end of 28S RNA in the 60S subunit in the eukaryotic ribosome that causes a failure in the binding of the elongation factor-2. Adapted from Cummings and Etzler 2009.

Under control of the UAS/Gal4 system, it is possible to express RicinA in specific tissues or subsets of cells. However, the transcription of RicinA occurred to be leaky, thereby causing unwanted depletion of cells (Kunes and Steller 1991). Different attempts have been made to control the expression pattern more reliably. Temperature-sensitive RicinA mutations were isolated and successfully used for temperature sensitive ablation. It has been hen the temperature shift is given and further, the toxin does not affect neighbored cells. In the following example, it is shown how effective RicinA can be used to ablate single photoreceptors in the eye of *Drosophila melanogaster*. Sevenless-Gal4 was used as driver line, which gives a specific expression pattern within R7 photoreceptors (Basler and Hafen 1989). The transgenic RicinA flies were temperature-sensitive and thus RicinA activity was induced though temperature shift. By doing so, R7 photoreceptors were completely ablated. This was additionally proven in EM sections.

RicinA has been demonstrated to be a powerful toxin that can be used to ablate subsets of cells. However, for enabling a more directed ablation specific to single cells, another control mechanism for the expression is needed. In this thesis, I will use a transgenic fly line that possesses a FRT flanked Stop cassette upstream of the Ricin sequence. This allows regulating RicinA expression through Flipase activity. Here, heatshock-Flipase was used to adjust the temporal onset of Flipase transcription to a very small time frame during development and with that, RicinA is tunable to the developmental onset of LPTCs.

2.5.3 Viral tracers shedding light on neuronal connectivity and circuits

Knowing the physiological properties of LPTCs, the question occurs as to which neurons are providing input information to these neurons. Here, only a single electron microscope (EM) study has provided the evidence that T4 and T5 neurons might be presynatically connected to LPTCs (Strausfeld and Lee 1991). However, since specific driver lines have been missing there have not been further studies since then. In *Drosophila melanogaster*, the only way to prove unequivocally the synaptic connectivity between two neurons has been by EM-studies. Therefore, the aim was to look for an alternative and less time-consuming method. In the mammalian system, viruses have been used for tracing neuronal circuits and various genetic methods have been established to utilize characteristic properties. Use of viruses allows

numerous advantages including highly detailed and stable cell labeling properties, fast spreading throughout the cell and identification of transsynaptic connected neurons, etc. which have been demonstrated in numerous studies (Conzelmann 1998; Ugolini 1995).

2.5.4 Tracing neuronal circuits with the Rabies Virus

The Rabies Virus belongs to the family of *Rhabdoviridae* and is a member of the *lyssavirus* genus. The virion has a distinct bullet shape with a helical nucleocapsid and envelope with about 400 large trimeric glycoprotein spikes on the surface. The sizes are approximately 75 nm in width and 180 nm in length. The single stranded, negative sense RNA is linear and encodes for five proteins in total: Nucleocapsis protein (N), Large protein (L), Phosphoprotein (P), Matrix protein (M) and Glycoprotein (G) (Fig. 18). The genome is tightly wrapped by around 1200 molecules of N proteins. In addition, this nucleoprotein complex is tightly associated with approximately 50 molecules of L proteins and 500 molecules of P proteins. The L and P proteins are part of the RNA polymerase complex, which transcribes the genomic RNA to a small leader RNA and 5 mRNAs. The M and the G proteins form the envelope of the virus and are supposed to determine host specificity. The reproduction cycle, which is common to all RNA viruses, takes place within the cell cytoplasm and is initiated by the fusion of the Rabies Virus envelope to the host cell membrane (adsorption). In this adsorption step, the G protein might recognize cell specific surface receptors (Fig. 19). The virus is taken up by endocytosis. The acid pH within the endosome allows the G protein to facilitate fusion of the virus membrane with that of the endosome. Because of the fusion, the nucleocapsid of the viron is released into cytoplasm of the host cell where genome replication of the viron takes place.

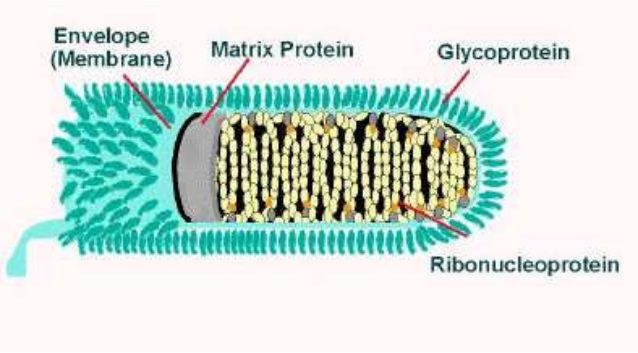

Fig. 18 The structure of Rabies Virus.
The bullet shell consists of spine-like Glycoproteins (G), Nucleocapsis proteins (N), Phosphoproteins (P), Large proteins (L) and Matrix proteins (M). They enwrap the genomic RNA which encodes 5 genes and package the transcribing ribonucleoprotein complex. Adapted from www.rabies.net

RNA replication is the process by which new copies of genome-length RNAs are created. It is carried out through the viral polymerase. The full length plus strand is coated with nucleocapsid protein and is copied into full length minus strand, which is also being coated with nucleocapsid protein. The envelope proteins are synthesized on ribosomes bound to the endoplasmic reticulum and modified at the Golgi body of the host cells. The viral RNA polymerase complex associates with the nucleocapsids when they are formed. Nucleocapsids bud out through modified areas of the membrane with G and M-proteins. The M-protein is involved in assembly: It interacts with patches of G proteins in the membrane and with nucleocapsids. After completing the entire assembling process within the host cell, the following offspring generation buds from the plasma membrane. The entire cycle takes only 1.5 hours post initial infection that makes the duration of reproduction extremely fast.

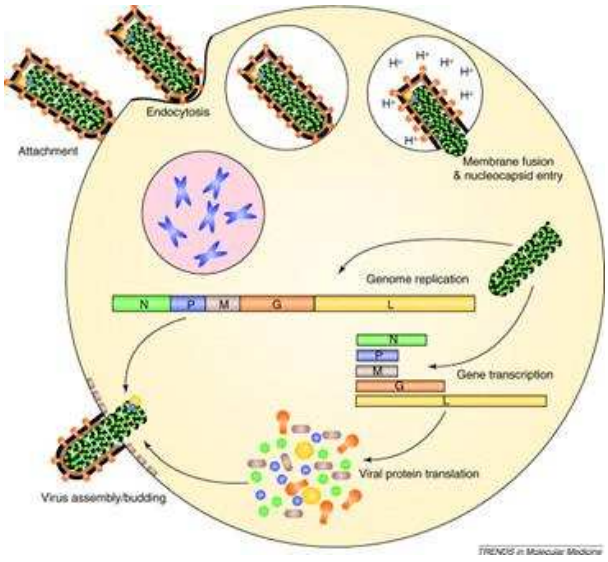

Fig. 19: Reproduction cycle of the Rabies Virus

The virus adsorbs to cell surface. Glycoprotein (G) is the attachment protein, which binds to a receptor on the host cell surface. The attached virus is taken up by endocytosis. The membrane of the virus fuses with the endosome membrane. As a result of fusion of the viral membrane with the endosome membrane, the nucleocapsid is released into cytoplasm. There, the RNP complex is activated and the genome is replicated. The viral protein assembles at the membrane surface where finally the new virus buds from the cell. Scheme adapted from 'Trends in Molecular Medicine'.

Rabies virions are transported in a retrograde fashion in infected cells (Wickersham et al. 2007) and in addition, they spread exclusively at synaptic connections. However, it is still speculative which of the five proteins encoded by the viral genome

defines these characteristics. Most probably, the G protein is involved in the retrograde transportation system as well as the presynaptic budding location.

In the past decade, the ability to recover negative-strand RNA viruses entirely from cDNA has been established with which a detailed analysis of molecular genetics and biology of viruses was enabled. Furthermore, the replication machinery of RNA viruses allows heterologous sequences to be expressed from other species like enhanced GFP (EGFP) (Tamamaki et al. 2000; Tomioka and Rockland 2006). Therefore, the advantages of the viral system in terms of easy manipulation of constructs, high capacity for foreign sequences, genetically stable expression, and the possibility of adjusting expression levels have been made accessible (Conzelmann 1998). Since then, in various studies the Rabies Virus has been successfully used as trans-synaptic tracer that infects neurons through axon terminals and spreads between synaptically coupled neurons in an exclusive retrograde way (Ugolini 1995).

Another major advantage of labeling cells by virus infection is the resulting high intensity of fluorescence in these cells that provides detailed information about their anatomical structures even without immunohistochemical amplification. Manipulations of the viral genome itself led to the production of a mutant virus in which the envelope G protein is deleted from the genome and replaced by the encoding sequence for EGFP (Fig. 20). These viruses are not able to infect cells due to the missing G-proteins that are needed for the adsorption step (Mabatsion et al. 1996, Etessami et al. 2000). However, through growth in complementing host cells the G protein is incorporated into the viral particle's membrane despite the lack of the coding sequence in its genome. The procedure whereby the viral envelope protein is exchanged is called pseudotyping and it allows G protein deletion viruses to infect contacted cells normally. However, the newly created progeny are trapped within the initial infected cells without the ability to synthesize the G protein themselves. The result is a high copy number of the viral core and EGFP within single cells allowing anatomical identification in living tissues (Wickersham et al. 2007).

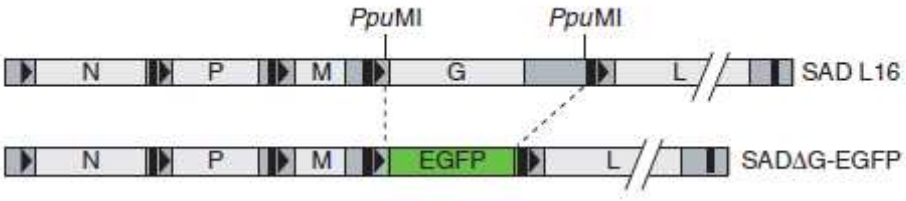

Fig. 20: Replacement of the viral G-protein though EGFP in the genome.
In the Rabies Virus deletion mutant SAD-dG-EGFP, the G protein open reading frame is replaced with that of EGFP. Light gray boxes show viral open reading frames, non-coding sequences are shown in gray and transcription signals are in black. Modified from Wickersham et al. 2007.

A problem of the viral infection is the different rates through which tracers cross synapses due to individual cellular transportation mechanisms on which they depend. Therefore, stronger synapses will be crossed and spreading occurs from these presynaptic cells even before the virus can label weaker connected neurons. The consequences are an ambiguity in the number of crossed synapses and no distinction between direct connected weak connection and strong indirect ones. Wickersham and colleagues constructed a virus that can only cross one synaptic step from the initial infected cell population, allowing the labeling of unambiguous connected monosynaptic cells. These viruses are genetically constructed like G deletion viruses mentioned before in which the G protein encoding sequence is replaced by that of EGFP.

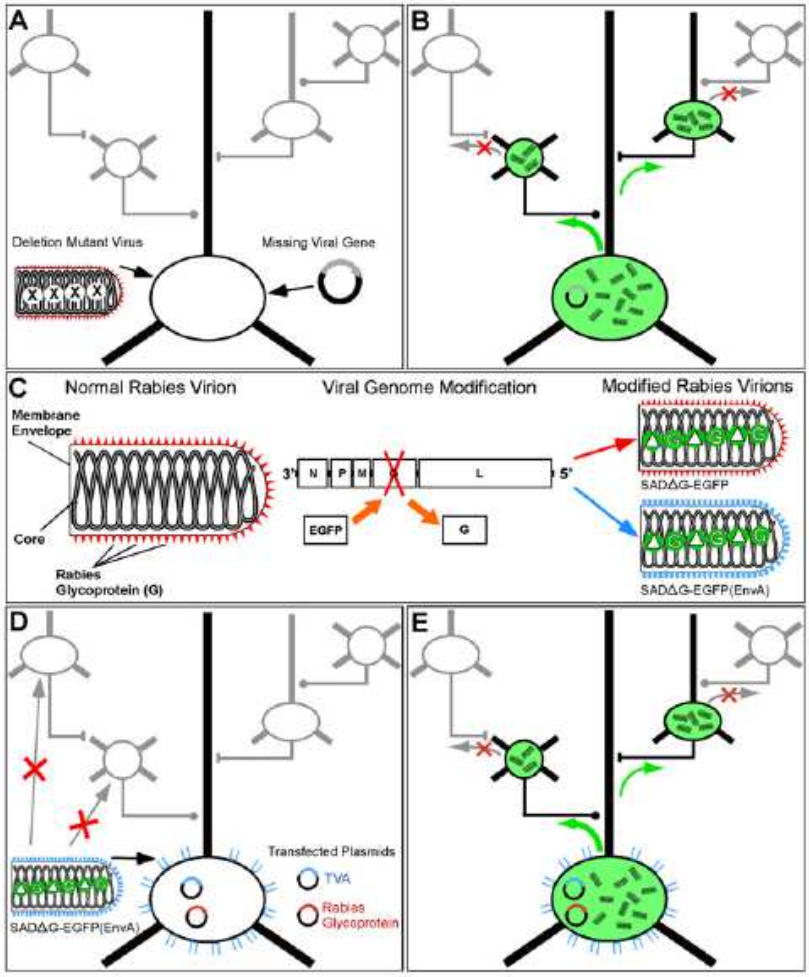

Fig. 21: Monosynaptic restriction of the viral infection through the EnvA/TVA system.
(A-B) Here, the Rabies strain: St. Augustine Decline (SAD) is used. A two component system derived from the ASLV-A virus is used for specific targeting of the virus to the cells of interest. The G-protein deletion mutant virus in which the G-protein encoding sequence is replaced by EGFP sequence is pseudotyped with EnvA. These VSVdG-EGFPpt (EnvA) target only host cells which express the complementary TVA receptor which is achieved through transfection of the cells with a plasmid encoding for TVA. Co-transfection of the G-protein encoding plasmid allows the newly created viral progeny to spread normally (B). However, without the ability to produce the G-protein by themselves, these viruses are trapped within these cells and cannot spread further (D+E). Scheme modified from Wickersham et al. 2007.

However, for a higher specification of host tropism these viruses were pseudotyped with EnvA. This protein is derived from ASLV-A virus (avian sarcoma and leukosis virus subgroup A) and it targets exquisitely the TVA receptor. Brain culture slices from the cortex of adult rats were co-transfected with plasmids encoding for dsRed and TVA, which labeled successfully transfected cells in red and form TVA receptors on their membrane surfaces. EnvA encoated viruses will only target TVA expressing

cells leading to a dual labeling of infected cells with dsRed and EGFP. By additionally providing the G protein *in trans*, the virus is enabled to spread once. With that, all direct presynaptic neurons are labeled by viral EGFP, allowing an unambiguous identification of initial infected cell population and presynaptic connected ones.

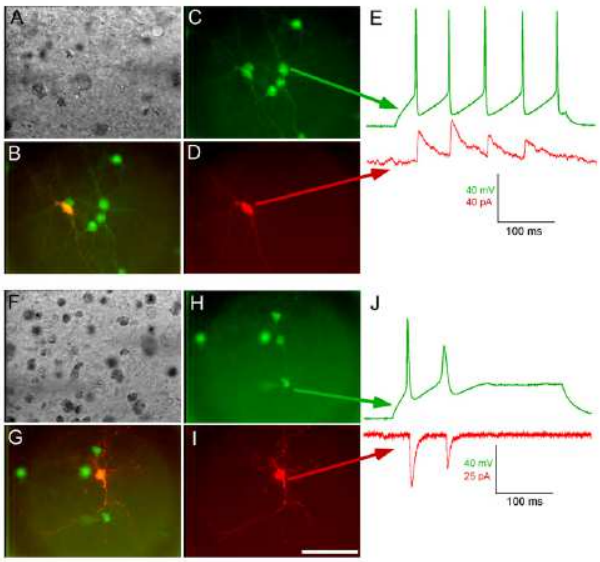

Fig. 22 Neuronal recordings reveal specificity of viral spread.
(A+F) Bright field images of the recorded region in the cortical slice. (C+H) Infected cells are labeled by viral EGFP and initiator cells are additionally marked in red through transfection with a ds-Red encoding plasmid (D+I). Merged images of green and red fluorescence channels are illustrated in B+G. In both cases, one can measure coincident responses between postsynaptic current injections and presynaptic recordings (E+J). This experiment proves the unambiguous monosynaptic spread to presynaptic cells. Modified from Wickersham et al. 2007.

Another important aspect to using attenuated *Lyssaviruses* as neuronal tracers is their significantly lower cytotoxicity and infection efficiency compared to commonly used tracer viruses from other families. The viability of host cells was tested by electrophysiological recordings. Both primarily infected cell and the marked one respond to current injection revealing synaptic connectivity (Fig. 22). This study provided strong evidence that Rabies Viruses have been successfully used to unravel synaptic connectivity and with that neuronal circuits.

The Rabies Virus has been demonstrated to be a powerful tool for anatomical identification of neuronal circuitries. However, viruses are specialized to specific host

species and infection has been only shown in mammalian species. No reports on its function in insect neurons have yet been published.

2.5.5 Using Vesicular Stomatitis Virus for labeling neurons.

The Vesicular Stomatitis Virus (VSV) belongs to the same family of *Rhabdoviridae*. Its genome is capable of accommodate an insert up to 4.5 kb. The VSV G-protein is affected by many different cell types including neuronal and glia cells. In contrast to Rabies Virus, it has been reported that within infected cells VSVs spread primarily through diffusion but also via directed anterograde and retrograde transport. Genetic manipulation of the VSV genome has opened up a wide range of possibilities, e.g. observing neuronal structure and tracing neuronal development and circuits (Van den Pol et al. 2009). However, the major advantage of the VSV is its broad host tropism: Infections of rats, mice, swines and flies have already been reported (Howerth et al. 1997; Schnitzlein and Reichmann 1985; Llewellyn et al. 2002; Van den Pol et al. 2009). In addition, the virus particles are small enough to be transported into submicron structures like dendritic spines supporting detailed anatomical studies. Time-lapse studies have revealed how effectively these viruses spread among cells without changing the cell structure or its vitality. With that, it is possible not only to take a closer look at anatomical features of neurons but also to trace neuronal circuits if the virus can be restricted to propagating only through cell-specific transportation systems.

Here, the functional combination of components from different viruses of the *Rhabdoviridae* family could create a new virus that combines the ability of VSV to infect insect neurons with the advantages of Rabies Virus like retrograde transportation and transsynaptic spread.

3 Materials

3.1 Buffers, solutions and media

Name	Recipe
Flyfood	5 l H_2O 28 g agar 110 g treacle 400 g malcine 400 g corn flour 50 g soy flour 90 g dry yeast 31.5 ml nipagin
Injection Buffer pH 6.8 10x	0.2 ml 0.5 M NaPi 5 ml 1M KCl 94.8 ml H2O sterile filtration of 1x solutions
TAE Buffer 50x (Tris-Acetate-EDTA)	242 g Tris base 57.1 ml glacial acetic acid 100 ml 0.5 M EDTA add ddH2O to 1 l and adjust pH to 8.5
TE Buffer 1x (Tris EDTA)	10 mM Tris-Cl (pH 7.5) 1 mM EDTA (pH 8) autoclave solution
PBS 10x (Phosphate Buffered Saline)	1.37 M NaCl 27 mM KCl 43 mM Na_2HPO_4 14.7 mM KH_2PO_4
PBT 10x	1 l PBS 10x 5 ml 100 % Triton X-100
Lysis Buffer for Western Blot	250 mM Tris-HCl 2% SDS

Standard brain culture medium	1 %	penicillin (10 000 U/ml)
	1 %	streptomycin (10 mg/ml)
	10 %	Foetal Bovine Serum
	10 µg/ml	insulin
	mixed into the Schneider's *Drosophila* Medium	

3.2 Flystocks

Stockname	Chromosome Location(s)	Source
DB331-Gal4	1	Reinhardt Stocker
G73-Gal4 (NP282)	3	Kei Ito
Bl/CyO; UAS-Dscam 1.30.30.1 Bl/CyO; UAS-Dscam 7.27.25.1 Bl/CyO; UAS-Dscam 2.9.19.2 Bl/CyO; UAS-Dscam 1.34.30.2, Dscam 1.6..19.2 Bl/CyO; UAS-Dscam 7.19.2 Bl/CyO; UAS-Dscam 11.31.25.1 Dscam^23 Dscam^21/CyOGB; Exon^2-FRT Dscam^21/CyO; Exon^6-FRT FRT40A, Dscam^21/CyO FRT42D, UAS-Dscam^21/CyO FRT42D, tubGal80/CyO	2,3	Dietmar Schmucker
UAS-mCD8::GFP	2	Liqun Luo
UAS-cytoGFP	3	Liqun Luo
UAS-FRT40A	2	Bloomington Stock Center
UAS-hs-Flp	1	Liqun Luo
UAS>Stop>RicinA	2	Liqun Luo
UAS-synaptotagmineHA	1	Andreas Prokop

UAS-synaptobrevine mRed	1	Shamprasad Raghu
UAS-tubGal80ts	3	Ron Davis
UAS-hsFlp, UAS-mCD8::GFP;UAS-tubp-Gal80,FRT40A/CyO	2,3	Bloomington Stock Center
GR27B03-Gal4	3	Gerald Rubin
GR42H07 GRR35F02 GR54A03	3	Gerald Rubin
Dscam RNAi 3115 25622 25623 36233 108835	2	Vienna *Drosophila* RNAi Center (VDRC)
Dcr2	2	Vienna *Drosophila* RNAi Center (VDRC)

3.3 Consumables

Consumables	Cat.number	Source
Falcon Petri dishes	351008	Becton Dickinson Biosciences
Primaria Cell culture dish	353801	Becton Dickinson Biosciences
14 ml Polypropylene Round-Bottom Tube	352051	Becton Dickinson Biosciences
Blaugel	9351.1	Carl-Roth GmbH
Silica Gel Orange	T199.1	Carl-Roth GmbH
1,5 ml / 2 ml Tubes	0030 125.150	Eppendorf AG
PCR tubes	0030 125.215	Eppendorf AG
Femtotips	5242 957.000	Eppendorf AG
Microloader	5242 956.003	Eppendorf AG

Fast Digest Enzymes		Fermentas GmbH
FastAP/SAP	EF0651 EF0511	Fermentas GmbH
T4 DNA ligase	EL0011	Fermentas GmbH
Inoculation loop	146051	Greiner Bio-One
Gateway recombination enzymes	BP: 11789013 LR: 11791019	Invitrogen GmbH
Propidium iodide	P1304MP	Invitrogen (P1304MP)
pDonR221	12536017	Invitrogen
Voltalef 10S	9036-80-0	Labscientific
Primers synthesis		Metabion / MWG
Restriction Enzymes		New England Biolabs
Wizard SV Gel and PCR Clean-Up	A9281	Promega GmbH
Triton-X 100	X100	Sigma Aldrich Co.
Micropistill	211-2100	VWR International GmbH
pUAST-Destination		VDRC
Neurobiotin	SP-1120	Vector Labs

3.4 Antibodies

Antibody	Cat.	Dilution factor	Source
α-Dlg (mouse)	4F3 anti-discs large	1:200	Hybridoma Bank
α-DscamIC 357 (rabbit)	gift	1:200 + 4% NGS	Dietmar Schmucker
α-mCD8 (rat)	RM2200	1:200	Invitrogen/Caltag
α-bungarotoxin, Alexa Fluor® 647 conjugate	B35450	1:200 + 4% NGS	Molecular Probes
Alexa Fluor 488 goat anti-rat-IgG	A11006	1:200	Molecular Probes

Alexa Fluor 568 goat anti-rabbit-IgG	A11011	1:200	Molecular Probes
Alexa Fluor 594 goat anti-mouse-IgG	A11005	1:200	Molecular Probes
Anti-GFP, rabbit IgG fraction, Alexa Fluor 488 conjugate	A-21311	1:200	Molecular Probes
Normal Goat Serum	G9023	4%	Sigma Aldrich

3.5 Electronic equipment

Electronic equipment	Model
Confocal microscope	Confocal Leica NT Confocal Leica SP2 Confocal Leica SP2-UV
Fluorescence Microscope (FL)	Leica M205 FA
Bright light appliance for (FL)	Schott FOSTEC LLC
UV light appliance for (FL)	Ebq 100
Binocular Microscope	Leica MZ6 Leica MZ9
Waterbath	Thermo Haake DC10
Table Centrifuge	Eppendorf Centrifuge 5415 D
Thermoshaker	peQ-Lab TS100
Photometer	Eppendorf Biophotometer Plus
PCR cycler	DNA Engine DYAD
DNA injector	Eppendorf Femtojet
Vortexer	Scientific industries Vortex Genie-2
Gel Doc	BioRad GelDoc2000
Incubator	Binder

3.6 Primerlist

Primer	Sequence	Comments
Project: UAS>Stop>TNXXL		
JS1	GTG AGC AAG GGC GAG GAG CT	forward primer pcDNA3-TNXXL
JS2	CTT AGT CCT CGA TGT TGT GGC	reverse primer pcDNA3-TNXXL
JS3	GGG GAC CAC TTT GTA CAA GAA AGC TGG GT	attB2 sequence
JS4	GGG GAC CAC TTT GTA CAA GAA AGC TGG GTC TTA GTC CTC GAT GTT GTG GC	reverse primer pcDNA3-TNXXL with attB2 site
JS5	GTG AGC AAG GGC GAG GAG ATG GTG AGC AAG GGC GAG GAG CT	overlap Primer 5'Stop with 3'TNXXL
JS6	CTC CTC GCC CTT GCT CAC	reverse primer pUAST-Stop-YC3.6
JS7	AGC TCC TCG CCC TTG CTC ACC ATC TCC TCG CCC TTG CTC AC	overlap Primer 3'Stop with 5'TNXXL
JS8	GGT ACC CGG GGA TCT TGA AG	forward primer pUAST-Stop-YC3.6
JS9	GGG GAC AAG TTT GTA CAA AAA AGC AGG CTT CGG TAC CCG GGG ATC TTG AAG	forward primer pUAST-Stop-YC3.6 with attB1 site
JS10	GGG GAC AAG TTT GTA CAA AAA AGC AGG CT	attB1 Sequenz
JS11	GTG AGC AAG GGC GAG GAG GCC GCC ACC ATG GTG AGC	replacement for JS5
JS12	GCT CAC CAT GGT GGC GGC CTC CTC GCC CTT GCT CAC	replacement for JS7
JS13	CCG TGC GGC CGC CCT CCT CGC CCT TGC TCA C	NotI Schnittstelle JS7

JS14	GGG GAC CAC TTT GTA CAA GAA AGC TGG GTG CCA GTG TGA TGG ATA TCT GCA G	TNXXL reverse primer new in backbone with attB2 JS4
JS15	CCA AGC TTG GTA CCG AGC TCG G	TNXXL forward without attB site
JS16	ACA TCG GAG AAT CTG GTA CCC GGG GAT CTT GAA G	
JS17	ATC GGA GAT CTC TCC TCG CCC TTG CTC AC	
JS18	GGG GAC CAC TTT GTA CAA GAA AGC TGG GTG CGG CCG CCT CCT CGC CCT TGC TCA C	attB2-Not-Stop Primer
JS19	TAT CTA GCG GCC GCC GCC TCC TCG CCC TTG CTC AC	
Project: pCasper-lexA		
JS20	ACA TCG GGG TAC CCC AGT CTT AAG CTC GGG CCC C	forward Primer: KpnI_ccd_Chloramp_attP2_KpnI (gateway)
JS21	TGC CAT CCA GCT GAT ATC CCC TAG GTA CCG ATG T	reverse Primer: KpnI_ccd_Chloramp_attP2_KpnI (gateway)
Js22	ACA TCG GGG ATC CCC AGT CTT AAG CTC GGG CCC C	forward primer: BamHI_ccd_Chloramp_attP2_BamHI (gateway)
JS23	TGC CAT CCA GCT GAT ATC CCC TAG GAT CCG ATG T	reverse primer: BamHI_ccd_Chloramp_attP2_BamHI (gateway)
JS24	GGG GAC AAG TTT GTA CAA AAA AGC AGG CTT CGA CGG AAT TCC TTG CTG SCT GC	forward Primer_gateway_NP282 with attB1
JS25	GGG GAC CAC TTT GTA CAA GAA	reverse Primer_gateway_NP282

	AGC TGG GTT TTC CTC GCC GGG CGA ACG	with attB2
JS26	GGG GAC AAG TTT GTA CAA AAA AGC AGG CTT CTA GCT TGA GTG CCA GCG AAG CAC	forward primer_gateway_NP1049 with attB1
JS27	GGG GAC CAC TTT GTA CAA GAA AGC TGG GTT CTT CAC CAC TGA ATT GGA ATC TG	reverse primer_gateway_NP1049 with attB2
JS28	GGG GAC AAG TTT GTA CAA AAA AGC AGG CTT CGT TTC TGC AAC GAC TTT GTA CCT AAA	forward primer_gateway_NP1195 with attB1
JS29	GGG GAC CAC TTT GTA CAA GAA AGC TGG GTG AGG TGG CAA CGC CGC TGC	reverse primer_gateway_NP1195 with attB2
Project: UAS-Bungarotoxin and UAS-Conotoxin		
pFU-ppV-aBtx-GPI		
JS30	GGT ACC GGT ATG TCT GCA CTT CTG ATC	forward primer
JS31	ATC GAA TTC TTA CAG CAA GCT CCA GAA GG	reverse primer
JS32	GGG GAC AAG TTT GTA CAA AAA AGC AGG CTT CGG TAC CGG TAT GTC TGC ACT TCT GAT C	forward primer with attB1
JS33	GGG GAC CAC TTT GTA CAA GAA AGC TGG GTA TCG AAT TCT TAC AGC AAG CTC CAG AAG G	reverse primer with attB2
pFU-PE		

JS34	GGT ACC GGT ATG TCT GCA CTT CTG AT	forward primer
JS35	GAA TTC TTA CTT GTA CAG CTC GTC C	reverse primer
JS36	GGG GAC AAG TTT GTA CAA AAA AGC AGG CTT CGG TAC CGG TAT GTC TGC ACT TCT GAT	forward primer with attB1
JS37	GGG GAC CAC TTT GTA CAA GAA AGC TGG GTG AAT TCT TAC TTG TAC AGC TCG TCC	reverse primer with attB2
pFU-GIDs-PE		
JS38	ACC ATG TCT GCA CTT CTG ATC CTA	forward primer
JS39	GGC CGC TTT ACT TGT ACA GCT CG	reverse primer
JS40	GGG GAC AAG TTT GTA CAA AAA AGC AGG CTT CAC CAT GTC TGC ACT TCT GAT CCT A	forward primer with attB1
JS41	GGG GAC CAC TTT GTA CAA GAA AGC TGG GTG GCC GCT TTA CTT GTA CAG CTC G	reverse primer with attB2
JS42	ACA TCG GGG TAC CAA TCG ATT TCA ATG TCA ATG TGG AAC G	forward primer KpnI
JS43	ACA TCG GGA GCT CGT TTG ATG CTG GCT ACT AAC GGC	reverse primer
JS44	ACA TCG GCC GCG GGT TTG ATG CTG GCT ACT AAC GGC	new reverse primer SacII
JS45	CTA GCA AAA TAG GCT GTC CC	forward primer for sequencing
JS46	ACT AAT TGA GAT GCA GAT CGC A	reverse primer for sequencing

JS47	GGG GAC AAG TTT GTA CAA AAA AGC AGG CTA ATC GAT TTC AAT GTC AAT GTG GAA CG	forward primer vGat for gateway with attB1
JS48	GGG GAC CAC TTT GTA CAA GAA AGC TGG GTG TTT GAT GCT GGC TAC TAA CGG C	reverse primer vGat for gateway with attB2
JS49	ACA TAC ATA CTA GAA TTC GGT AC	pChs sequencing forward primer
JS50	GAT CCA CTA GTG GCC TAT GCG G	pChs sequencing reverse primer
JS51	ACA TCG GGG TAC CTC TCG AGT TCC AGT TTG TGT CTC TC	forward primer vGat 4kb with KpnI
JS52	ACA TCG GGG TAC CTA ATC GAT TTC AAT GTC AAT GT	forward primer vGat 3kb with KpnI
JS53	ACA TCG GCC GCG GTA CGA GTA TAT TAT ACA TATCC	reverse primer vGat 3kb with SacII
JS54	ACA TCG GGG TAC CTA ATC GAT TTC AAT GTC AAT GT	forward primer vGat 6kb with KpnI
JS55	ACA TCG GCC GCG GAA TCT TAA GCC TGA GGG AGA A	reverse primer vGat 6kb with SacII
Project: Virus TVA and G-Protein		
JS56	GGG GAC AAG TTT GTA CAA AAA AGC AGG CTT CAT GGC GCG GCT GCT GCC CGC GCT	TVA forward primer attB1
JS57	GGG GAC CAC TTT GTA CAA GAA AGC TGG GTT TAC AGG AAC AGG TGG TGG CGG	TVA reverse primer attB2
JS58	GGG GAC AAG TTT GTA CAA AAA AGC AGG CTT CAT GAA TAT ACC TTG CTT TGC TGT	Mokola-G primer attB1

JS59	GGG GAC CAC TTT GTA CAA GAA AGC TGG GTT CAA GTA CCT GGG AGC CCT TTA	Mokola-G primer attB2
JS60	GGG GAC AAG TTT GTA CAA AAA AGC AGG CTT CAT GAA GTG CCT TTT GTA CTT AGC	VSV-G primer attB1
JS61	GGG GAC CAC TTT GTA CAA GAA AGC TGG GTT TAC TTT CCA AGT CGG TTC ATC	VSV-G primer attB2
JS62	GGG GAC AAG TTT GTA CAA AAA AGC AGG CTT CAT GTT ACT CTC TAC CGC CAT ATT	BH-G primer attB1
JS63	GGG GAC CAC TTT GTA CAA GAA AGC TGG GTT TAT GAC TCA CCA GTG GCC CCC	BH-G primer attB2
JS64	GGG GAC AAG TTT GTA CAA AAA AGC AGG CTT CAT GGT TCC TCA GGC TCT CCT GTT	SAD-G primer attB1
JS65	GGG GAC CAC TTT GTA CAA GAA AGC TGG GTT TAC AGT CTG GTC TCA CCC CCA	SAD-G primer attB2
JS66	GGG GAC AAG TTT GTA CAA AAA AGC AGG CTT CAT GGT TCC TCA GGT TCT TTT GTT TGT A	CVS-G primer attB1
JS67	GGG GAC CAC TTT GTA CAA GAA AGC TGG GTT TAC AGT CTG ATC TCA CCT CCA CTC TT	CVS-G primer attB2
Degenerative PCR		
JS68	GCA GAA GCT TTG CGT ACT CGC	T1BUAS
JS69	ATT CAA ACC CCA CGG ACA TG	T2D
JS30	WGT GNA GWA NCA NAG A	AD3

JS31	AAT CAT ATC GCT GTC TCA CTC A	T2En

4 Methods

4.1 Molecular Biology

4.1.1 Plasmid DNA Extraction

For plasmid isolation and purification of DNA for subsequent cloning procedures, an extraction kit (Plasmid Mini Kit from QIAGEN) was used. From each transformation plate, a single colony was picked with sterile inoculation loop (Greiner Bio One) and transferred to a 14ml polypropylene round-bottom tube (Falcon) containing 4 ml LB medium with the appropriate selective antibiotic. This primary cell medium was incubated for approximately 8 h at 37℃ with vigoro us shaking (approx. 300 rpm). Bacterial cells were harvested by centrifugation at 6000 x g for 15 min with an Eppendorf table centrifuge. Therefore, the medium was transferred to 2ml Eppendorf tubes and twice spun down. The bacterial pellet was resuspended in 0.25 ml of Buffer P1 by vortexing them vigorously for several minutes. Afterwards 0.25 ml of Buffer P2 was added and mixed thoroughly by inverting the tube 4–6 times. The lysate should appear viscous addition of Buffer P2. Mixing should result in a homogeneously colored suspension. In the next step 0.35 ml of N3 was added and mixed immediately and thoroughly by vigorously inverting 4–6. After addition of Buffer N3, a fluffy white material formed and the lysate became less viscous (“The precipitated material contains genomic DNA, proteins, cell debris, and KDS”). The suspension should be mixed until all trace of blue had gone and the suspension was colorless. The final mixture was centrifuged at maximum speed in a microcentrifuge for 10 min. The supernatant containing plasmid DNA was transferred to a column with filter and spun down for 1minute. The solution in the column was discarded and the DNA within the filter washed by applying 0.5ml PE buffer. The buffer was again centrifuged for 1minute and afterwards discarded. After washing step, the emptied column with filter was centrifuged for another 1minute in order to remove remaining ethanol. For eluting, the DNA 50µl prewarmed (65℃) EB buffer or DNAse free H2O was dropped onto the center of the filter and incubated for 5minutes. At the end the filter was put into a 1.5ml Eppendorf tube and centrifuged for 1minute at maximum rpm. The final concentration of the DNA should be around 500ng/µl.

4.1.2 Polymerase Chain Reaction (PCR)

This method was originally developed by Kary Mullis and allows the amplification of a distinct strand of DNA. Therefore, a thermo-stable variant of polymerase is used. Depending on the chosen polymerase the speed and amplification accuracy varies. In this thesis for all PCRs the “iProof High Fidelity Master Mix” (BioRad) was used. This high-fidelity DNA polymerase offered an extreme enhanced performance rate for all PCR applications by comprising a unique *Pyrococcus*-like proofreading enzyme fused to a dsDNA binding protein, Sso7d. This results in a thermostable polymerase that accurately amplifies long products from a variety of DNA templates. The “iProof High Fidelity Master Mix” has already polymerase, nucleotides, included in an optimized reaction buffer. Therefore, no further PCR components need to be added. For each 50µl reaction volume, 1µl of DNA template was given to 25µl of 2x Master Mix and filled up with DNAse and RNAse free water. The following setting adjusted to the length of PCR product was used in this thesis:

Step	Degree (℃)	Time (min/sec)
Denaturation	98	1’30’’
Annealing	98	30’’
Elongation	Primer Tm	Length of product
End	70	1’
Cycle	From Annealing till End	40x
Termination	70	10’
Storage	4	forever

4.1.3 Restriction of DNA vector backbone and insert

Restriction sites are short (~6bp) DNA palindomic sequences which can be recognized by specific restriction endonucleases. These enzymes break the double stranded DNA sequence at those sites hence usually a single stranded end (sticky end) is left over; In some cases blunt ends, in which both DNA strands are evenly cut, do also occur. Restriction of the DNA is performed for preparing the vector backbone or PCR product for subsequent cloning procedures or for analyzing the correct introduction of an insert after ligation into a given vector. Control digestion was made

with a sample of 1-2µl of DNA (100-200ng). For nearly all DNA restriction-procedures, “Fast Digest enzymes” from Fermentas were used and proceeded after following protocol:

2-5µg DNA
10U restriction enzyme
8µl 10xbuffer
Add H2O to a total volume of 80µl
Incubate 1hour at 37℃

4.1.4 Preparation of DNA for ligation

After treatment with restriction enzymes, vector backbones were treated with CIP/CIAP or SAP (Fermentas) for 3hours in order to dephosphorylate the endings. Neither digestion enzymes nor dephosphorylation enzyme were heat inactivated. Purification of the digestion product was done through gel electrophoresis. Appropriate DNA strand was identified under UV light and excised out of the gel.

4.1.5 Vector backbone purification

In order to discriminate cut from uncut vector, digested DNA was analyzed via gel electrophoresis. Cut vectors were identified under UV light and excised out of the gel. With “Wizard SV Gel and PCR Clean-Up System” (Promega) the DNA was extracted out of the gel and restriction enzymes removed. Therefore, the gel slice was put into a 2ml Eppendorf tube and 10µl Membrane Binding Solution per 10mg of gel slice was added into the tube. For PCR purification, the same volume of Membrane Wash Solution was added to the PCR product, respectively. The gel slice was incubated 50–65℃ until gel slice was completely dissolved. For each DNA sample, one SV Minicolumn was inserted into a Collection Tube. Dissolved gel mixture or prepared PCR product was transferred to the Minicolumn assembly and incubated at room temperature for 1 minute. Then the Minicolumn was centrifuged at 16,000 × g for 1 minute. The flow through was discarded and Minicolumn reinserted into Collection Tube. 700µl Membrane Wash Solution (ethanol added) was added onto the column and centrifuged at 16,000 × g for 1 minute. Again flow through was discarded and

Minicolumn reinserted into Collection Tube. The washing step was repeated with 500µl Membrane Wash Solution and centrifugation at 16,000 × g for 5 minutes. The Collection Tube was emptied and the column-assembly re-centrifuged for 1 minute with the microcentrifuge lid open (or off) to allow evaporation of any residual ethanol. The Minicolumn was transferred to a clean 1.5ml microcentrifuge tube and adding 50µl of Nuclease-Free Water to the Minicolumn. At room temperature, the water was inoculated for 5 minute. For elution of the DNA the assembly was centrifuged for 1minute at 16,000 x g. Minicolumn was discarded and the DNA was stored at 4℃ or –20℃.

4.1.6 Insert purification

Insertion products were accordingly digested with same enzymes as the vector was treated and remaining nucleotides and primers removed though inoculation with ExoSAP-IT (USB). The advantage ExoSAP-IT is the possibility to remove unused primers and nucleotides with absolutely no sample loss and therefore, ideal for small sample volumes. This reaction is an alternative to the common gel purification procedure. It was used for all PCR products, which were used later on for gateway cloning. ExoSAP-IT was directly given to the PCR products and incubated in commonly used PCR buffers.

5µl PCR product
2µl ExoSAP-IT
Incubate 15minutes at 37℃
Incubate 15minutes at 80℃ for inactivation.

4.1.7 Ligation

A perquisite way to introduce DNA fragments into a vector backbone is to put restriction sites at each end of the desired insert. Treatment of DNA components, vector and insert with the same set of restriction enzymes enable a directed introduction of the insert into the vector backbone. The molar ratio of vector to insert

should be 1:3 or 1:5. The concentrations were determined prior via DNA photometer and ligation performed after following protocol:

5µg PCR product
1µg of plasmid DNA
0.5µl of T4DNA ligase (Fermentas)
1µl of 10xbuffer
H2O was added to a total reaction volume of 20µl
Incubation at 16℃ overnight

4.1.8 Gateway Cloning System

The gateway cloning system offers a great alternative to commonly ligation systems for cloning DNA fragments into appropriate expression vectors. This cloning system is based on "Bacteriophage lambda *att* site recombination". In bacteria, there is a stretch of DNA called *att*B, (B stands for bacteria), and in the phage there is a stretch of DNA called *att*P (P stands for phage). When the phage infects a bacterium, the injected lambda DNA recombines with the corresponding bacterial DNA via the *att* sites in the presence of integration-specific enzymes. When an *att*B site recombines with an *att*P site, the outcome is integration of the phage DNA into the bacterial genome. Once integrated, the hybrid recombination sites are called *att*L and *att*R (L stands for left, R stands for right). These recombination reactions ("LR" and "BP") are the basis of the Gateway® Cloning System. The *att*B × *att*P reaction is mediated by Gateway® BP Clonase™ II enzyme mix; the *att*L × *att*R reaction is mediated by Gateway® LR Clonase™ II enzyme mix. *ccd*B is the F plasmid-encoded gene that inhibits growth of *E. coli.*

BP-reaction

1-7 µl of *att*B-PCR product (15-150 ng)
1 µl pDonor 221 vector (150 ng/µl)
TE buffer, pH 8.0 was added to a total volume of 8 µl
2 µl of BP Clonase™ II enzyme was added and mixed by brief vortexing

Incubation at room temperature overnight
1 µl of the Proteinase K solution was added to each sample
10minutes incubation at 37℃ the reaction for termi nating the reaction

2 µl of the final mixture was taken for transformation and 50 µl of transfected cells were spread onto LB agarose plates containing Kanamycin.

LR reaction

For the LR reaction the same procedure was performed. Instead of *att*B-PCR product, 1-7 µl of the Entry clone was taken and 2 µl LR Clonase- II enzyme mix for each reaction. In this step, incubation period was always overnight. Here again, 2 µl of the final mixture was taken for transformation of chemical competent cells and finally, 50 µl of the transfected cells were spread onto LB agarose plates containing Ampicillin.

4.1.9 Transformation of chemical competent *E.coli* strains

For transformation an aliquot (50µl, stored at -80°C) of chemical competent cells (e.g. DH5α from Invitrogen) was thawed on ice for 15minutes. 150ng Plasmid DNA or 3µl of ligation product per 50µl cells was set for transformation and therefore inoculated within the cells on ice for another 30 minutes. Afterwards the mixture was given heatshock at 42℃ for 30 seconds and chilled on ice for 1,5minutes. The cells were incubated in 250µl of prewarmed S.O.C medium or LB medium for 1hour, at 37℃ in a thermoshaker, with 300rpm. 20µl of that suspension was plated onto an agar plate containing the appropriate selective antibiotic. These plates were incubated overnight in 37℃ incubator.

4.1.10 Rapid small-scale isolation of *Drosophila* DNA

With the following protocol it was possible to isolate small-scale DNA samples in a high quality, i.e. very pure and highly concentrated (>1µg/µl) from adult flies; but can be used equally well to extract DNA from other developmental stages. DNA prepared

accordingly to that method and used in this thesis primarily for isolation of promoter regions and location of P-element insertions within transgenic flies.
Therefore, flies were first anesthetized with CO2. Around 1-20 flies were put in an Eppendorf tube and kept on ice until next step. Solution A which contained 0.1 M Tris-HCl, pH 9.0; 0.1 M EDTA; 1% SDS and 0.5-1% DEPC (added directly before use) were added into the tube and homogenize a sterile micro pistil (VWR). 100 µl of solution A was used for extracting DNA from 1-5 flies, 200 µl for 6-10 flies and 500 µl for up to 50 flies. The mixture was then incubated for 20-30 minutes at 70℃. Afterwards, 14 µl of 8 M potassium acetate was added for each 100 µl homogenate and left on ice for 30 minutes. For DNA extraction 100 µl Phenol-Chloroform (1:3) mixture was added, briefly vortexed and spun 10' at RT. The supernatant containing DNA was moved to a new tube. Precipitation of DNA was done by adding 0.5 volumes of isopropanol at and spun for 5 minutes at RT. The pellet was washed carefully with 70% EtOH, respun, dried and redissolved in 10 (1 fly) to 100 (50 flies) µl DNAse free H2O.

4.1.11 Degenerative PCR

The degenerative PCR enables to determine the exact insertion site of the P-element in the genome of transgenic *Drosophilas*. This method was derived from the so called "nested PCR". Here, three different primers with specific binding properties are needed for distinguishing the chromosomal location. In the first PCR, one primer has to bind inside of the UAS or Gal4 vector (T1BUAS or T1BGal4). The second one is degenerated (AD3) this means binds at several positions within the genome. The second PCR does base on the PCR product of the first one. Here, the first primer is exchanged by another one (T2D) that binds more specifically in the primed out regions. Both primers, T1BUAS and T2D, are sitting within the 3'P-element site but not within the terminal repeat in the 5' site whereas the T1BUAS primer is sitting with its final 8nts in the 3' Pelement site thus the rest of the primer is vector specific since T2D is located within the 3'P. Therefore, T2D can be used with any P element. The 2nd PCR is usually checked on gel and subjected to EXOSAP-IT. Primer stock concentration is 10 pmol/µl (= 10 µM). The 3rd PCR with the T2Den Primer is only used if the concentrations after the 2nd PCR are too low.

In the 1st PCR T1BUAS and AD3 primer were used. The PCR reagent contained:
0.4 µl T1BUAS/T1BGal4
8µl AD3
1 µl DNA template (150ng)
10 µl iProof Master Mix
Add H2O to a total volume of 20 µl

In the 2nd PCR T2D and the same AD3 primer that had been used for 1st PCR. The PCR reagent contained:
0.4 µl T2D
4µl AD3
1 µl DNA from 1st PCR diluted 1:50
10 µl iProof Master Mix
Add H2O to a total volume of 20 µl

Degenerative PCR protocol:

PCR1

1	Incubate	93℃	1min
2	Incubate	95℃	1min
3	Incubate	94℃	1min
4	Incubate	62℃	1min
5	Incubate	72℃	2min30sec
6	Cycle to step3 for 4more times		
7	Incubate	94℃	1min
8	Incubate	25℃	3min
9	Incubate	72℃	2min30sec
	Ramp to 72℃ at 0.2℃ per sec.		
10	Incubate	94℃	30sec
11	Incubate	68℃	1min
12	Incubate	72℃	2min30sec

13	Incubate	94℃	30sec
14	Incubate	68℃	1min
15	Incubate	72℃	2min30sec
16	Incubate	94℃	30sec
17	Incubate	44℃	1min
18	Incubate	72℃	2min30sec
19	Cycle to step10 for 14 more times		
20	Incubate	72℃	5min
21	Incubate	4℃	forever
PCR2			
1	Incubate	95℃	1min30sec
2	Incubate	94℃	30sec
3	Incubate	64℃	1min
4	Incubate	72℃	2min30sec
5	Incubate	94℃	30sec
6	Incubate	64℃	1min
7	Incubate	72℃	2min30sec
8	Incubate	94℃	30sec
9	Incubate	44℃	1min
10	Incubate	72℃	2min30sec
11	Cycle to step 2 for 11 more times		
12	Incubate	72℃	5min
13	Incubate	4℃	Forever
PCR3			
1	Incubate	94℃	30sec
2	Incubate	44℃	1min
3	Incubate	73℃	2min30sec
4	Cycle to step 1 for 30 more times		
5	Incubate	72℃	5min
6	Incubate	4℃	forever

4.2 Transgenic flies

4.2.1 Flyfood

Flies were raised on standard corn meal medium supplemented with dry yeast. Soy, corn and dry yeast were mixed in one liter of cold water. Agar was oaked before adding another liter of cold water. Three liters were heated to 98 ℃ and the agar was added. After one hour of heating, malcine and treacle the mash were mixed with the boiling water. The solution was then filled up to five liters and cooled down to 65 ℃. Propionic acid was added. The food was filled into plastic vials.
Breeding Fly stocks were kept at 18 ℃ and transfer ed to fresh vials every 14 days. Experimental flies and crosses were kept at 25 ℃ a nd were flipped every week. All flies were kept at 70 % relative humidity at a 12 hour light/dark cycle. One development cycle (from egg to adult) takes approximately seven days at 29 ℃, nine days at 25 ℃, eleven days at 22 ℃, or 19 days at 18 ℃ (source: Bloomington stock center). In our incubators this was somewhat slowed down to 11 days at 25 ℃.

4.2.2 Egglaying medium

Grapeagar dishes were prepared for flies to lay eggs on 200 ml red grape juice (Rio D`Oro, Aldi) were warmed up in the microwave for 2 minutes and mixed with 3 g Select Agar. After reheating, the solution was poured into petri dishes. Fresh plates were prepared on day of injection. After removing all eggs from a plate it was reused.

4.2.3 Generating transgenic flies

For preparing the DNA injection mix 6µg of DNA and 2µg of transposase, Δ2-3, were diluted in 100µl DNAse and RNAse free water and gently mixed by turning the tube 2-3 times. For precipitation $^{1}/_{10}$ Volumen 3M Na-Acetat pH 5, 2µl pellet paint for marking the DNA and 2.5x Volumen 100% EtOH were added and incubated on ice for 15min. Afterwards the mixture was spun down at 15000rpm, 15min, 4^{0}C. The supernatant was removed and afterwards the DNA was washed one time with 70% EtOH and once more with 100% EtOH. The DNA pellet was dried on air for >15min. The DNA pellet was finally diluted in 20µl 1x injection mix. Afterwards the DNA was

checked by gel electrophoresis. For P element mediated germline transfection of *Drosophila* embryos 2 day old flies were allowed to lay eggs on grape agar plates for 20 to 30 min and then flies were transferred on a fresh plate. Eggs were collected, washed in PBT, washed in 50 % Klorix for 4.5 min to remove the chorion, rinsed in water and aligned smoothly with a paintbrush side by side on an agar block. Aligned eggs were transferred onto a cover slip coated with glue, such that the posterior end faced the edge of the slip. The slip was then transferred to a drying chamber with Blaugel (Roth) for 14 min. Eggs were fixed to a microscope table, where injections were done using an electrode holder, connected to Femtojet injector. Femtotips were back filled with 3 µl of injectionmix. The electrode tip was gently pushed against the side of the cover slip to widen the tip. Each egg was injected with a small volume of injection mix to its posterior end, where the polar cells formed which set up the germline. Importantly, injections needed to be performed in the syncytial stage of embryos. Cell membranes developed after the 13th nuclear division, at room temperature approximately 1 h after egg delivery. Polar cells were the first cells to form in the developing embryo. Eggs were then coated with oil (Voltalef 10S) and transferred to a humidified agar plate for embryos to hatch on. The first day the injected eggs were put in an 18℃ incubator and later on they were transferred to a 25℃ incubator. Embryos were collected during the next 2 days and transferred to fresh yeast vials. Freshly hatched adults were collected and individually crossed to freshly hatched w– wild type BT (originally collected in Bayreuth, Germany) flies. Successful transfection was indicated by red-eyed progeny. These again were collected right after hatching and crossed individually to balancer flies (sp/CyO;TM6/MKRS), recognizable by the marker phenotypes "curly wings" and "tubby larva". Progeny was collected for red eyes and presence of the balancers, yielding stable lines if insertions hit 2nd or 3rd chromosome. Flies with X chromosomal insertions were backcrossed to yield homozygous stable lines.

4.2.4 Anatomical analysis

4.2.4.1 Fly crossings

Drosophila melanogaster were grown on standard corn medium at 25℃, with 12:12 hours dark: light cycle and 60% humidity. In all experiments, flies were kept in 30-ml

vials containing 10 ml food. For all crossing experiments, 5-8 female virgin flies were kept together with 3 male flies in one vial and transferred to a fresh one after 5 days.

RicinA project

In the Ricin experiment virgin females from the stock DB331; hsFlp/CyO were crossed to males from the following stock: UAS-RicinA,UAS-mCD8::GFP/CyO. Heatshock treatment was made after the developed protocol mentioned in the results part of the thesis. Heatshock was given for 1-2hours and flies were kept afterwards in vials containing standard medium at room temperature.

UAS>Stop>TN-XXL project

For testing the construct female virgins from the stock UAS>Stop>TN-XXL were crossed to males of the following stock: DB331-Gal4; hsFlp/CyO. After 48hours egg laying, adult flies were transferred to another fresh food vial and the egg containing vials were given heatshock for 1hour at 37℃. After wards the vials were kept at room temperature.

UAS-Btx project

For testing the construct female virgins from the stock UAS-Btx were crossed to males from the following stock: DB331-Gal4

.

vGat-Gal4 project

For testing the vGat-Gal4 constructs female virgins from the different vGat-Gal4 stocks were crossed to males of the following stock: UAS-mCD8::GFP and also to males of the stock: UAS-cytoGFP.

Dscam project

For the Dscam localization experiment virgin females from the stock GR27B03-Gal4 (gift from Gerald Rubin) were crossed to males from the following stock: UAS-mCD8::GFP/CyO (Bloomington Stock Center). Progenitors were selected after GFP expression.

For the overexpression experiment in HS neurons virgin females from the stock DB331-Gal4; UAS-mCD8::GFP (DB331-Gal4: gift from Reinhardt Stocker) were crossed to males from the following stock: 1. Bl/CyO; UAS-Dscam 11.31.25.1 (gift

from Dietmar Schmucker). Progenitors with following genetic background were taken for all experiments described in this study: DB331-Gal4/+; UAS-mCD8::GFP/Bl; +/+ (Dscam overexpression flies). For generating control flies with appropriate wildtype background and balancer Dscam overexpression flies were crossed inter se. Flies with the wildtype background of the UAS-Dscam stock were kept as a stock: +/+;Bl/CyO;+/+. Male flies from that stock were crossed to virgin females from the stock DB331-Gal4; UAS-mCD8::GFP. Progenitors with following genetic background: DB331-Gal4/+; +/Bl; +/+ were taken as control flies in behavior and electrophysiology assays. As wildtype reference flies from following stock: *new wildtype* were compared to control flies in both electrophysiology and behavior assays. No obvious differences occurred.

Reconstructions of HS cells are based on confocal images that were taken from dissected brains after the staining procedure (s.Immunohistochemistry). For wildtype HS cell reconstruction an additional cytosolic GFP marker was added for enhancing the outline of fine structures. Males from the stock UAS-GFPcyto (Bloomington Stock Center) were crossed to virgin females of the following stock: DB331-Gal4; UAS-mCD8::GFP resulting in: DB331-Gal4/+; UAS-mCD8::GFP/+; UAS-GFPcyto/ + progenitors of which confocal images were taken.

For deficiency and null constructs virgin female flies from the stock: Dscam^23,mCD8::GFP/CyO; G73,UAS-Flp/TM6 were crossed to males of the following stock: Dscam^21/CyOGB; Exon2^ (Exon6)-FRT.

For the developmental onset study males from the stock: tub-Gal80ts/CyO; DsI/TM6 were crossed to virgin females of the following stock: DB331-Gal4; UAS-mCD8::GFP/CyO. For inactivating Gal80ts, the vials containing the experimental flies were shifted to a 30℃ incubator.

For the MARCM experiment (Lee, T. and Luo, L. 2001) male flies from the stock: DB331-Gal4/y; FRT40A/CyO; DsI/TM6 flies were crossed to virgin females of the following stock: UAS-hsFlp, UAS-mCD8::GFP; tubp-Gal80,FRT40A/CyO flies. 30-40 L3 larvae were treated with half an hour heatshock in waterbath at 37℃ and afterwards kept in fresh food vials at room temperature.

For the Dscam null MARCM experiment males from the stock: FRT42D, UAS-Dscam^21/CyO; UAS Flp flies were crossed to virgin females of the following stock: DB331-Gal4; FRT42D, tubGal80/CyO; UAS-mCD8::GFP. Crossings were kept in grape-agar plates at 25℃ and parental flies discarded after 3 days egg laying. After

reaching pupa stage flies were selected under fluorescent microscope after GFP expression and transferred to a fresh vial. Flies were kept at RT.

For Dscam RNAi silencing experiments males from the individual UAS-RNAi (3115, 25622, 25623, 36233 and 108835) stocks were crossed to female mCD8::GFP/ G73-Gal4 flies. When in addition Dcr2 was expressed then UAS-RNAi flies were crossed to mCD8::GFP/ FM7; Dcr2/ CyO; G73/TM6 flies.

For overexpression in T4 and T5 cells male flies from the following stocks: GR42H07, GRR35F02 and GR54A03 were crossed to virgin female flies of the following Stock: UAS-mCD8::GFP. GFP positive offspring was selected under fluorescent microscope and subsequently crossed to following stock: Bl/CyO; UAS-Dscam 11.31.25.1.

4.2.4.2 Immunohistochemistry

For cell reconstruction, female flies 3–5 days after eclosion were dissected. Flies tested in electrophysiology and behavior assays were immediately dissected after performances. Therefore, flies were anesthetized with CO2. The head was then removed and placed on a drop of PBS. The head cuticle was first cut open with forceps at the frontal part and then the rest was torn off. After discarding the neurolemma, brains were fixed in 4% PFA for 30 minutes at room temperature. Subsequently, brains were rinsed in phosphatebuffered saline (PBS), pH 7.2, including 1% Triton X-100 (PBT). For antibody staining, samples were further incubated in PBT including 4% normal goat serum (Sigma Aldrich) and primary antibodies were added according to their individual dilution factors overnight at 4℃. Antibodies were removed by several washing steps (3 x 20 minutes in PBT) and secondary antibodies were applied 1:200 overnight at 4℃. Finally, excessive antibodies were removed by a 3 x 20-minute washing protocol (PBT). Stained brains were mounted in Ibidi Mounting Medium (Ibidi GmbH) and analyzed via confocal microscopy.

The following primary and secondary antibodies were used in the present study. Primary antibodies included: Alexa Fluor 488 conjugate rabbit IgG anti-GFP (Molecular Probes) used in all anti-GFP staining procedures unless otherwise stated, rat anti-mCD8 (Invitrogen Caltag) only used together with rabbit anti-DscamIC (gift from Dietmar Schmucker) in the Dscam localization experiment and mouse anti-Dlg (4F3 anti-discs large; DSHB) used for background staining.

4.2.4.3 Confocal microscope setup

Serial optical sections were taken at 0.3-0.5 µm intervals with 1,024x1,024 pixel resolution and 4 times frame average using confocal microscopes (Leica TCSNT and Leica SP5) and oil-immersion 40x (n.a. 1.25) for cell reconstruction images and 63x (n.a. 1.4) Plan-Apochromat objectives. In most cases, frontal sections were taken from the posterior side of the brain. For Figure 1 b, horizontal sections were taken in the dorsal region of the brain. The individual confocal stacks were analyzed in Amira 5 (Zuse Institute Berlin (ZIB)) software. The size, contrast, and brightness of the resulting images were adjusted in Photoshop CS3 (Adobe Systems).

4.2.5 Whole brain culture

All manipulations were performed in a clean environment using disinfected equipment (forceps, pipettes, PCR tubes, etc.) in order to prevent bacterial or fungal contamination.

For whole brain culture (modified from Ayaz, D. 2008) Millicell low height culture plate inserts (Milipore) were placed in a sterile Petri dish (Falcon) containing 1 ml of sterile PBS Dulbecco's (DPBS). On top of the membrane a freshly prepared coating, solution of Laminin (3.3 µg/mL; BD Biosciences) and Polylysine (33.3 µg/mL; BD Biosciences) in sterile D-PBS was added. The culture plate inserts were incubated overnight at 37℃. The next day they were washed extensively with sterile D-PBS and were stored at 4℃ for up to three weeks. Just before use, the coated inserts were transferred to an empty sterile Petri dish. For making the brain explants, adult female flies of the desired genotype were collected within 4 days after eclosion. After CO_2 anesthesia, the flies were placed in a 1.5 ml centrifuge tube on ice, keeping them alive but immobile. Before dissection, flies were washed in 70% Ethanol for a few seconds and placed into a sterile Petri dish containing ice-cold Schneider's *Drosophila* Medium (GIBCO). The brains were dissected out in that medium as careful and as fast as possible (< 3 min). Parts of the eyes and lamina were left attached when they were difficult to remove. Damage to the brain or delay in the speed of the dissection reduced the quality of the brain culture and therefore, all damaged brains were discarded. The dissected brains were collected in a PCR tube containing Schneider's Medium on ice and then washed with ice-cold dissection

medium. After dissection and washing, the brains were placed in a drop of medium on the membrane of the culture plate insert, using a pipette. Therefore, the pipette tip was cut a bit open with a scissor and rinsed with Schneider Medium. This prevents the brain to be stuck at the inner wall of the pipette tip. Up to five brains were transferred from the PCR tube onto the same insert. When all brains were in place, their antero-posterior orientation was verified and corrected if necessary. Excess medium was removed using a pipette, leaving only a thin film of medium covering each brain. 1.1 ml of culture medium was then added to the Petri dish containing the insert. The culture dishes with the explants were kept in a plastic box in a cell culture incubator at 25℃. The culture medium was refreshed every two days.

4.2.6 Behavior setup

All tested flies developed in vials with medium under constant conditions. The incubators were set 25℃ and 60%humidity. In all cr osses, maximum 10 virgin female flies were crossed with 3-5 male ones. In the behavior-setup-room, air humidity was put constant through a custom air humidifier. Test specimens were first put onto ice for making them immobile. Afterwards they were tethered to a torque via UV sensitive glue. Tethered flies were kept one day on a rack for starving and only fed with water and sugar solution. At the following day, the flies were put into the stimulation arena.

4.2.6.1 LED arena

Visual stimulation was presented with a custom built LED arena consisting of 30 by 8 TA08-81GWA dot matrix displays (Kingbright, California, USA), each harboring 8 by 8 individual green (568 nm) LEDs, covering 360° in azimuth and 85° in elevation of the fly's visual field with an angular resolution of about 1.4° between adjacent LEDs. The arena is capable of frame rates above 600 fps with 16 intensity levels.

4.2.6.2 Assays

All stimuli were presented monocular with a 30-degree gap at the frontal area in order to avoid binocular view. At the beginning, a whole field stimulus was presented 5seconds in one direction then 5 seconds in the other one. Afterwards stimulation for

elevation, azimuth, and contrast were in following sequence: 1. 1second break 2. 1second null direction 3. 5seconds preferred direction 4. 5seconds null direction. At the end of all assays, again 5seconds whole field stimulation was presented.
The elevation stimuli were presented randomly at different heights (38.6-30.9 deg , 30.9-21.8 deg, 21.8-11.3 deg, 11.3-0 deg, 0 - -11.3 deg, -11.3 - -21.8 deg, -21.8 – 30.9 deg, -30.9 - -38.6 deg) as well as those in different azimuth angles (-180 - -15deg or 15 - 180deg) on dark background.
For contrast assay the pattern was presented at the entire arena but only at certain azimuths (-180 - -15 deg und 15-180 deg) the pattern was moved.

4.2.6.3 Analysis

For calculating the response strength the average response of the last 2seconds while PD stimulation subtracted from the average of the last 5seconds while ND stimulation were calculated and then divided by 2. The torque strength results from subtraction of the winbeat amplitude left from that of the right one.
Data were acquired and analyzed with the data acquisition and analysis toolboxes of Matlab.

4.2.7 Electrophysiology setup

4.2.7.1 Visually Guided Whole-Cell Recording

Detailed information about all electrophysiology procedures is provided in the recent publication from Schnell et al. 2010.
Flies were anesthetized on ice and waxed on a Plexiglas holder whereby extended proboscises were fixed. The head was bent down to expose the caudal backside of the head and with Aluminium-foil with a hole of ~1–2 mm sustained by a ring-shaped metal holder was placed on top of the fly. The upper wet part (covered with ringer solution (Wilson et al. 2004)) of the preparation was thereby separated from the lower dry part. A small window was cut into the backside of the head, and during mild protease treatment, the neurolemma was partially digested and the main tracheal branches and fat body were removed. The protease was rinsed off and replaced by ringer solution. A saline jet was generated with a ringer-filled electrode in order to remove the extracellular matrix and to expose the HS-cell somata for recording. Water immersion optics were used from above and visual stimuli were presented to dry and fully intact compound eyes. Genetically labeled green fluorescent cells were

approached with a patch electrode filled with a red fluorescent dye and recordings were established under visual control. During the recordings, the fluorescence excitation was shut off to prevent blinding of the fly. After the recording, several images of each Alexa-filled LPTC were taken at different depths along the z-axis.

4.2.7.2 LED arena

For visual stimulation, a custom-built LED arena was used based on the open-source information of the Dickinson Laboratory. The arena consists of 15 by 8 TA08-81GWA dot matrix displays (Kingbright, California, USA), each harboring 8 by 8 individual green (568 nm) LEDs, covering 170° in azimuth and 85° in elevation of the fly's visual field with an angular resolution of about 1.4° between adjacent LEDs. The arena is capable of frame rates above 600 fps with 16 intensity levels. Matlab was used for programming and generation of the patterns. The luminance range of the stimuli was 0-8 cd/m^2.

4.2.7.3 Assays

To study contrast dependency, a square-wave grating of 34° spatial wavelength moved at a constant angular velocity of 34°/s corresponding to a temporal frequency of 1Hz. Contrast was calculated as $(I_{max} - I_{min})/(I_{max} + I_{min})$. With the 16 intensity levels of the LEDs, seven pattern contrasts could be obtained ranging from 100 % down to 6.7 % at the same mean luminance. To obtain a lower contrast of 3.3 %, four consecutive image frames were used to define one image as described above. The square-wave grating (spatial wavelength: 22.4°, angular velocity: 22.4°/s) used either ispilateral or contralateral stimulation covered about 56° in azimuth and 85° in elevation and was displaced by ±15° relative to frontal gaze. The local response characteristics of HS-cells were determined using a previously described stimulus (Nordstrom et al. 2008; Wertz et al. 2009). A small bar of 5.6° length and 1.4° width was moved horizontally from the contra- to the ipsilateral side and back again at different elevations or vertically downward and upward at different positions along the azimuth thereby an area of 12 about 145° along 250 the azimuth and 85° of elevation was covered.

Data were acquired and analyzed with the data acquisition and analysis toolboxes of Matlab. Receptive fields were calculated by binning the responses of single HS-cells mean response during null direction from the mean response during preferred direction motion. The receptive fields of all HS-cells of a certain type were averaged, smoothed by convolving them with a 3x3 kernel approximating an isotropic Gaussian function, and normalized to maximal value.

4.2.7.4 Analysis

In order to identify the cell type from which recording were taken an intracellular dye filling was done. Therefore, flies were decapitated and cut heads were fixed in a layer of glue in a way that the facet eyes were looking downward into the glue. After hardening of the glue (~2 min) the specimen were covered with Ringer's solution, and the cuticle at the backside of the fly's head was removed with sharp needles. This procedure allowed direct access to the brain. The main tracheal branches were removed. Dye fillings were performed using quartz electrodes. Electrodes were filled with a 10 mM Alexa Fluor 594 solution (Invitrogen) and backfilled with 2 M KAc/0.5 M KCl solution. Impaled cells were loaded by negative current pulses for a few seconds. For the determination of electric coupling between HS cells 2 - 4 % Neurobiotin (Vector Labs, Burlingame) was added to the intracellular solution. Neurobiotin and Alexa Fluor-568 were coinjected via ± 0.2 nA current pulses for up to 10 min. Whole fly heads were decapitated and fixed in 4 % paraformaldehyde for two hours before dissection in PBS

4.2.8 Cell reconstruction

The image stacks taken by confocal microscope were transferred to Matlab (Mathworks, Natick, MA) and all reconstruction analysis was performed there in custom written software combined with the "TREES" software (Cuntz et. Al 2008). Based on 2-D images cylinder models of the main branching structures were obtained in a semi-automated way: interactive software allowed switched viewing of either Z-projection or an individual slice of an image stack. Z-values were attributed to each cylinder directly from the depth-map according to their 2D location. Quick tracing results (30 min) were achievable working corrections based on individual

slices were necessary in all reconstruction steps. Jumps in the Z-axis were smoothed by use of linear interpolation. With that procedure hull areas of HS cell dendrites were calculated.

In order to obtain a measure for the convexity of dendrites, the convex hull was drawn around all dendrite nodes. The surface ratio between the dendritic spanning field and this convex hull was chosen as a characteristic spanning field parameter, the convexity index.

4.3 Virus injection into living flies

First 5 µl of the virus solution was backfilled to an injection electrode. The tip of the electrode was broken open with a forceps. Flies were anesthetized on a CO2 pad and magnified under stereomicroscope (Leica). The fly was positioned with a brush and forceps in a way that the caudal backside of the head was exposed. The loaded electrode was carefully stabbed into the cuticle in a very sharp angle thereby avoiding strong penetration of the brain itself. The fly together with the electrode is connected to the electrode holder of the Femtojet injector. After two injection pulses with minimal pressure (100/20) the fly was removed off the electrode and put into a food vial. 2 days after infection flies were anatomically analyzed.

5 Results

5.1 The role of Dscam1 in the development of Lobula Plate Tangential Cells

HS neurons possess characteristic dendritic structures covering the frontal layer of the lobula plate. The dendritic ramifications of neighboring HS cells were overlapping each other. In addition, these neurons were connected to each other via gap junctions (Schnell et al. 2010). In order to determine how their complex anatomical features were important in fulfilling their function of motion detection HS cells were genetically manipulated by overexpressing single *Dscam1* (Down Syndrome Cell Adhesion Molecules) isoforms. This kind of overexpression has been reported to elicit repulsion between overlapping neurons (Schmucker et al. 2007), a phenomenon that might also occur in HS cells. However, so far it has not been clarified whether HS cells possess an endogenous Dscam code at all and which potential role Dscams might play in establishing neuronal targeting and pattern formation in HS cells. In order to shed light on these questions an extensive anatomical study was carried out using immunohistochemistry combined with genetic manipulations in *Drosophila melanogaster.*

5.1.1 HS cells possess an endogenous Dscam code that is required for self-avoidance and pattern formation

As a first step in establishing whether Dscams were endogenously present within wildtype HS cells, an immunolabeling assay was carried out in which a monoclonal antibody (357; kindly provided by Dietmar Schmucker) directed against the entire intracellular domain of Dscams in order to reveal the localization within the optical lobe. Furthermore, GR27B03-Gal4 was used to drive an expression pattern that is restricted to HS cells within the lobula plate. Here, membrane-tagged Green Fluorescent Protein (mCD8::GFP) was used as a cell marker. The Dscam antibody staining illustrated a massive presence of Dscams in the entire optical lobe (Fig. 23 A). Notably, horizontal sections showed that Dscams were located in all four lobula plate layers, thereby collocating with the HS-cell layer and also with the VS cell layer (Fig. 23 C, D). Furthermore, Dscams were unambiguously present in the dendrites,

somata, as well as axonal terminals of HS cells (Fig. 23 B, E, F). Immunolabeling was also repeated in other driver lines giving consistent results (not shown).

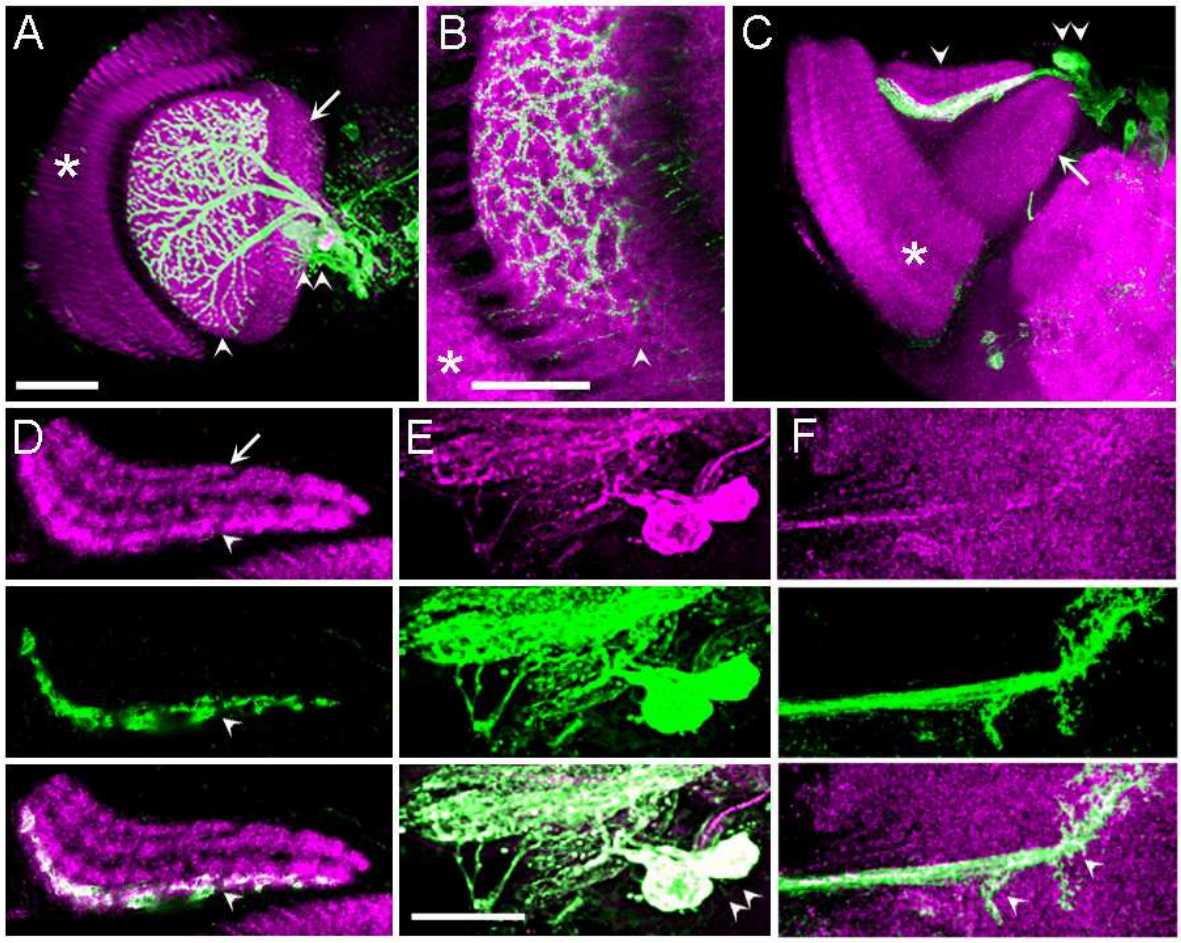

Fig. 23: Dscam is expressed in HS cells, the entire fly visual system.

Three giant neurons of the horizontally sensitive (HS) system (green) express GFP (GR27B03-Gal4; UAS-mCD8::GFP). Their large overlapping dendrites are stacked along the dorsal-ventral axis and cover the entire lobula plate where they colocalize with Dscam. (A) In the frontal section, double immunolabeling of Dscam (magenta) and GFP (green) shows Dscam expression in all neuropils of the fly visual system. Furthermore, coexpression of Dscam can be observed in GFP labeled HS-cells. Immunolabeling of Dscam highlights columns and layers in the lamina (arrowhead, only partially included), medulla (triangle), lobula (arrow), and the lobula plate (asterisk) of the fly visual system. (B) Close-up of the lobula plate shown in A, GFP and Dscam colocalize in dendritic branches of HS cells. (C) The horizontal section shows how the dendritic arborizations of HS cells are restricted to the thin, most-anterior layer of the lobula plate. (D) Close up of the lobula plate reveals Dscam expression in all four layers of the lobula plate. The most-anterior layer colocalizes with GFP expressing dendrites of the three HS cells. (E) Further colocalization of Dscam and GFP in HS cell somata and (F) as well as HS axon terminals. Dscam was labeled with an antibody raised against the intracellular domain (Dscam IC, magenta). Confocal image stacks were taken with a z-increment of 0.3 µm, a 63X

objective and minimized pinhole. Composite images in A, B and C were generated by collapsing 150, 29 and 40 images respectively. Scale bar 50 µm in A, C and 30 µm in B. D-F are single confocal images, scale bar 30 µm.

In order to support the results and further to study the functional role of Dscams in HS cells, Dscam null flies were generated. Here, DB331-Gal4 was used to drive expression of GFP and Flipase activity in HS and VS cells (Raghu et al. 2007). Dscam null cells had the following genetic background: DB331-Gal4; FRT42D, tubGal80/ FRT42D, Dscam^21; UAS-mCD8::GFP/ UAS-FLP. The genetic design of the transgenic flies based on the MARCM technique (Lee and Luo 2001) ensured that only homozygous cells lacking GAL80 were Dscam null as well as GFP labeled. The rest of the fly still possessed the intact Dscam code and thus did not express the marker gene. This method has been successfully implemented before for selective labelling of Dscam null cells (Chen et al. 2007).

Dscam null cells display strong dendritic and axonal disorders (Fig. 24 A, B). In the dendritic regions, fasciculation of first order sister branches were detectable as well as self-crossing events in higher order branches (Fig. 24 E). Furthermore, the general density of higher order branches appeared to be increased (Fig. 30). In the axonal regions, the fibers were diverging at their destination areas and did not reach their target regions. Furthermore, the terminals of HS cells appeared clumpy (Fig. 24 D). Regarding VS cell terminals, the dendrites seemed to be much smaller than in wildtype flies. In addition, the axonal pattern was cluttered, which would indicate fasciculation between the terminal branches. In addition, some clumped structures at the endings were clearly visible (Fig. 24 F). Furthermore, the somata of VS and HS cells were dislocated and no longer associated with each other (Fig. 24 C).

Together, these findings provided the first evidence that HS cells possessed an endogenous Dscam code, which was required for correct targeting and pattern formation. In the next step, I wanted to evaluate how many isoforms were required in order to provide an identification system that ensures a proper branching structure in HS cells.

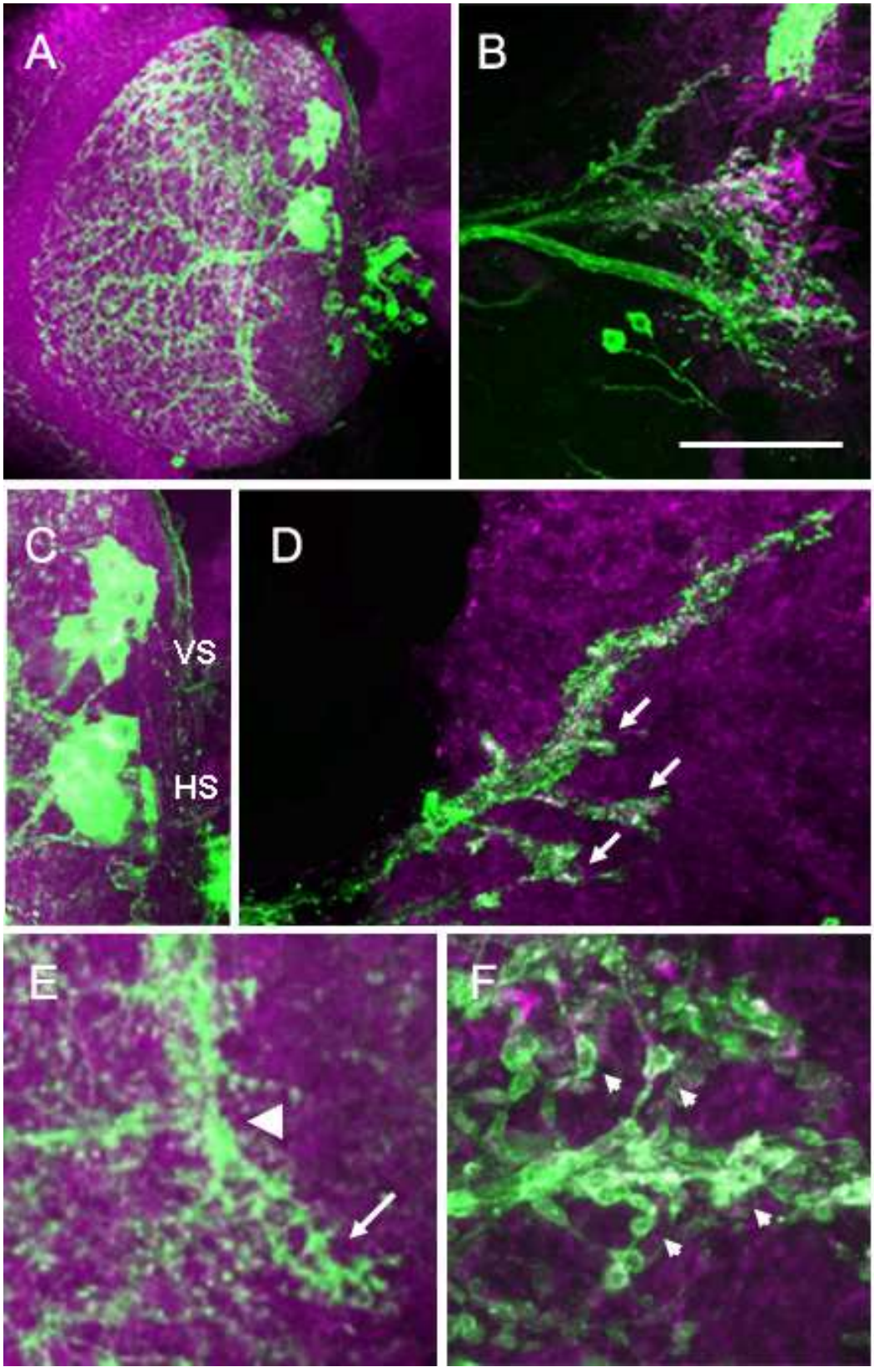

Fig. 24: Dscam null causes loss of self-avoidance and clustering of dendritic and axonal branches in LPTCs.

(A-B) Overview images of the dendritic and axonal regions of GFP labeled LPTCs (green) which lack the endogenous Dscam code (DB331-Gal4; FRT42D, tubGal80/ FRT42D, Dscam^21; UAS-mCD8::GFP/ UAS-FLP). Background staining was provided by immunolabeling with anti-disc-large (magenta). (C-F) Close up images reveal mislocation and altered clustering of HS and VS cellbodies (C). Axonal terminals of HS cells separate at the protocerebral region but possess clustered endings and projection errors (D: arrows). The axonal endings of VS cells are partially fasciculated and the endings are clumpy (F: arrows). At the dendritic areas in the lobula plate, clustering of high order branches is visible (E: triangle). However, only weak dendritic fasciculations could be detected in VS cells (E: arrows). Confocal image stacks were taken with a z-increment of 0.3 µm, a 63X objective and minimized pinhole. Composite images were generated by collapsing 150 (A, C, E) and 60 (B, D, F) images respectively. Scale bar 50 µm in A, B; 25 µm in C; 18 µm in D and 12 µm in E, F

5.1.2 Thousands of isoforms are essential to provide HS cells with a robust self-avoidance mechanism

Dscam loss-of-function experiments showed that Dscams were necessary for the proper development of dendritic shape and ramification of LPTCs. However, does reduction of Dscam variability also have an impact on complexity and formation of dendritic branching in HS cells? In order to answer this question, flies with restrictions in splicing variability were generated and anatomically analyzed. Here, flies with Dscam delta exon 2 and delta exon 6 in a heterozygous Dscam null background were generated restrictively to the G73-Gal4 (original: NP282 from Kei Ito lab) expression pattern which includes HSN and HSE. Excision of Exon 6 reduced the variability from 19008 to only 1584 potential isoforms (Fig. 25 A) and excision of Exon 2, which does not possess endogenous splicing variability, was leading to Dscam null (Fig. 25 B) in the affected cells. Flies with the genetic background: Dscam^23, mCD8::GFP/ Dscam^21; G73-Gal4, UAS-Flp/ Exon2^ (Exon6) were generated. These flies possessed a homozygous lethal Dscam null (Dscam^21/ Dscam^23) background that was rescued by a heterozygous reinsertion of the entire Dscam allele in which the excisable exons were flanked by FRT sites (UAS-Dscam FRT Exon 2/ 6). Through UAS-Flipase activity, the exons could be removed from the rescue-allele, thereby resulting in the reduced Dscam variability (delta Exon 6; Fig. 25 B) and the null ‘mutant’ (delta Exon 2; Fig. 25 D) in the expression pattern of G73-Gal4.

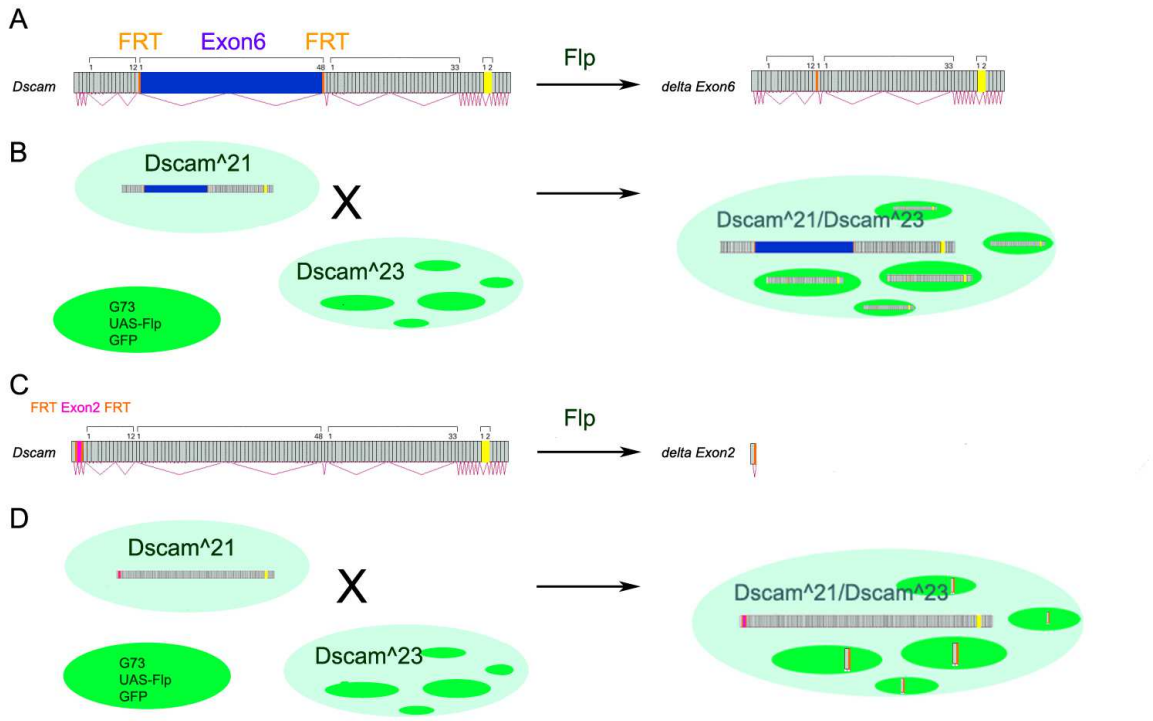

Fig. 25: Single Exon excision elicits reduced Dscam variability and Dscam null.
(A) The 'Exon 6' construct consists of the entire *Dscam* gene sequence in which exon6 is flanked by FRT sites. This allows the excision of exon6 by Flipase activation. (B) Crossing two flies, one carrying Dscam^21 and Exon 6 construct and the other Dscam^23, G73-Gal4, UAS-Flp and UAS-mCD8::GFP, results in offspring with a lethal Dscam null background (Dscam^21/Dscam^23) that is rescued by the Exon6 construct. However, green-labeled cells driven by G73-Gal4 possess Flipase activity that leads to the excision of Exon 6 off the gene. This reduces the hypervariability of exon 6 from 18 down to 1. (C) The 'Exon 2' construct consists of the entire *Dscam* gene sequence in which exon 2 is flanked by FRT sites. This allows the excision of exon 2 by Flipase activation. (D) Crossing two flies, one carrying Dscam^21 and Exon 2 construct, the other Dscam^23, G73-Gal4, UAS-Flp and UAS-mCD8::GFP, results in offspring with a lethal Dscam null background that is rescued by the Exon 2 construct. However, green-labeled cells driven by G73-Gal4 possess Flipase activity that leads to the excision of the entire Exon 2 off the gene. This leads to Dscam null in these cells.

Excision of Exon2 caused severe changes in the anatomy of HS cell dendrites. Here, loss of Dscam function elicited self-crossing events and subtle fasciculation of sister branches (Fig. 26 D' 1, 2, 5). In addition, an overall reduction of cell complexity, with partial lack of entire branching structures, was detectable (Fig. 26 D' 3, 4). This observation was contradicting previous results made in Dscam null cells, where the lack of Dscams led to an increase in complexity and the dendritic fields were not

impaired. Excision of Exon 6 elicited strong self-crossings and fasciculations between sister- branches (Fig. 26 C' 1, 4, 5). Comparable to the delta Exon 2 phenotype, the dendritic fields as well as branching complexity were reduced (Fig. 26 C' 2, 3). The phenotypical penetrance in both transgenic flies was very low with only 3 out of 10 HS cells showing anatomical changes in the dendrites.

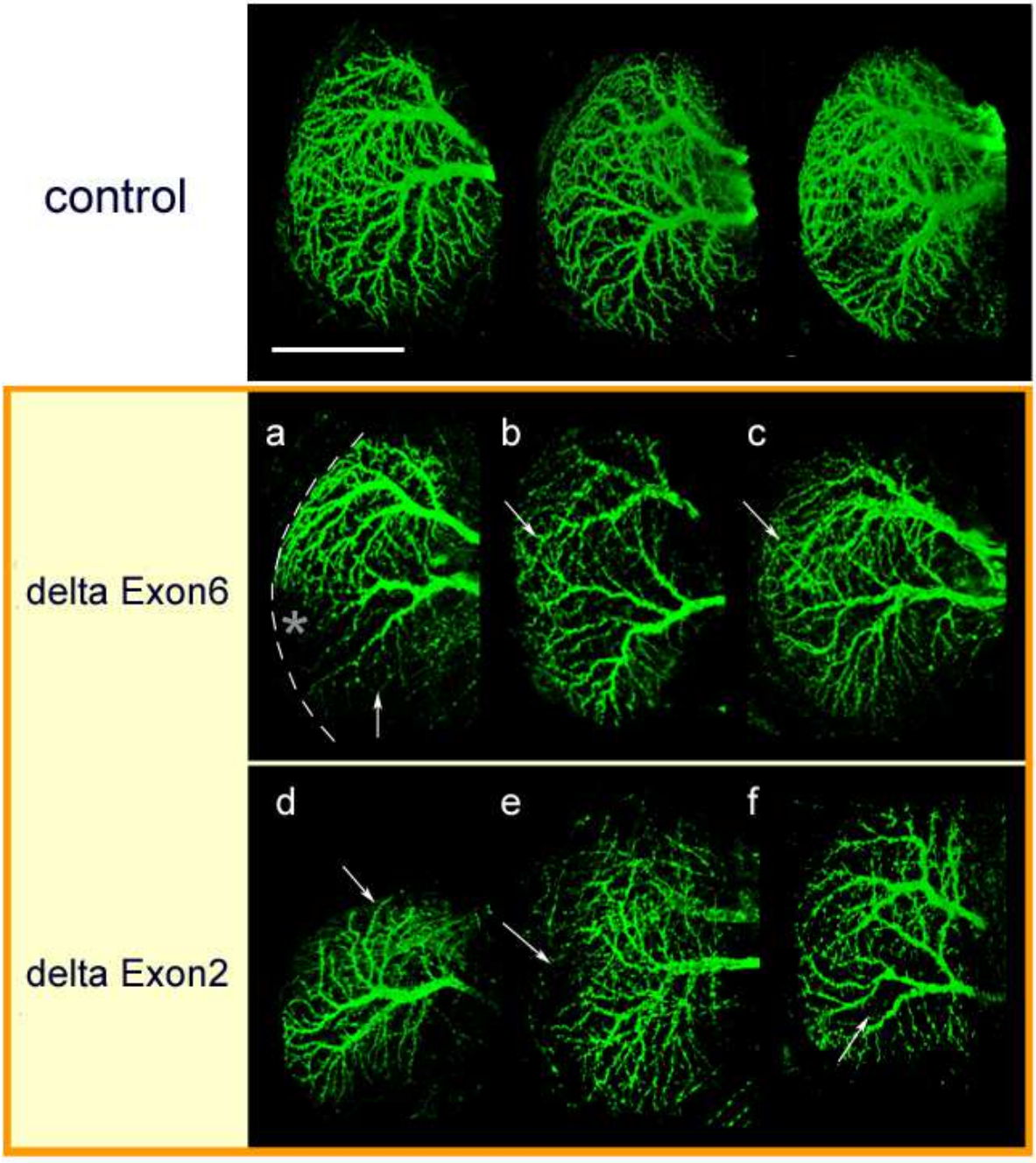

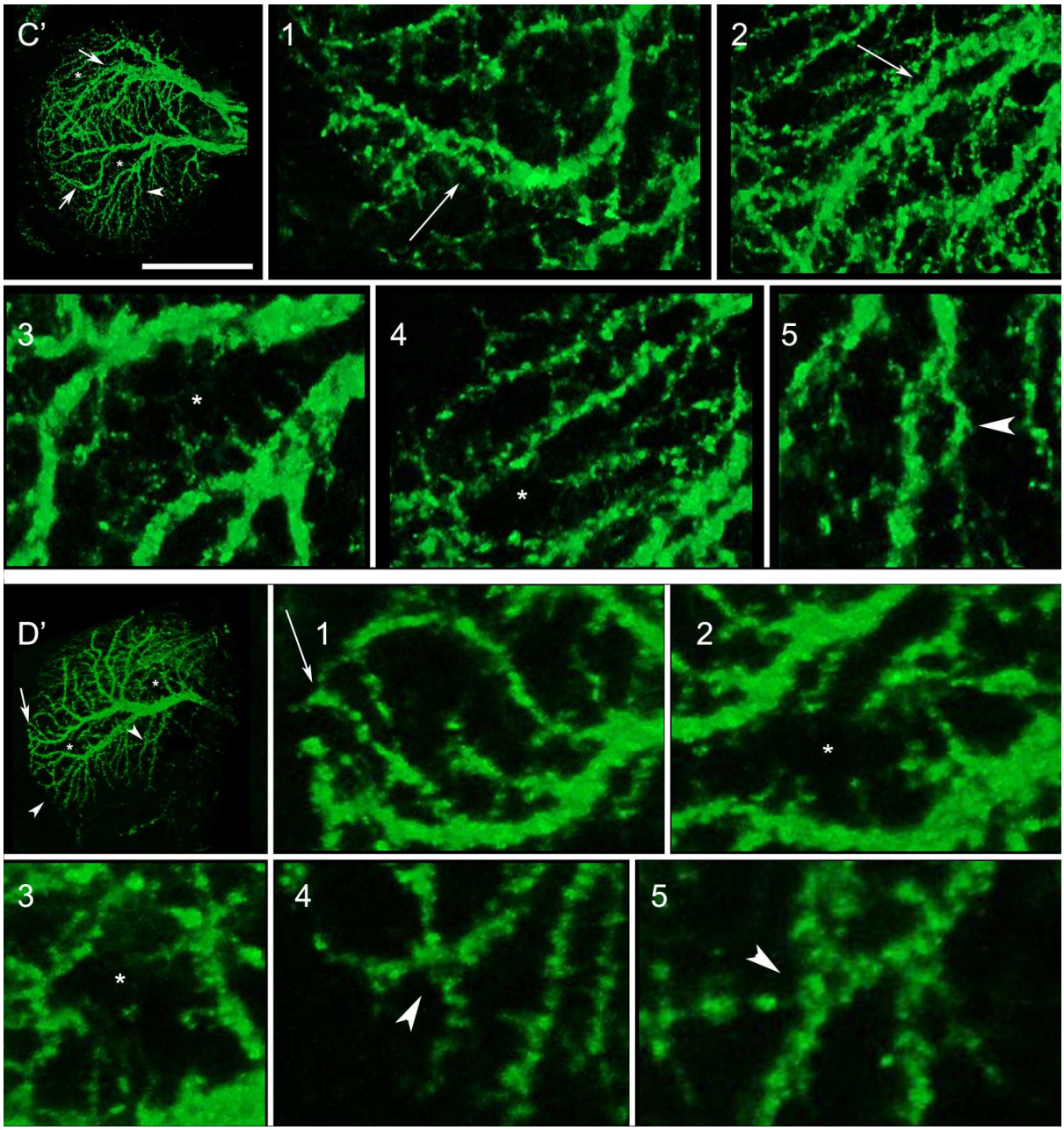

Fig. 26: Reduction of Dscam variability as well as Dscam null causes variable self-crossing phenotypes in HS cells.

This figure shows the dendritic arborization phenotype of HSN and HSE labeled with mCD8::GFP (green) driven with G73-Gal4 in which either Dscam exon6 or Dscam exon2 was excised specifically within that expression pattern. Control flies possessed the following genetic background: Dscam^23, UAS-mCD8::GFP/ Dscam^21; G73-Gal4/ Exon2^ (Exon6). Dscam deficiency flies possessed the following genetic background: Dscam^23, mCD8::GFP/ Dscam^21; G73-Gal4, UAS-Flp/ Exon2^ (Exon6). Control flies without Flipase activity display a normal dendritic arborization pattern indifferent from wildtype ones, whereas the reduction of Dscam variability causes changed phenotypes in the branching pattern. In (a) the HSE cell (arrow) seems to possess a decreased branching pattern and furthermore, the cell does not reach the distal lobula plate border (asterisk) which is schematically

depicted with the dashed line. In (b) and (c), the distal regions of the dendritic tips are self-crossing (arrows) and some main branches are approaching each other (a: arrow). In Dscam delta Exon 2 neurons, the arborization pattern is even more disrupted. In (d) HSN (arrow) is totally collapsed whereas HSE dendrites seem to be elongated to the direction of the missing cell. In cases where both cells are still present, the branching complexity is reduced (e and f: arrows). (C' + D') Close-up pictures from (C) and (D) depict areas in which fasciculations (C' 1, 2 and D' 1: arrows), self-crossings (C' 5 and D' 4, 5: arrowhead) and strong reductions of branching density (C' 3, 4 and D' 2, 3: asterisk) are prominent. Confocal image stacks were taken with a z-increment of 0.2 µm, a 63X objective and minimized pinhole. Composite images were generated by collapsing ~150 images. Scale bar 50 µm; Close up pictures: Scale bar 5 µm-12 µm.

The results showed that excision of Exon2 caused different phenotypes with higher variability and differing from the prior described Dscam null phenotype. This observation will be discussed later on.

Another possibility of assessing further Dscam null phenotypes was to use RNAi for silencing Dscam components. Five different UAS-RNAi lines targeted against Dscam were tested: 3115, 25622, 25623, 36233, and 108835 in the expression pattern of G73-Gal4. Only two UAS-RNAi lines elicited anatomical changes in the HS dendrites. Flies expressing UAS-RNAi 36233 and UAS-RNAi 3115 displayed dendritic self-crossings (Fig. 27 B1) and clustering in HS cells (Fig. 27 A1). Using additional UAS-Dicer2 enhanced neither the phenotype nor the penetration rate. In general, the RNAi phenotype was similar to that evoked by excising Dscam exon2.

So far, the results revealed that reduction of Dscam variability and Dscam null had a severe impact on the dendritic morphology of HS cells, thereby providing strong evidence that thousands of different Dscam isoforms might be needed for controlling correct pathway finding and pattern formation of the dendritic branches in these cells. The deficiency experiments revealed how the phenotypes varied according to the number of potential available Dscam isoforms.

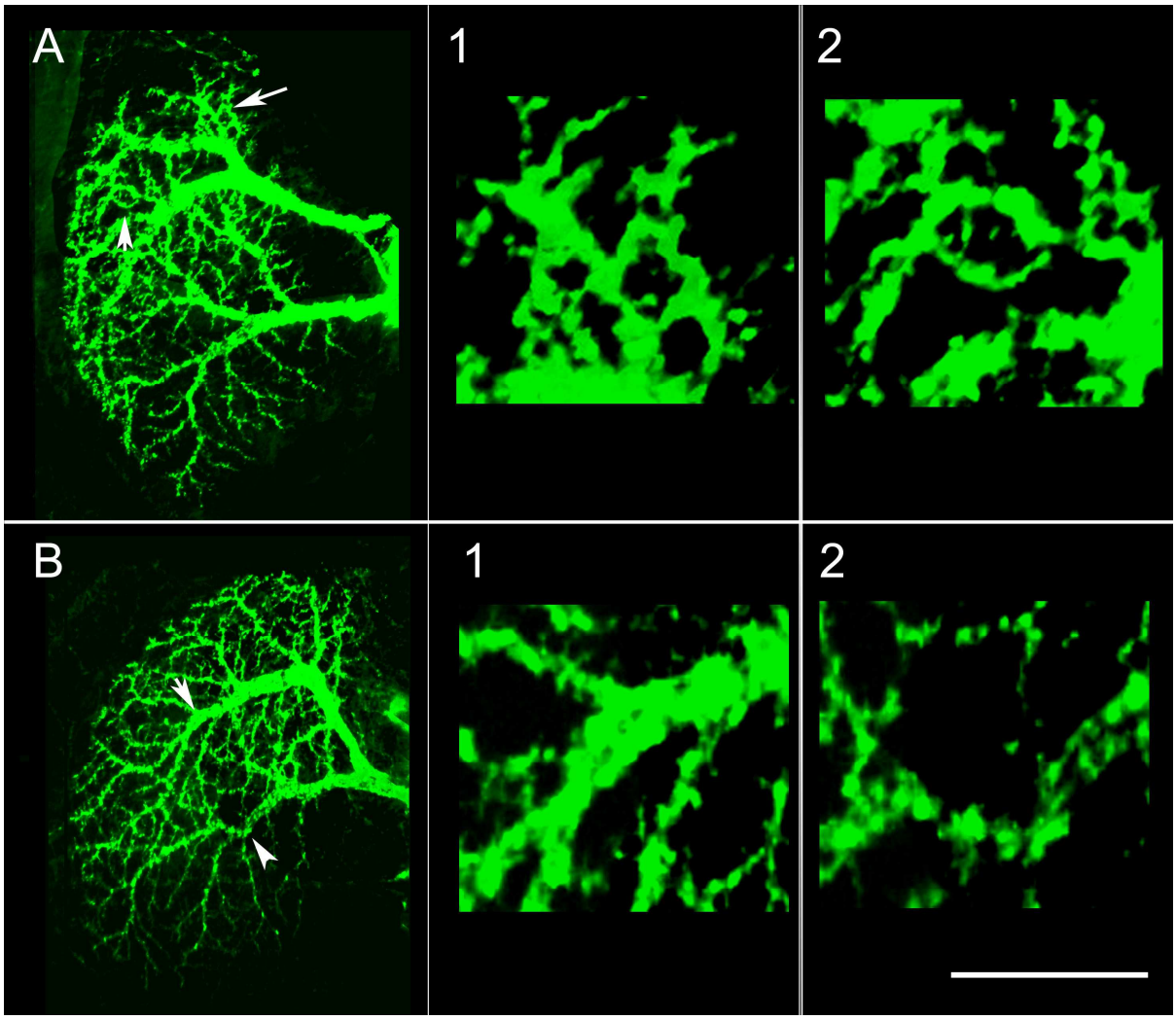

Fig. 27: RNAi silencing elicits loss of self-avoidance and dendritic clustering.

Flies expressing UAS-RNAi targeted against Dscam (mCD8::GFP/ UAS RNAi; G73-Gal4/+) are showing dendritic clustering and self-crossings. (A 1+2) Overview of the HS cell dendrites in which Dscam is silenced by the expression of RNAi 3115 reveals reduction of dendritic ramification density. (A 1+2) Close-up images reveal dendritic clustering and self-crossings. (B) Similar phenotypes are elicited by silencing with RNAi 36233. Self-crossing events (1) and impaired dendritic pathway finding (2) are visible. Confocal image stacks were taken with a z-increment of 0.2 µm, a 63X objective and minimized pinhole. Composite images were generated by collapsing ~150 images. (A+B) Scale bar 50 µm; Close up pictures (1-2): Scale bar 10µm.

5.1.3 Overexpression of single Dscam isoforms in HS cells results in strong gain-of-function phenotypes

In total, six different Dscam isoforms were overexpressed in addition to the endogenous expressed Dscam code (Fig. 28). As cell marker, protein membrane tagged mCD8::GFP was used. The HS cells in UAS-mCD8::GFP/ +; G73-Gal4/ UAS-Dscam isoform flies were visually inspected. At first sight, overexpression of Dscam 1.30.30.1, Dscam 7.27.25.1, Dscam 2.9.19.2 and Dscam 1.34.30.2 + Dscam 1.6.19.2 did not elicit any strong morphological changes, i.e. based on experiences with the wildtype anatomy, visual analysis of the taken confocal images resulted in the conclusion that no or only minor changes were caused by overexpression of these Dscam isoforms. In contrast, HS cells in which Dscam 7.6.19.2 (+7.6.19.2) or Dscam 11.31.25.1 (+11.31.25.1) was overexpressed revealed severe alterations in the dendritic arborization pattern of HS cells. A major reduction in arborization density was present in +7.6.19.2 cells leading to the assumption that higher order branches were missing. +11.31.25.1 cells were partially lacking the entire distal area of their dendritic field. In +7.6.19.2 neurons the phenotype ranged from “fishbone”-like dendrites with practically no higher-order branches to wildtype branching patterns. Around 20 % of all +7.6.19.2 flies examined revealed severely reduced higher order branches. However, in +11.31.25.1 flies, the penetration was much higher. Around 80 % of the flies showed non-wildtype dendritic fields. Sometimes only rudimentary dendritic trees of HSE remained. Furthermore, Dscam overexpression exhibited only partially penetrated phenotypes (Fig. 29) in which either HSN or HSE was affected.

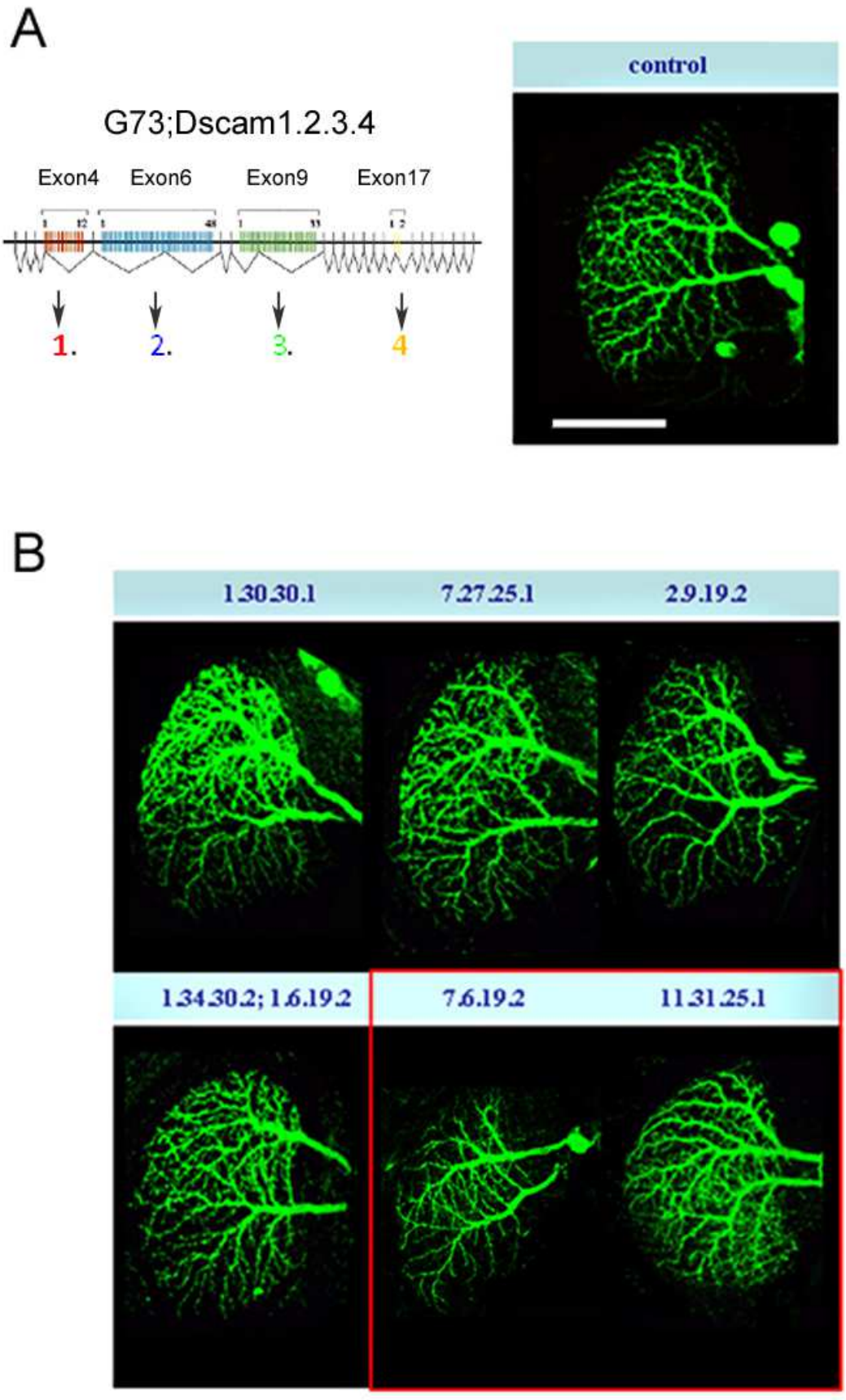
A
G73;Dscam1.2.3.4
Exon4
Exon6
Exon9
Exon17
1.
2.
3.
4
control
B
1.30.30.1
7.27.25.1
2.9.19.2
1.34.30.2; 1.6.19.2
7.6.19.2
11.31.25.1

Fig. 28: Overexpression of different single Dscam isoforms in HS cells elicits different dendritic branching phenotyps.

The coding of single Dscam isoforms is built up of 6 constant domains and 4 different hypervariable exon domains that are individually spliced and assembled (A: scheme). (A) Control flies (UAS-mCD8::GFP; G73-Gal4) in which the wildtype dendritic branching pattern of HSN and HSE are visible (green). (B) Six different single Dscam isoforms were overexpressed in HS cells (UAS-mCD8::GFP/ +; G73-Gal4/ Dscam isoform). In cells with Dscam 7.6.19.2 overexpression the number of higher order branches seems to be reduced and in Dscam 11.31.25.1 overexpression the entire dendritic field of HSE is in general reduced (B: red box). Here, a direct comparison is possible between normal-sized HSN and the smaller HSE dendrites. Other Dscam isoforms elicit a similar reduction in dendritic branching density (Dscam 2.9.19.2) but less severe than Dscam 7.6.19.2. Confocal image stacks were taken with a z-increment of 0.2 µm, a 63X objective and minimized pinhole. Composite images were generated by collapsing ~100images. Scale bar 50 µm.

For testing stability and dosage dependence on penetrance and uniqueness of the elicited phenotypes, Dscam +7.6.19.2 and Dscam +11.31.25.1 were expressed with a different driver line: DB331-Gal4. Here, both isoforms elicited constant phenotypes whereas the penetrance rates changed. In case of +11.31.25.1, penetration rose up to 100 %, i.e. all three HS cells in heterozygous Dscam overexpression flies (DB331-Gal4; UAS-mCD8::GFP; UAS-Dscam 11.31.25.1) displayed smaller dendritic fields. Moreover, the dendrites of VS cells also seemed to be anatomically affected. However, this phenomenon has not yet been analyzed in detail (Fig. 30 G-I). In order to underline the major lack of dendritic ramifications of HS cells in the distal region of the lobula plate, background staining was applied with anti-disc-large (Dlg) antibody staining, a postsynaptic marker that highlights all neuropils of the optical lobe (Fig. 30).

These complicated, wide-ranging anatomical distortions revealed the importance of a phenotypic analysis of individual neurons. In order to support the anatomical findings and allow further dissection of the Dscam elicited gain-of-function phenotype, additional reconstructions of HS cells were performed by Friedrich Förstner.

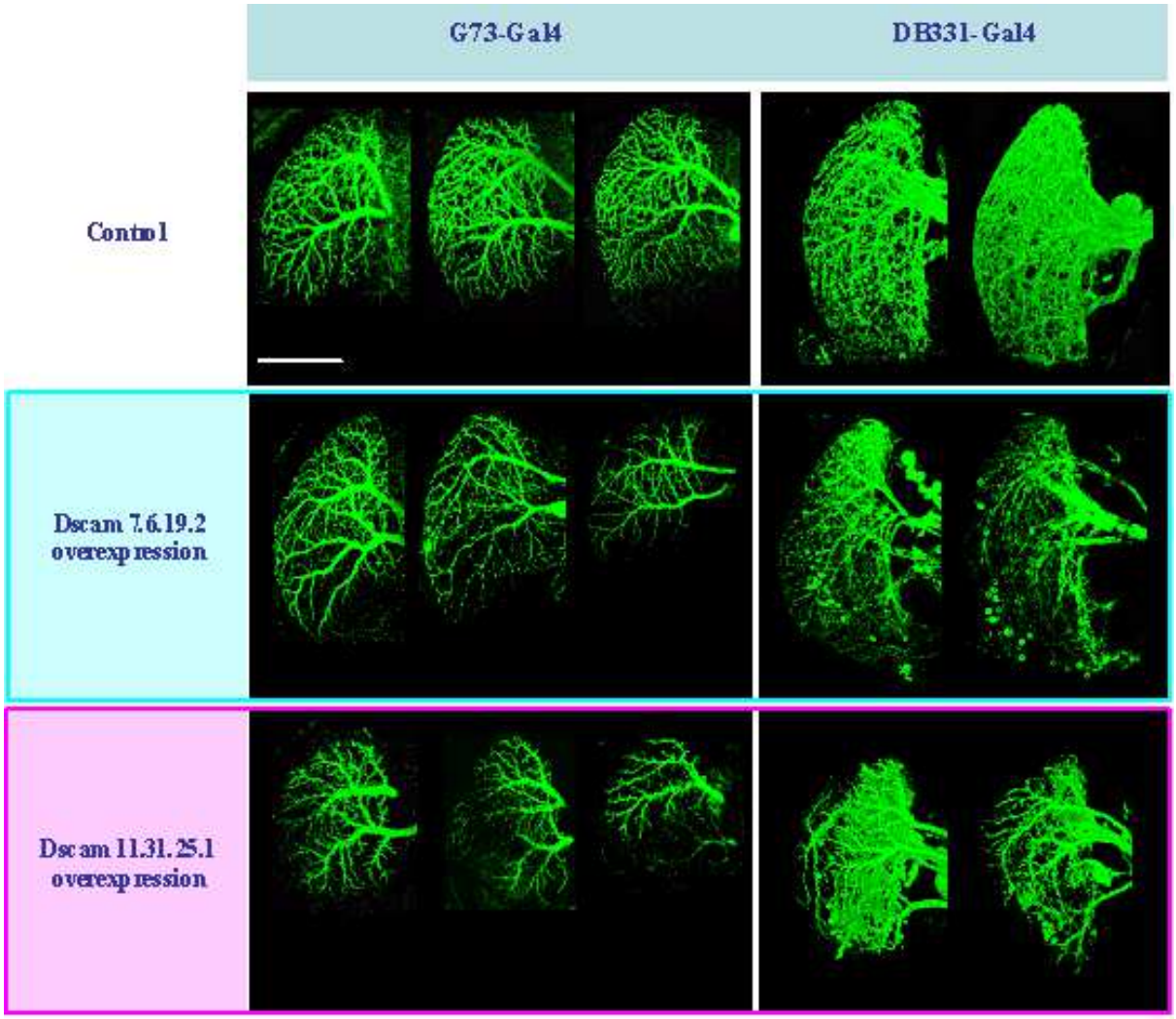

Fig. 29: Uniqueness of individual Dscam phenotypes is independent of transgenic expression level.

Images from control flies (UAS-mCD8::GFP; G73-Gal4 and DB331-Gal4; UAS-mCD8::GFP) illustrate the expression patterns of the used driver lines in the lobula plate: G73-Gal4 and DB331-Gal4. Here, the phenotypes elicited in the HS cell dendrites by Dscam +7.6.19.2 and +11.31.25.1 are shown to be highly variable in penetrance but the elicited changes are constant and independent from the used driver lines (UAS-mCD8::GFP/ +; G73-Gal4/ Dscam Isoform or DB331-Gal4/ +; UAS-mCD8::GFP/ +(Bl), Dscam Isoform/ +). When driven by DB331-Gal4, the elicited Dscam +11.31.25.1 overexpression phenotype occurs stable whereas the penetrance rate of Dscam +7.6.19.2 overexpression is not significantly increased (right side). Confocal image stacks were taken with a z-increment of 0.2 µm, a 63X objective and minimized pinhole. Composite images were generated by collapsing ~100 images. Scale bar 50 µm.

5.1.4 Reconstruction and statistical analysis of HSN and HSE dendrites elucidate further characteristics of the Dscam gain-of-function and loss-of function phenotypes

For reconstruction of the main dendritic branches of HS cells an open-source software package, the ‘‘TREES toolbox,’’ was used by Friedrich Förstner. This package provides a general set of tools for analyzing, manipulating, and generating dendritic structure, including a tool to create synthetic members of any particular cell group and an approach for a model-based supervised automatic morphological reconstruction from fluorescent image stacks (Cuntz, H. 2010). Confocal images were taken as a basis for model-based reconstructions (Fig. 30). The expression pattern driven by DB331-Gal4 included two different subgroups of LPTCs: HS and VS cells. Nevertheless, tracing and reconstruction of the main dendritic branches in HS cells was very feasible due to the separate locations of VS and HS cells in different lobula plate layers (Fig. 30). In control flies, UAS-mCD8::GFP and an additional cytosolic GFP (UAS-cytoGFP) marker were both expressed. This dual labeling resulted in a clear outline of the branching structures that enabled tracing of the dendritic processes. In Dscam +11.31.25.1 flies, expression of the mCD8::GFP marker turned out to be sufficient for reconstructing the remaining cell branches. Dscam gain-of-function phenotype decreased the density of cell structures, which simplified tracing of the main branching patterns. Therefore, Dscam loss-of-function and Dscam gain-of-function were eliciting opposing phenotypes in HS cells.

The dendritic density of HS cells was enhanced to such an extent in Dscam null flies that only a detailed reconstruction of the entire branching pattern of HSN revealed the high frequency of self-crossing events in Dscam loss-of-function cells (Fig. 31 B: arrowheads). In control flies, the endogenous self-avoidance mechanism prohibited any self-crossing events (Fig. 31 D).

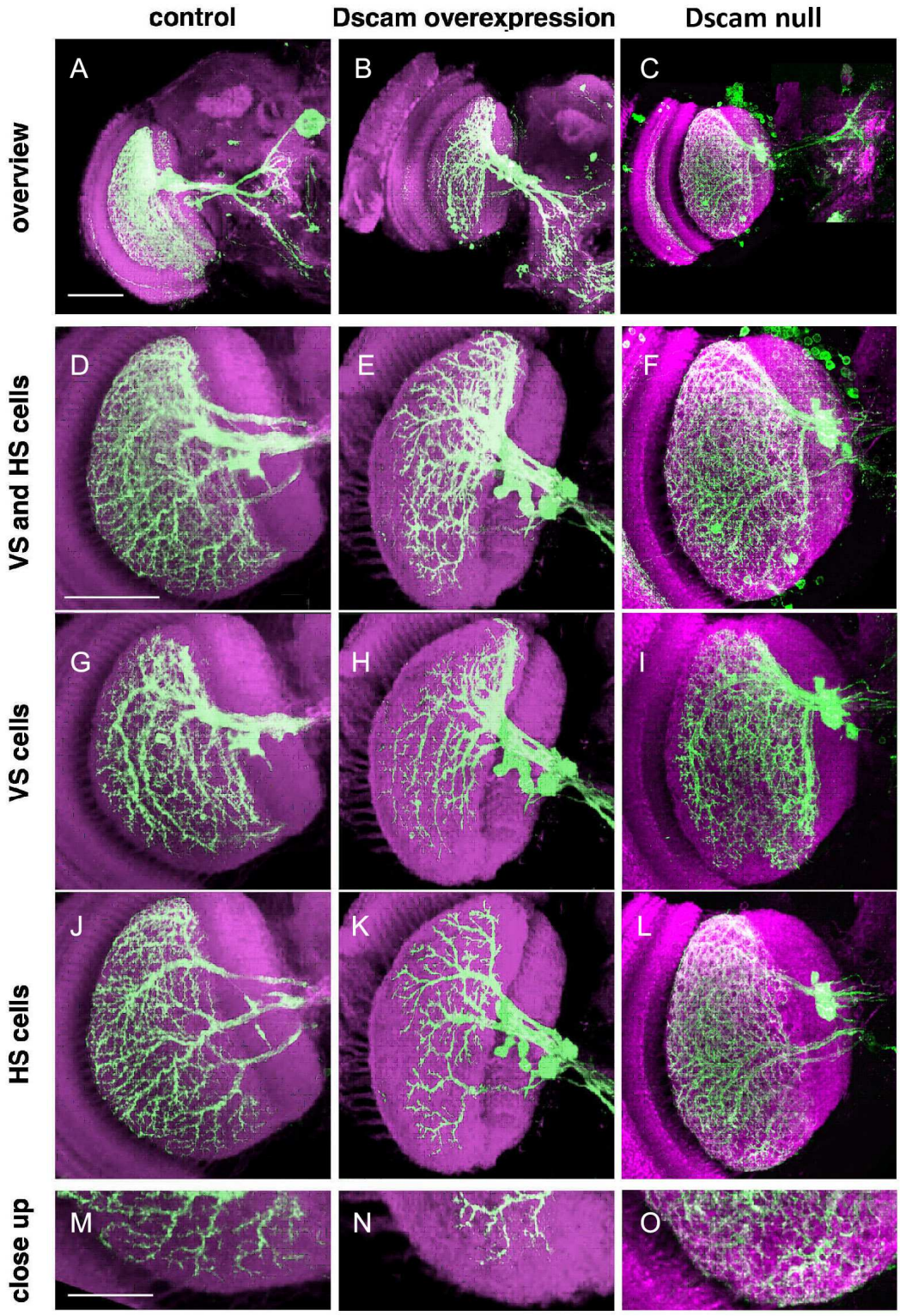

Fig. 30: Different phenotypes elicited by genetic manipulations of the endogenous Dscam codes in LPTCs.

Here LPTCs in control (DB331-Gal4; mCD8::GFP/ Bl), Dscam gain-of-function (DB331-Gal4/ +; mCD8::GFP/ Bl; Dscam +11.31.25.1/ +) and Dscam loss-of function flies (DB331-Gal4; FRT42D,

tubGal80/ FRT42D, Dscam^21; UAS-mCD8::GFP/ UAS-FLP) are shown. The expression pattern driven by DB331-Gal4 includes 3 HS and 6 VS cells labeled with mCD8::GFP (green). The lobula plate contours are labeled with anti disc-large (magenta). (A-C) Overview images already allow some differences to be assumed in the cell anatomy between control and Dscam +11.31.25.1 and Dscam null cells. (D-F) Images of the lobula plate show a dense expression pattern within the lobula plate. By using the Amira 'Oblique Slice' software toolbox, it was possible to separate the HS cells layer entirely from the VS cell layer. (G-I) Consistent with the findings made in HS cells, manipulation of the Dscam code elicits similar phenotypes in VS cells. Dscam +11.31.25.1 cells show reduced dendritic fields and Dscam loss-of-function elicits dendritic fasciculations. (J-L) Hence, HS cells can be observed independently. (M-O) Close up images of the ventral part of the lobula plate show lateral parts of HSS cells. In control cells (M) the ramifications extend to the lobula plate border whereas in +11.31.25.1 flies the dendritic tips do not reach that border (N). Furthermore, dendritic branching density is strongly reduced. (O) In contrast to the gain-of function phenotype, Dscam loss-of-function massively increases pattern density. The ability to separate HS from VS cells is also fundamental in reconstructing the neurons. Confocal image stacks were taken with a z-increment of 0.2 µm, a 63X objective and minimized pinhole. Composite images were generated by collapsing ~150 and 50 images respectively. Scale bar 50 µm. Reconstruction data was kindly provided by Friedrich Förstner.

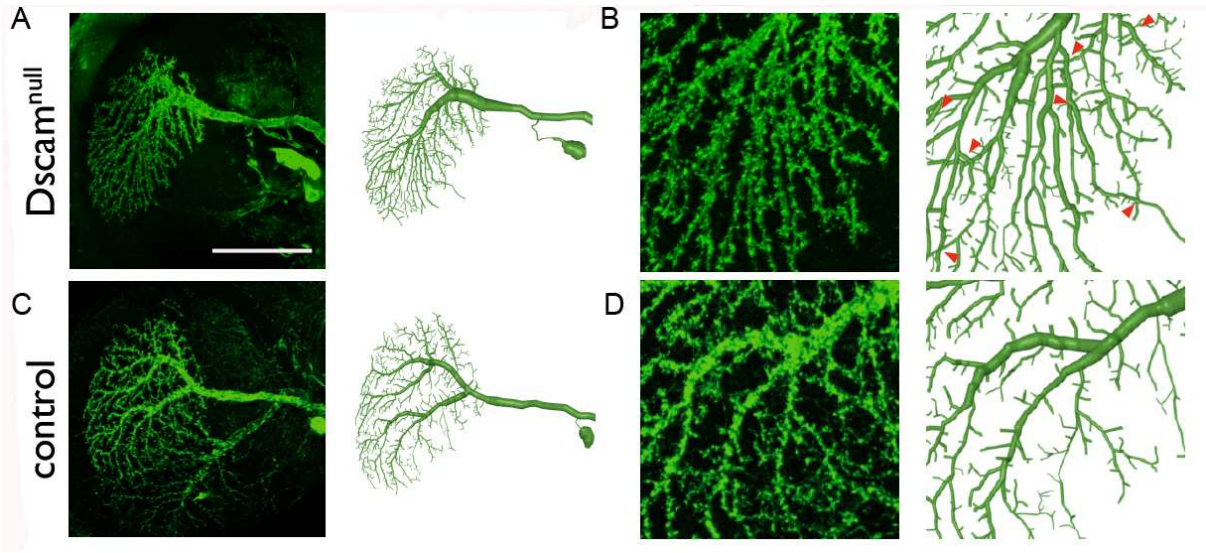

Fig. 31: Detailed reconstruction of the entire dendritic branching pattern reveals the high frequency of self-crossings in HS cells missing the Dscam code.

Image data taken for reconstruction are shown on the left sides. Corresponding reconstructions are illustrated on the right sides. (A +C) Overviews of the reconstructed HSN cell dendrites from control (UAS-mCD8::GFP; G73-Gal4) and Dscam null flies (DB331-Gal4; FRT42D, tubGal80/ FRT42D, Dscam^21; UAS-mCD8::GFP/ UAS-FLP). (B) Close up of the reconstructed cell in (A) reveal several self-crossing events caused by lack of the Dscam code (red arrowheads). (C) Close ups of the reconstructed wildtype cell in (B) show that in wildtype cells self-avoidance mechanisms prohibit crossing of sister branches. Confocal image stacks were taken with a z-increment of 0.2 µm, a 63X

objective and minimized pinhole. Composite images were generated by collapsing ~150 images. Scale bar 50 µm (A+C) and 15 µm (B+D). Reconstruction data was kindly provided by Friedrich Förstner.

Statistical analysis of ten reconstructed HSN/ HSE pairs (Fig. 32 A), further underlined the previous anatomical observations. The dendritic fields were strongly impaired in Dscam gain-of function cells. In Dscam +11.31.25.1 flies, the HS-cell dendrites covered a far smaller area in the lobula plate than in wildtype flies (Fig. 32 C). The coverage values were obtained by connecting the dendritic tips that were farthest away from the main branch. With that, the outline of the dendritic field was determined, which gave an approximated value for the coverage areas. In addition, the lobula plate areas were also defined for each set of reconstructed HS cells. By calculating the lobula plate areas covered by the HS cell outlines, the obtained values were normalized, excluding individual size variations from animal to animal. The wildtype HSN coverage values were on average around 38 % and reduced to 25 %. Moreover, the coverage by HSE was reduced from 60 % to 35 %. Furthermore, the overlap areas of HSN and HSE dendrites were determined, thereby demonstrating consistent results to the previous finding. The average areas significantly shrunk from ~2700 µm² to ~1000 µm².

As the analysis of the individual cell shapes demonstrated a clear decrease in size of the dendritic terminals, the question occurred whether something had changed within the lobula plate itself. Therefore, the size of the lobula plate was calculated and indeed revealed an increase of 15 % (from 9500 µm² to 11000 µm²) compared to control samples.

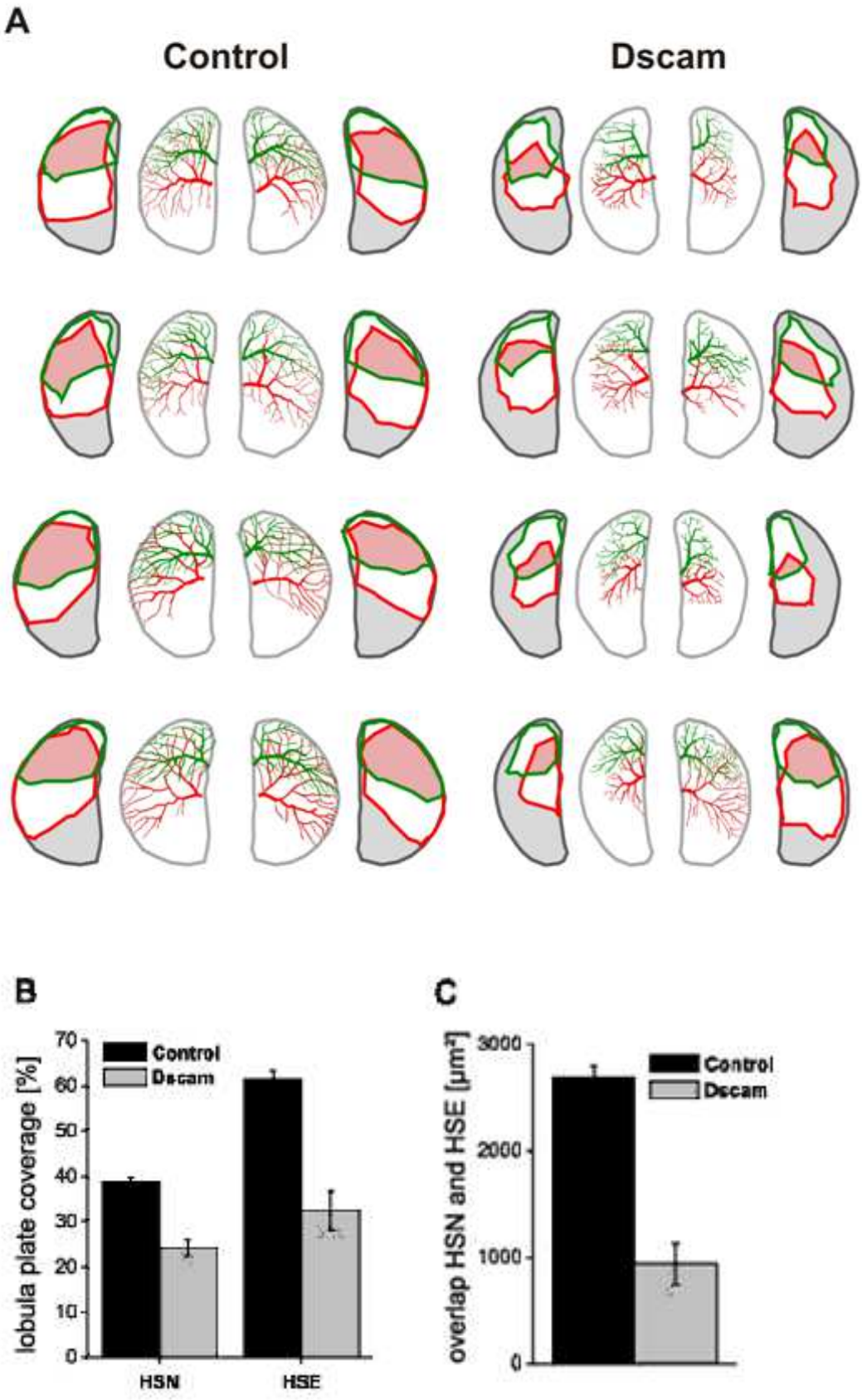

Fig. 32: Analysis of the reconstructed dendrites of HSN and HSE reveals a strong decrease in their dendritic fields.

8 pairs of HSN (green) and HSE (red) main dendritic branches were reconstructed from control flies (DB331 Gal4/ +; UAS-mCD8::GFP/ +; UAS-cytoGPF/ +) (A) and Dscam +11.31.25.1 flies (DB331 Gal4; UAS-mCD8::GFP/ Bl; Dscam +11.31.25.1/ +). The lobula plate borders are illustrated in grey. The approximated coverage areas in the lobula plate are shown in green for HSN and in red for HSE. The cross section areas in which HSN and HSE outlines share common areas are marked in red. In those overlap areas heteroneural interactions between both cells might take place. (B) Analysis of lobula plate coverage areas demonstrates that Dscam misexpression causes a reduction of around 35% in HSN cells (from 38% to 25%) and in HSE of around 42% (from 60% to 35%). (C) Analysis of the overlap areas of HSN and HSE dendrites reveals expected results. In control flies, both dendrites overlap at an area of ~2700 µm² that is more than 90% of the entire dendritic area of the cell. In +11.31.25.1 flies, this overlap is strongly reduced to a value of ~1000 µm². Reconstruction data and analysis were kindly provided by Friedrich Förstner.

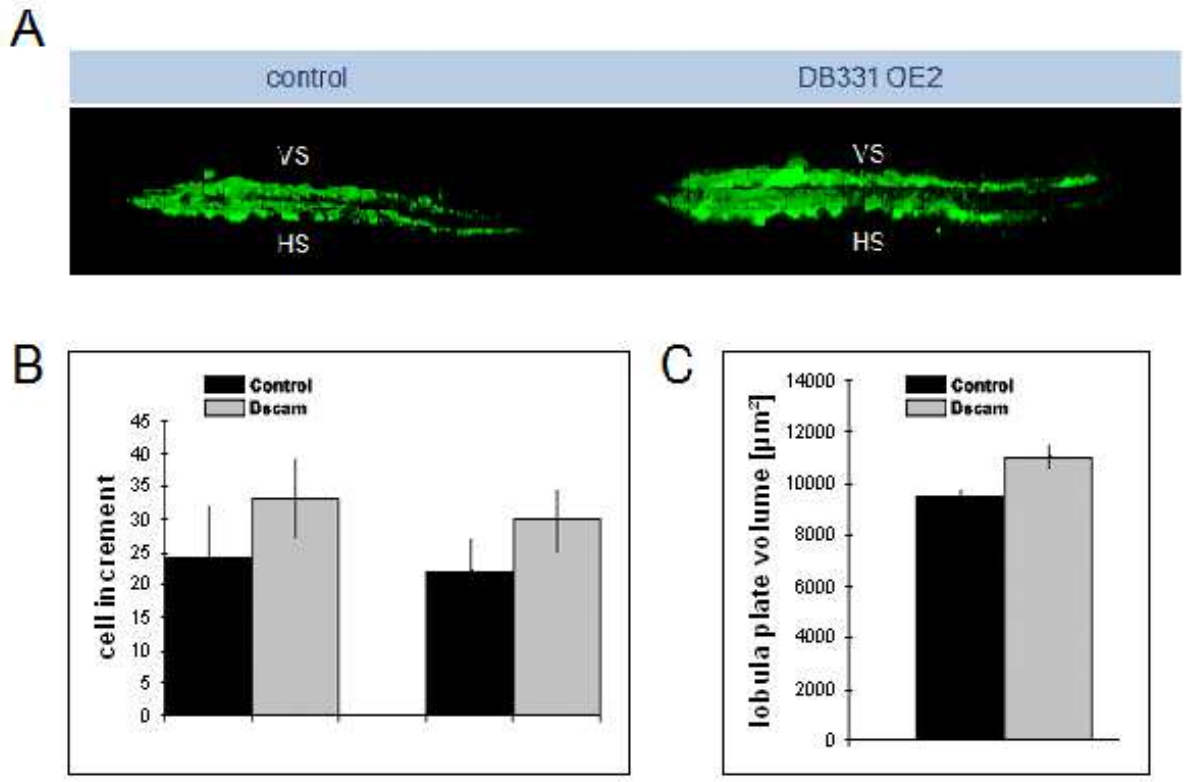

Fig. 33: Dscam +11.31.25.1 elicits increased spacing between HS and VS cell layers and expansion of the entire lobula plate.

(A) The horizontal view of HS and VS cell layers (green) in control (DB331-Gal4; UAS-mCD8::GFP; UAS-cytoGFP) and Dscam +11.31.25.1 flies (DB331-Gal4/ +; UAS-mCD8::GFP/ Bl; Dscam +11.31.25.1/ +) indicates the increased distance between the layers of both cell groups elicited by Dscam misexpression. For an appropriate view of the cell layers, the three-dimensional images from +11.31.25.1 and control flies were aligned and all parameters accordingly adjusted. Afterwards, oblique slices were selected. Statistical analysis in (B) demonstrates a stronger increment of HSN and HSE with Dscam overexpression and with that an increased penetration in the z-axis. In addition, the

entire lobula plate area is enlarged (C). Confocal image stacks were taken with a z-increment of 0.2 µm, a 63X objective and minimized pinhole. Images show single slices.

Further observations of the distance between the HS to VS cell layers in the lobula plate were performed, showing an increase in the space between. Calculations of the cell increment, i.e. the cell depth of HSN and HSE dendrites were analyzed by looking at the strength of HS cell bending in z-axis within the lobula plate. In wildtype flies, HS cells were also not planar but following the elliptic shape of the lobula plate until the outer borderline. There, the branches curve shapely into the other lobula plate layers like the outermost VS cell layer. Consistent with the previous findings, an increased bending of HSN and HSE cells in +11.31.25.1 flies was found (Fig. 33).

Taken together, this study provided a quantitative analysis of the elicited Dscam gain-of function phenotype in HS cell dendrites. The results underlined the anatomical observations and revealed a massive decrease in dendritic branches leading to smaller coverage areas of the HS cells in the lobula plate. However, +11.31.25.1 had an opposing effect on the entire lobula plate, causing an increased dendritic field of about 20% and hence a larger cell increment in the z-axis.

5.1.5 The elicited Dscam gain-of-function phenotype is a non-cell-autonomous effect

With a MARCM-analysis, Dscam +11.31.25.1 was overexpressed restrictively in single cells. This study was intended to answer the question whether the misexpression phenotypes were caused by direct interactions between HSN and HSE, between HS cells and columnar neurons or cell autonomous effects. If Dscam is acting cell autonomously in HS cells, then single clones should reveal Dscam +11.31.25.1 phenotype independently of the overexpression in other cells. Alternatively, if single Dscam +11.31.25.1 cells do not show any alterations in phenotype, then this would suggest a non-cell-autonomous effect. Around 500 brains needed to be dissected and analyzed in order to obtain a single HSN clone (Fig. 34). Consistent with the findings in various other studies, the labeled HSN did not show the characteristic lack of distal arborizations of the +11.31.25.1 phenotype. This result provided the first hint that the +11.31.25.1 phenotype was only elicited when two interacting cells both possess the same Dscam isoform on their membranes. However, due to the low number of observed single HS clones, a further experiment should provide supportive result.

This experiment was carried out by Bettina Schnell, in the electrophysiology setup. Here, Dscam null flies from a previous experiment (DB331-Gal4; FRT42D, tubGal80/ FRT42D, Dscam^21; UAS-mCD8::GFP/ UAS-FLP) were used. Dscam null cells were GFP labeled. Here, a fluorescent dye (Alexa-Fluor 569/ Invitrogen) was injected into non-fluorescent wildtype cells located close to HS cells, which were Dscam null in order to observe non-cell-autonomous effects of Dscam mutant cells. The wildtype cell in Fig. 35 did indeed show fasciculations of higher order branches (arrowhead) as well as self-crossings of sister branches (arrow) that were most probably caused by interactions with Dscam null cells.

In addition, the MARCM analysis revealed other cell types that were included in the expression pattern of DB331-Gal4 (Fig. 36). Notably, there were couples of lobula plate intrinsic neurons; trans-lobula plate neurons, trans-medulla neurons labeled. Whether these neurons were interacting with LPTCs has yet to be investigated.

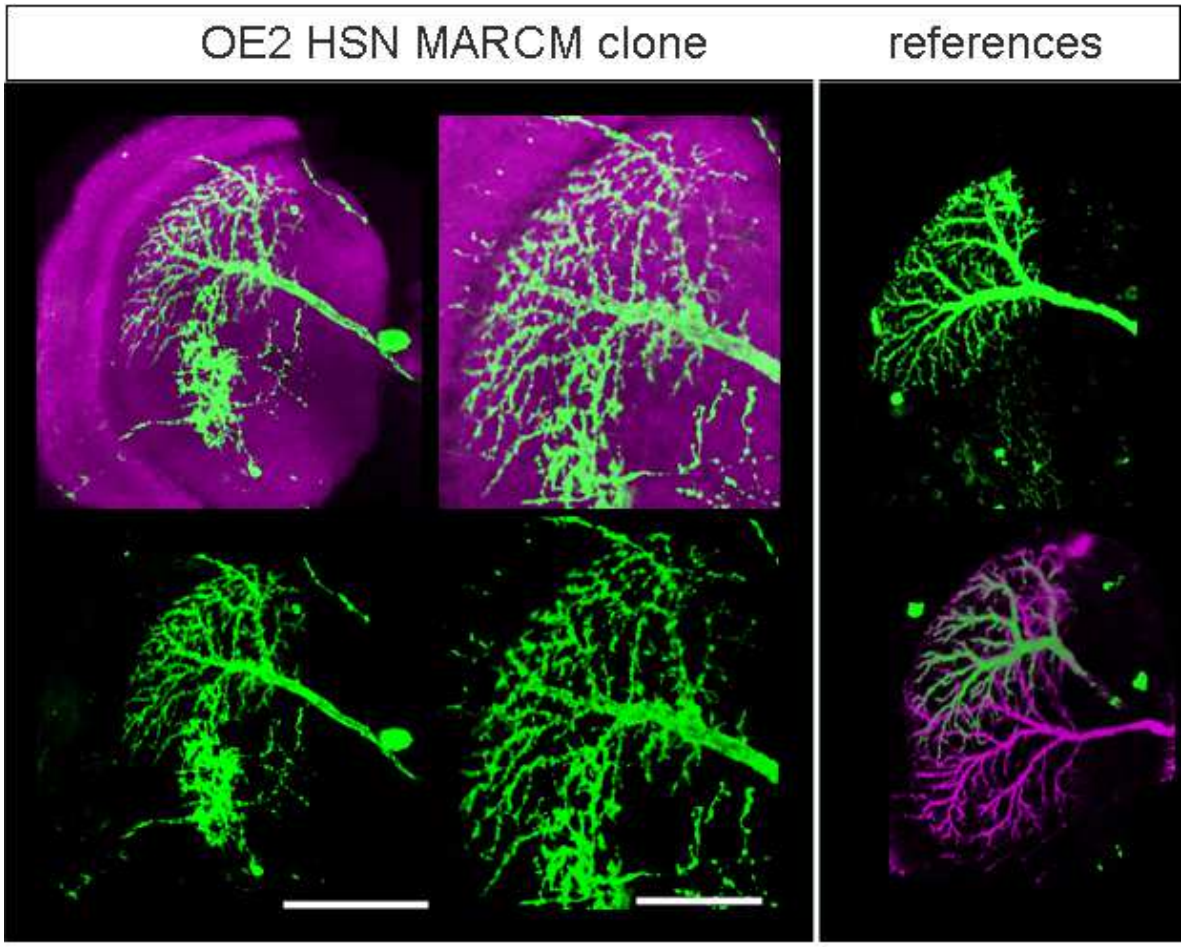

Fig. 34: Overexpression of Dscam +11.31.25.1 in single HSN cells does not elicit mutant phenotype.

Overexpression of Dscam +11.31.25.1 in single GFP labeled HSN cell (green) via MARCM does not change in the dendritic arborization pattern. DB331-Gal4 was used as driver line and mCD8::GFP to label cells. For background, staining anti-disc large (red) was used. As morphological wildtype references, single HS cells are depicted: Single HSN labeled with mCD8::GFP and HSE additionally labeled by Alexa Fluor 568 in G73 expression pattern. Single HSN cells with Dscam +11.31.25.1 are not morphological altered. Confocal image stacks were taken with a z-increment of 0.2 µm, a 63X objective and minimized pinhole. Composite images were generated by collapsing ~150 images. Scale bar 50 µm and 25 µm (close up).

These results provided the first evidences of a non-cell autonomous effect of Dscam gain-of-function phenotype in HS cells.

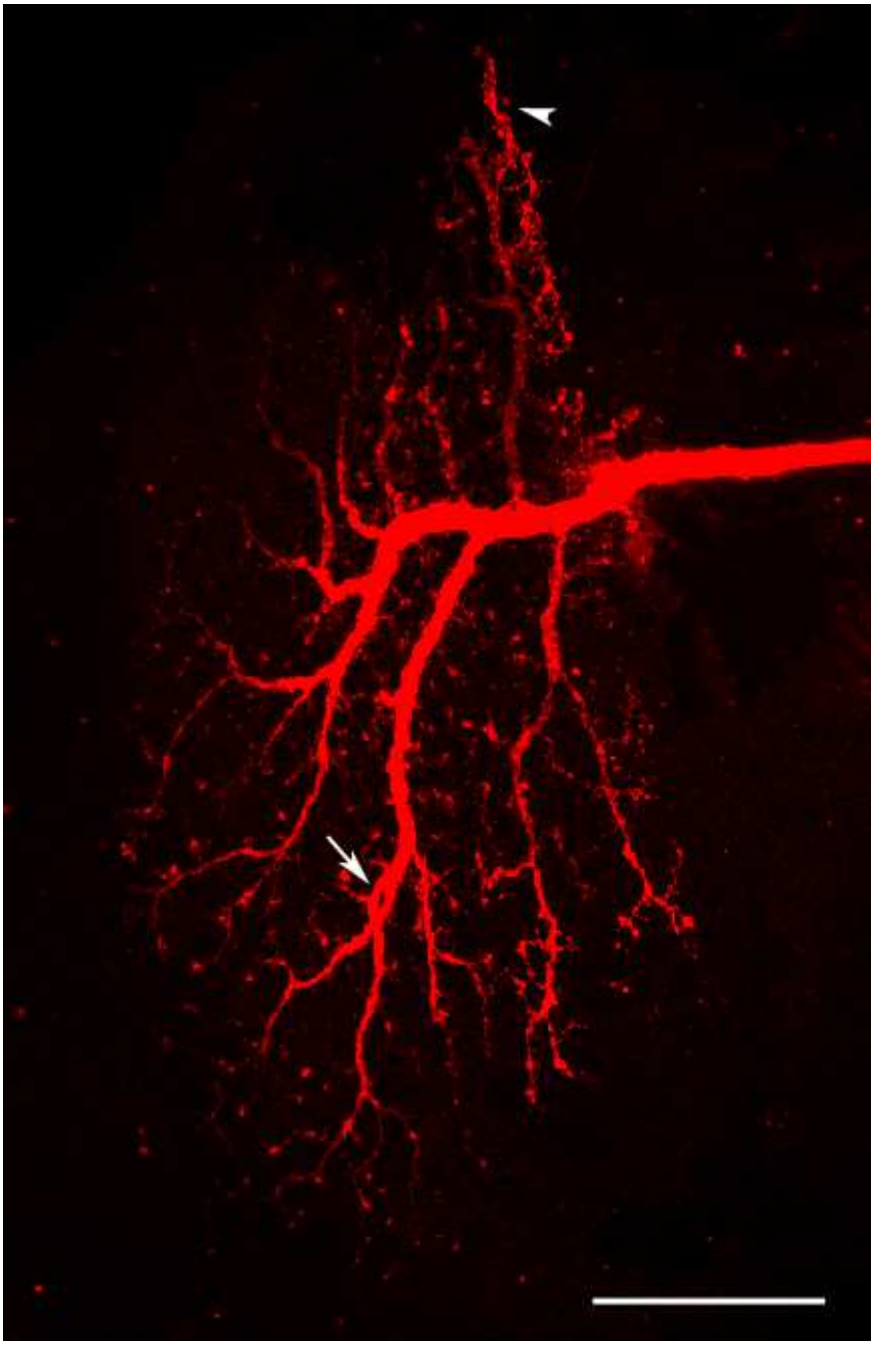

Fig. 35: Dscam null cells elicit self-crossings and fasciculations in wildtype cells.
In Dscam null flies (DB331-Gal4; FRT42D, tubGal80/ FRT42D, Dscam^21; UAS-mCD8::GFP/ UAS-FLP) a fluorescent dye (Alexa Fuor 568) was injected into the soma of a non-GFP labeled, wildtype cell located close to the HS cellbodies. The branching pattern located in the lobula plate shows clumping of higher order branches (arrowhead) as well as self-crossing of sister branches (arrow). As this cell still possesses its Dscam code, the observed phenotype is most probably elicited through interactions with neighbored Dscam null cells and points to a non-cell-autonomous Dscam effect. Confocal image stacks were taken with a z-increment of 0.2 µm, a 63X objective and minimized pinhole. Composite images were generated by collapsing ~150 images. Scale bar 25 µm.

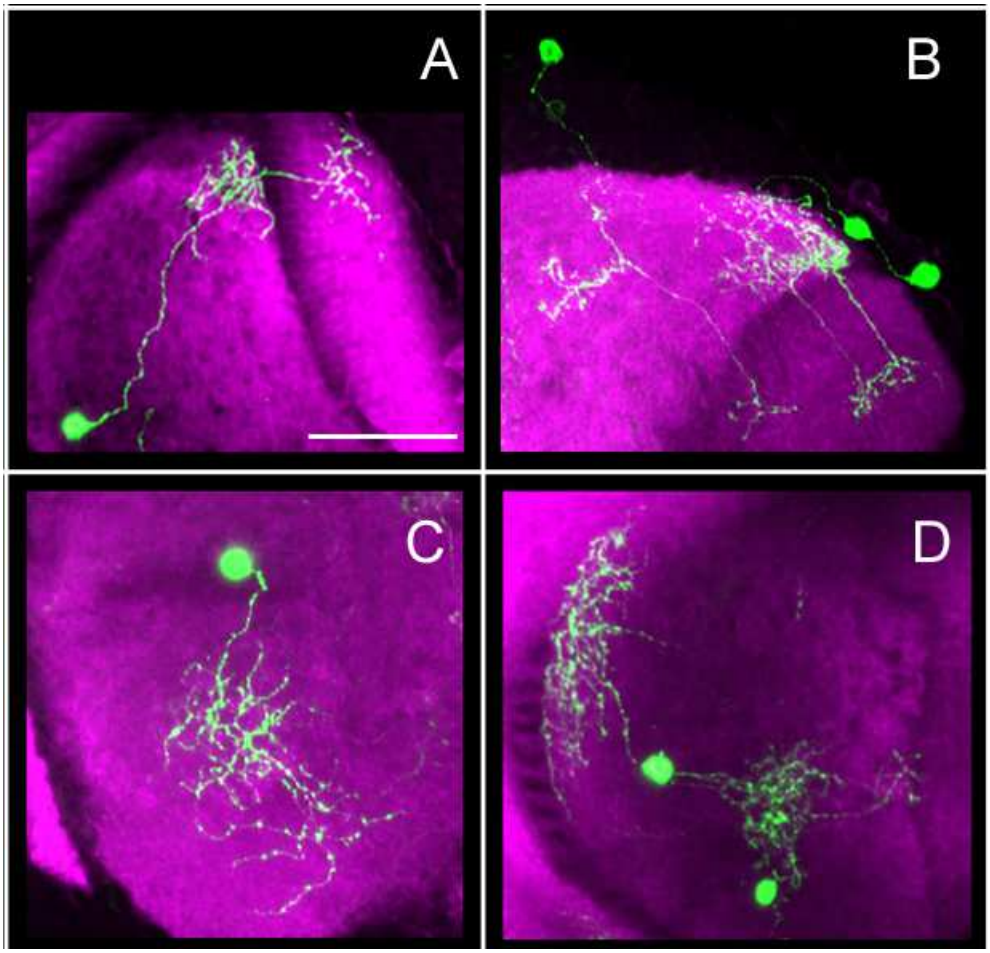

Fig. 36: MARCM analysis reveals different cell types within DB331-Gal4 expression pattern.
A number of various cell types within the expression pattern of DB331 were detected through MARCM analysis. There are various Trans-Lobula Plate cells GFP labeled (green) which possess ramifications both in the lobula plate and in the lobula and thus connect both neuropils (A+B). In addition, the expression pattern contains lobula plate intrinsic neurons (C+D). As background, staining anti-disc large (magenta) was used. Confocal image stacks were taken with a z-increment of 0.2 µm, a 63X objective and minimized pinhole. Composite images were generated by collapsing ~50 images. Scale bar 25 µm.

5.1.6 The Dscam +11.31.25.1 dendritic phenotype depends on the onset of expression during development

To indicate the developmental time points at which Dscams have an influence on the dendritic outgrowth and pathway finding in HS cells, the following transgenic flies were generated: DB331-Gal4/ +; tub-Gal80ts/ UAS-mCD8::GFP; +/ TM6. Here, temperature-sensitive tubulin-Gal80 was used to control Gal4 activity. As long as the flies were kept at 18℃, Gal80 was inhibiting Gal4. Therefore, flies were developing under wildtype conditions at 18℃. By shifting the temperature to 30℃, Gal80 became inactivated and Gal4 activated. With that, the onset of Dscam +11.31.25.1 was triggered to different developmental stages of the fly. The temperature shift was implemented at three different stages: larval stage L3, pupa stages P30-36 and P42-48 and flies were observed in adult stage. If different Dscam isoforms were regulating different processes at different time points during the development of HS cells, then the onset of Dscam +11.31.25.1 should be critical for the elicited phenotypes.

The results demonstrated that onset of Dscam +11.31.25.1 overexpression at 3rd instar larval (L3) stage or around P35 were both causing reduced dendritic fields and a decrease in branching complexity of LPTCs (Fig. 37). However, onset of Dscam +11.31.25.1 at P35 caused a more severe reduction of dendritic ramification than the onset at L3 stage. When Dscam +11.31.25.1 was induced at P45 or later on, then the dendrites retained the wildtype morphology. Dscam +11.31.25.1 onset between P42 and P48 elicited intermediate phenotypes. Here, the dendritic fields were unaltered as in case of control flies (DB331-Gal4/ +; UAS-mCD8::GFP/ CyO; +/ TM6) whereas the branching pattern appeared less dense with a decrease in higher order branches. These observations lead to the assumption that Dscam misexpression was not able to influence dendritic targeting once the branches were established their final patterning. In order to prove this hypothesis, the developmental growth of wildtype HS cells was observed. The results revealed that the main branches were covering their final dendritic fields at P45. This coincidence provides the evidence that Dscams might be mainly involved during dendritic outgrowth.

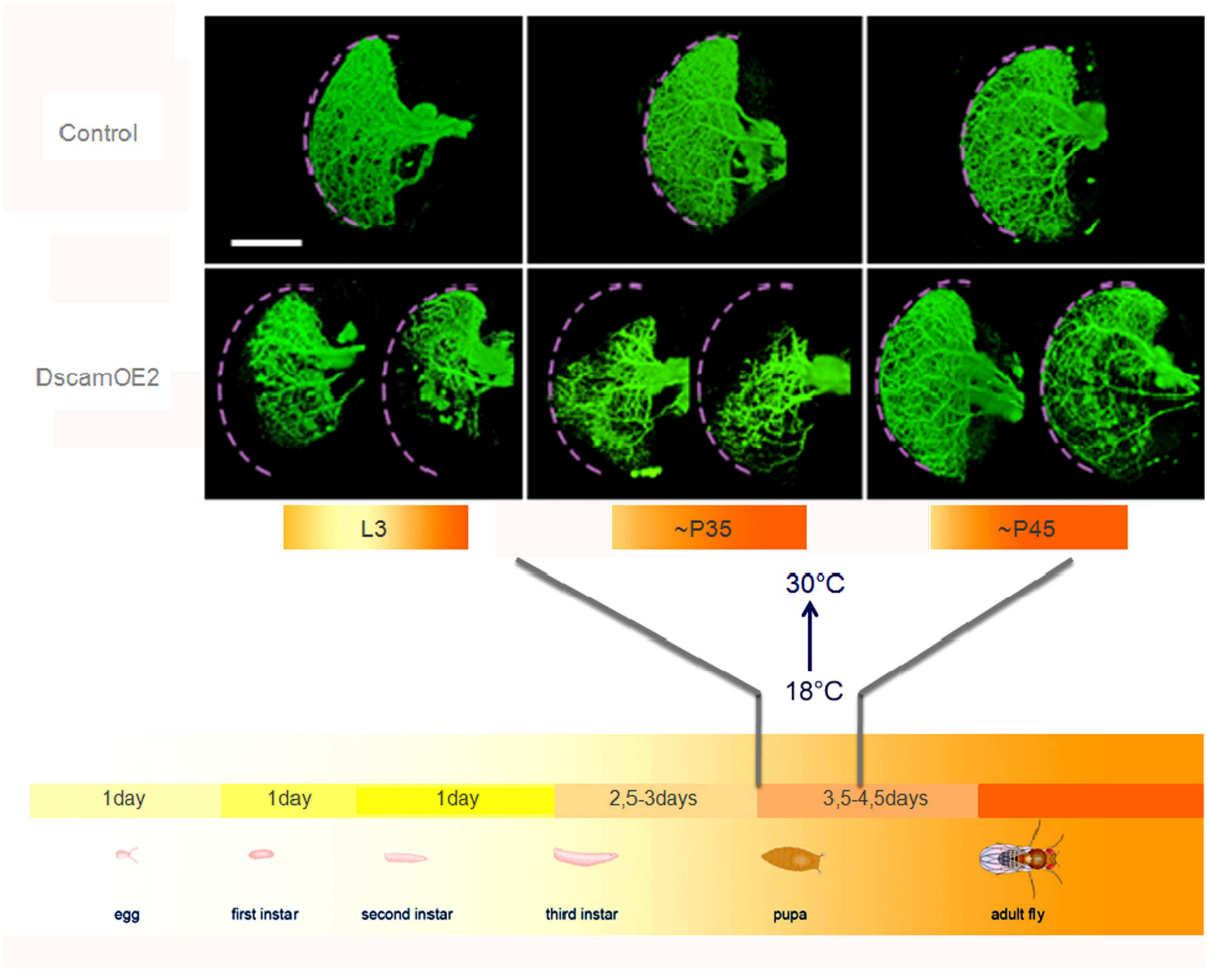

Fig. 37: Dscam +11.31.25.1 phenotype depends on the onset of expression in HS cells.

The scheme illustrates the developmental stages and corresponding temporal periods of *Drosophila*. DB331-Gal4/ +; tub-Gal80ts/ UAS-mCD8::GFP; +/ TM6 flies and control flies (DB331-Gal4/ +; UAS-mCD8::GFP/ CyO; +/ TM6) were kept at 18℃ until tem perature shift. At 18℃, no GFP expression was observable, corresponding with no Gal4 activity. A temperature shift to 30℃ was implemented at 3 different developmental stages: larval stage L3 and during pupa stages at ~P35 and ~P45. Flies were then constantly kept at 30℃ until adult stage. Bra ins from +11.31.25.1 induced flies as well as control flies were analyzed in adulthood. Confocal image stacks were taken with a z-increment of 0.2 µm, a 63X objective and minimized pinhole. Composite images were generated by collapsing ~150 images. Scale bar 50 µm.

5.1.7 HS cells with Dscam gain-of-function phenotype still possess fundamental connectivities

HS cells possess a density of nicotinic acetylcholine (nAchR) and gamma aminobutyric acid (GABA) receptors on their dendritic branches. In order to investigate whether nAchRs were still present on the remaining dendritic branches of Dscam +7.6.19.2 and +11.31.25.1 HS cells, staining with fluorescent α-bungarotoxin-Alexa 647 was performed. This peptide extracted from *Bungarus multicinctus* venom binds with high affinity to the α-subunits of the nAchR in the brain. A detailed description of the procedure is available in previous study (Raghu et al. 2009)

In fact, in Dscam +7.6.19.2 as well as Dscam +11.31.25.1 flies, α-bungarotoxin labeling revealed nAchRs expression on the remaining dendritic tips of HS cells (Fig. 38). However, the receptor density seemed to be strongly reduced in the entire distal area of the lobula plate according to the decrease in branching complexity and dendritic fields in Dscam overexpression flies.

Furthermore, on Dscam +11.31.25.1 cells staining accumulation was detectable (Fig. 38 arrows). All tested lines were stained separately following the same protocol. The α-bungarotoxin labeling revealed remaining nAchRs on the dendritic tips of Dscam overexpression cells.

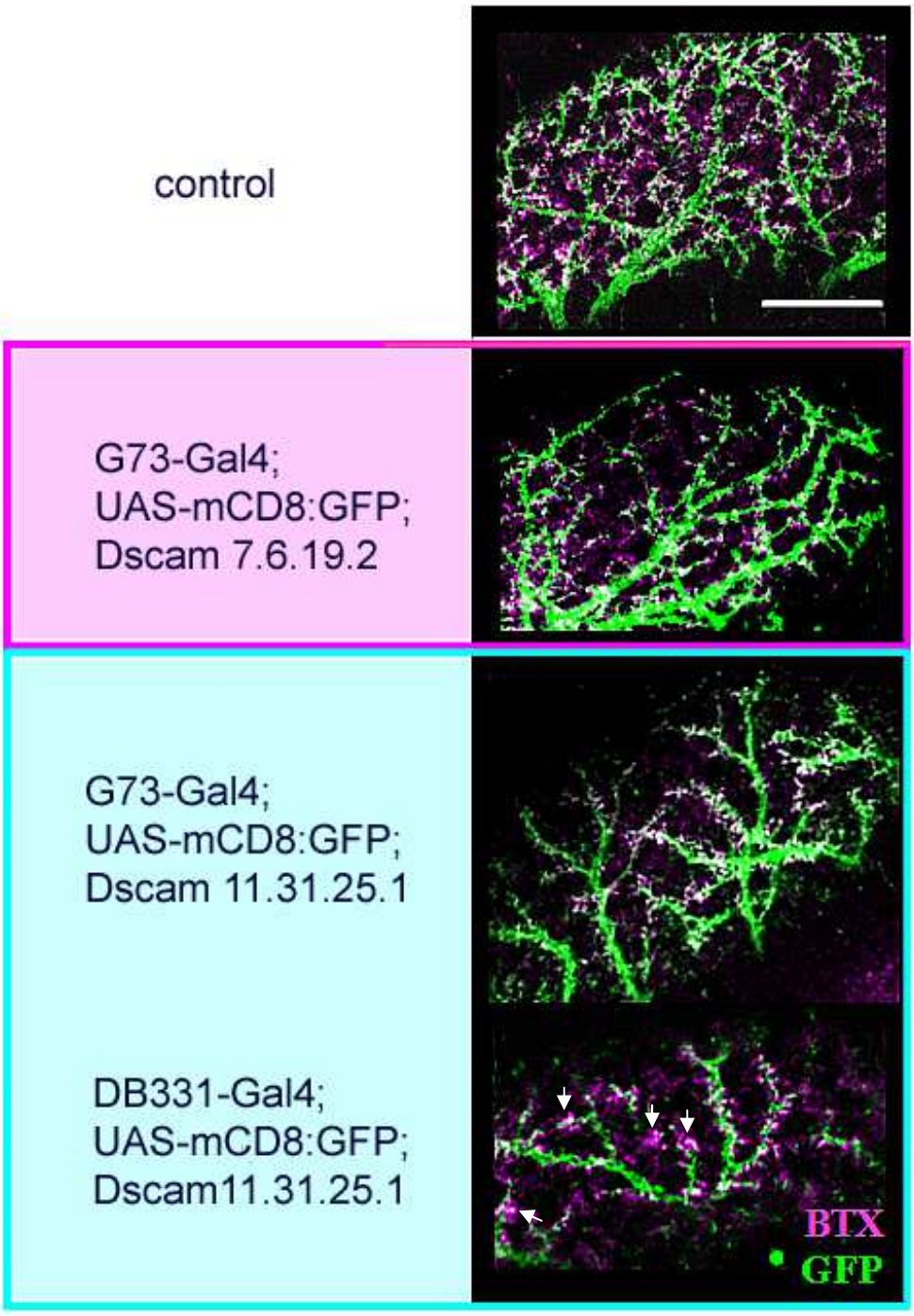

Fig. 38: HS cells with Dscam gain-of-function phenotypes possess detectable nicotinic Acetylchonlinreceptors on their remaining dendrites.

Immunostaining with α-Bungarotoxin (α-Btx) in magenta reveals the presence of nAchR at the GFP labeled dendritic tips of HS cells (green), both in control flies (UAS-mCD8::GFP; G73-Gal4) and the remaining branches of HS cells with Dscam overexpression. Here, Dscam 7.6.19.2 (+7.6.19.2) is depicted in the red box and Dscam 11.31.25.1 (+11.31.25.1) in the blue box. The number of labeled nAchRs seems to be decreased in Dscam overexpression cells. However, as the staining procedure

for each transgenic line was performed separately, differences in labeling intensity can be caused by variations in handling. Confocal image stacks were taken with a z-increment of 0.2 µm, a 63X objective and minimized pinhole. Composite images were generated by collapsing ~5 images. Scale bar 10 µm.

For observing the axonal terminals of LPTCs in Dscam overexpression flies, three specific Gal4 driver lines: GR42H07, GRR35F02 and GR54A03-Gal4 (generously provided by Gerald Rubin) were used, giving a very specific expression pattern of T4/T5 cells alone or including LPTCs (Fig. 39).

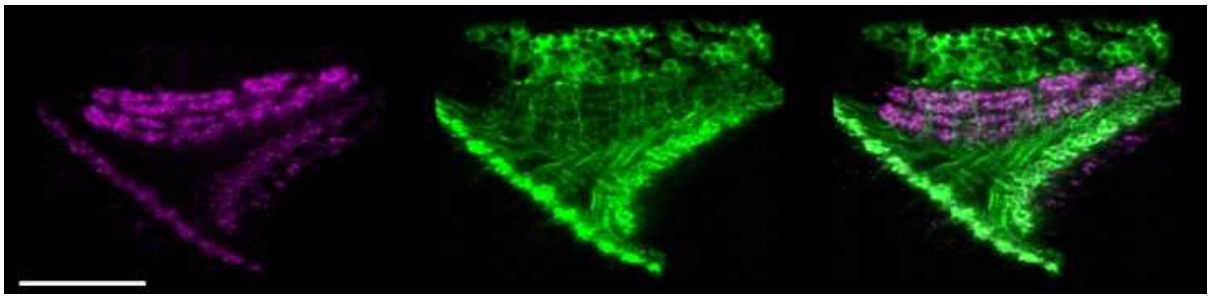

Fig. 39: T4 and T5 neurons possess axonal ramifications in all four layers of the lobula plate.
The driver lines: GR42H07 -Gal4 is used to label T4/T5 cells with mCD8::GFP (green). The additional presynaptic marker: synaptotagmine-HA (magenta) reveals the axonal terminals of these neurons after immunolabeling with a secondary fluorescent antibody. Horizontal sections reveal that T4 and T5 neurons ramify in all four layers of the lobula plate and thereby exhibit potential interactions to LPTCs. Confocal image stacks were taken with a z-increment of 0.2 µm, a 63X objective and minimized pinhole. Composite images were generated by collapsing ~150 images. Scale bar 50 µm.

In order to highlight presynaptic terminals of T4 and T5 synaptotagmine-HA (hemagglutinin) was expressed as a presynaptic marker. To label them anti-HA conjugated with Alexa Fluor 568 was used. Notably, the axonal ramifications of T4 and T5 cells terminated in the same lobula plate layers where the dendrites of LPTCs located. Close up images from horizontal sections as well as frontal sections show overlap areas between green-labeled LPTC dendrites and magenta-labeled T4/ T5 axonal terminals (Fig. 40). These findings support the results from previous studies (Bausenwein, B. 1992 a, b, Fischbach, KF. 1989) revealing potential connectivity between T4/ T5 cells and LPTCs.

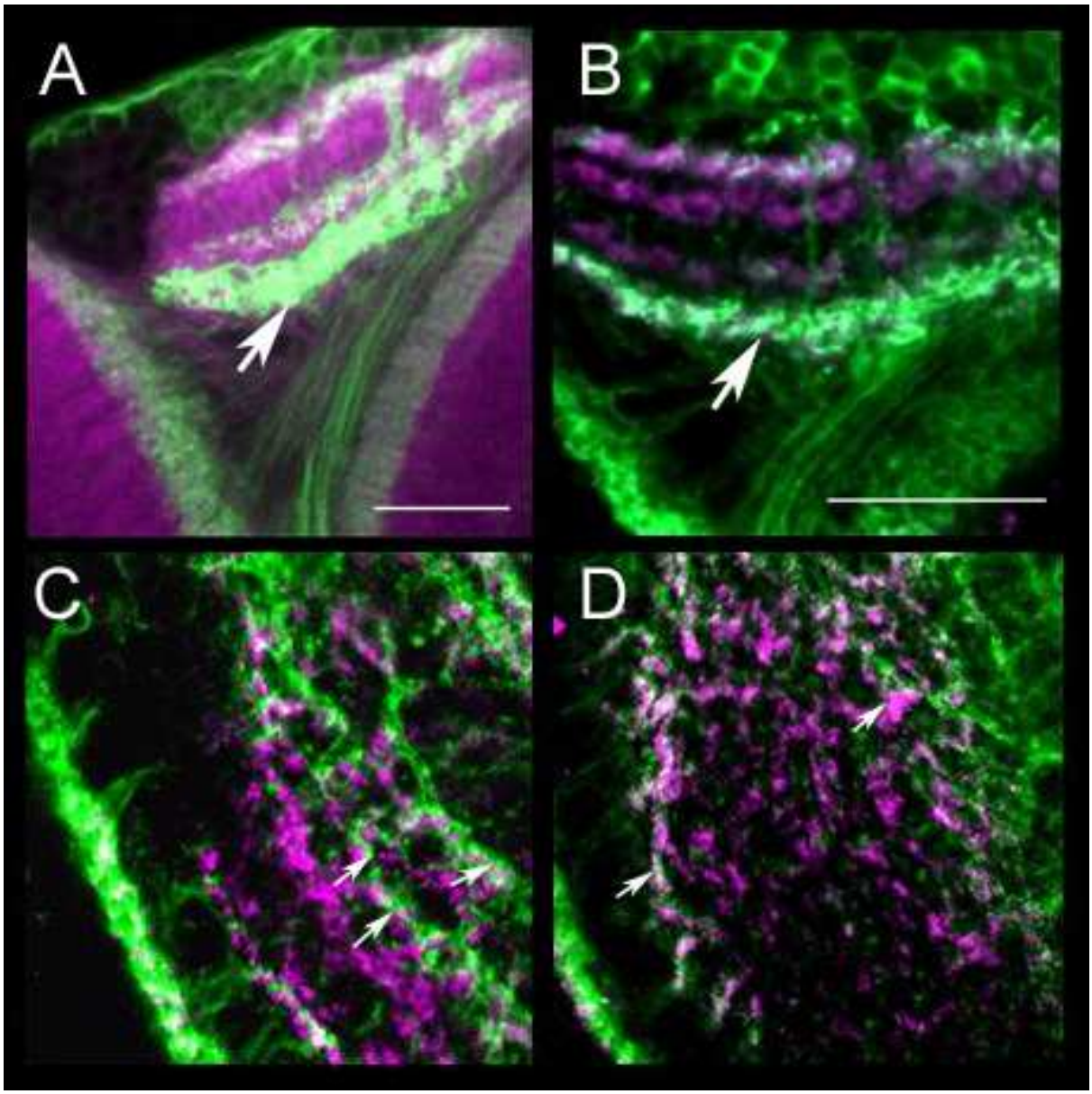

Fig. 40: Axonal terminals of T4/T5 neurons are overlapping with the dendrites of LPTCs.
(A) Horizontal sections of the expression pattern of GR54A03-Gal4 labeled with mCD8::GFP and anti disc-large as background staining reveal the four layers in the lobula plate in which T4 and T5 cells ramify. The section also shows neuritis in the medulla layer 10 and in the superficial most lobula layer. In this case, the expression pattern additionally includes LPTCs. HS cells are located in the innermost lobula plate layer (arrow). (B) Close up of synaptotagmine-HA, labeled terminals (magenta) suggest T4/ T5 cells synaptically contact on HS cell dendrites (arrow). (C) Frontal section supports this assumption and shows many areas where synaptotagmine-HA and GFP colocalize in VS cell dendrites (C) as well as HS cell dendrites (D). Confocal image stacks were taken with a z-increment of 0.2 µm, a 63X objective and minimized pinhole. Composite images were generated by collapsing ~150 images and 5 images respectively in frontal sections. Scale bar 25 µm.

In the next step, GR54A03-Gal4 was used to overexpress Dscam 11.31.25.1 in T4/ T5 cells and LPTCs. Here, the questions were whether Dscam gain-of-function in LPTCs would elicit the same phenotype as observed before and how T4 and T5 cells were impaired by Dscam misexpression. The results revealed that Dscam +11.31.25.1 elicited a constant phenotype in HS cell with a decrease of dendritic fields as well as reduction of branching density (Fig. 41 A). So far, three different driver lines were used for overexpressing the same Dscam isoform and each of them possesses different columnar neurons in its expression pattern. Therefore, the individual Dscam gain-of-function phenotype in HS cells seems to be independent from the Dscam code of surrounding neurons.

Observations of the axonal targeting of T4 and T5 neurons in the lobula plate revealed a disrupted termination pattern (Fig. 41 B, C). The four target layers in the lobula plate were not innervated in a structured way, whereas ramifications in the lobula and medulla could still be recognized in their target layers but were also partially mislocated (Fig. 41 C). For unknown reason it was not possible to express synaptotagmine-HA in parallel to Dscam +11.31.25.1 within T4/T5 and LPTCs. Another morphological change was observable in the locations of T4 and T5 cellbodies: They were forming clusters.

However, due to the lack of any Gal4 driver line that constantly gives an expression only in T4 and T5 cells, it was not possible to distinguish between anatomical changes caused by Dscam misexpression in these cells or non-cell-autonomous Dscam effect from LPTCs.

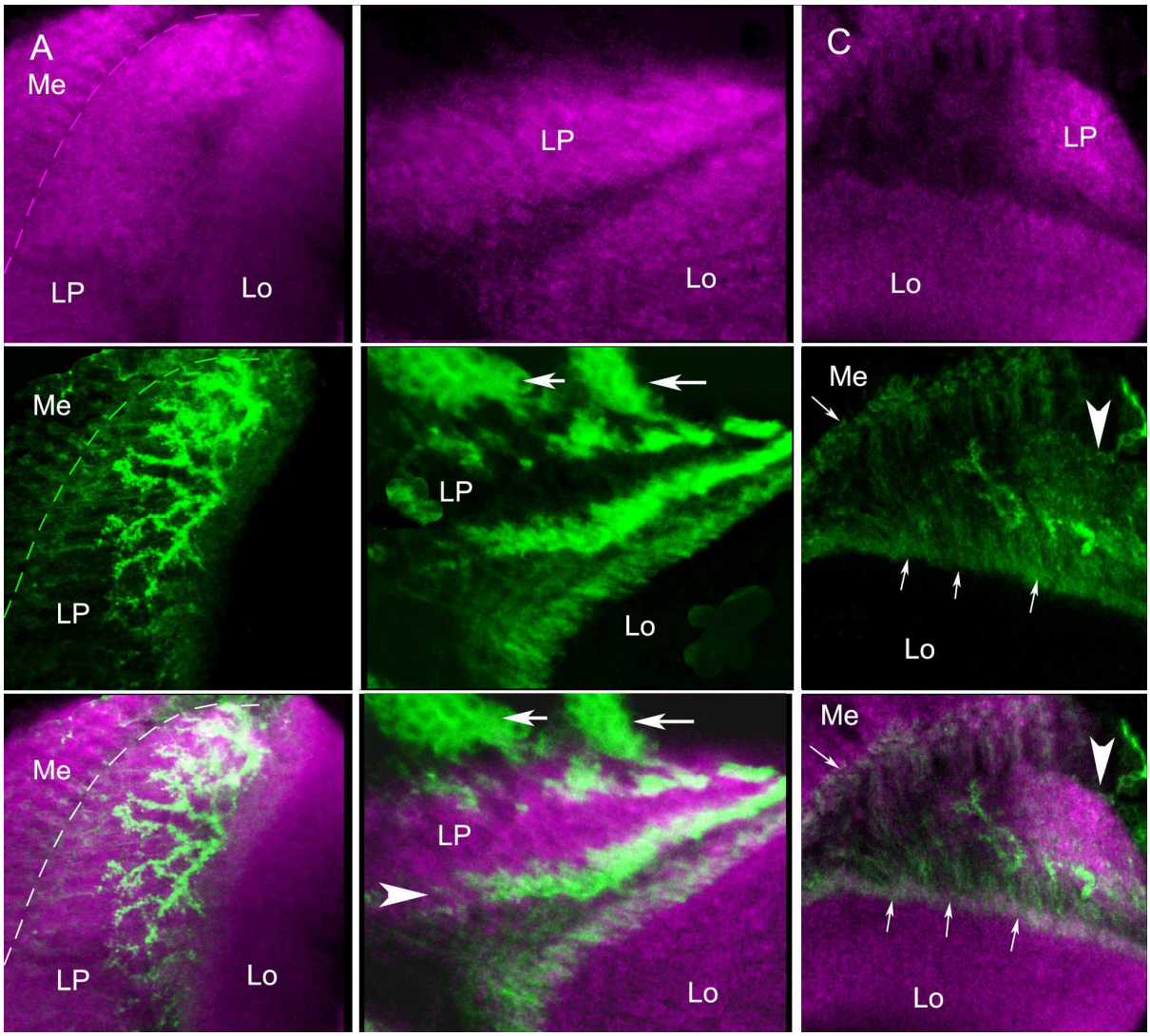

Fig. 41: Overexpression of Dscam 11.31.25.1 in T4/T5 cells disrupts axonal targeting.
GR54A03-Gal4 was taken to drive Dscam +11.31.25.1 in GFP labeled T4/ T5 cells (UAS-mCD:8-GFP/ +; GR54A03-Gal4/ Dscam +11.31.25.1). The background was stained by anti-dsic-large (magenta). (A) HS cell dendrites with Dscam +11.31.25.1 do not reach the distal lobula plate border (dotted line) and possess in general a reduced dendritic branching pattern. (B) The four termination layers of T4 and T5 in lobula plate layer are not detectable anymore. This leads to the assumption that T4/ T5 axons do not terminate in an ordered fashion within the defined layers of the lobula plate (arrowhead). Furthermore, the cellbodies of T4 and T5 cells are clumped together in two major clusters (arrows) located close to the lobula plate. However, this kind of disruption occurs less severely in the lobula and medulla where the pattern is still maintained (C: arrows). Confocal image stacks were taken with a z-increment of 0.2 µm, a 63X objective and minimized pinhole. Composite images were generated by collapsing ~50 images. Scale bar 25 µm.

Besides columnar information processing and connectivity, HS cells also possess a horizontal information flow. It is known that these cells are coupled with each other

via gap junctions (Schnell et al. 2010). Neurobiotin, a dye that passes gap junctions, was injected via a sharp electrode into the cellbody of a HS cell. This experiment was carried out by Bettina Schnell. The results revealed that all three HS cells were still connected in Dscam + 11.31.25.1 flies (Fig. 42). Therefore, the electric coupling was not affected by the reduction of dendritic fields. However, the location of the electric connections is still unknown.

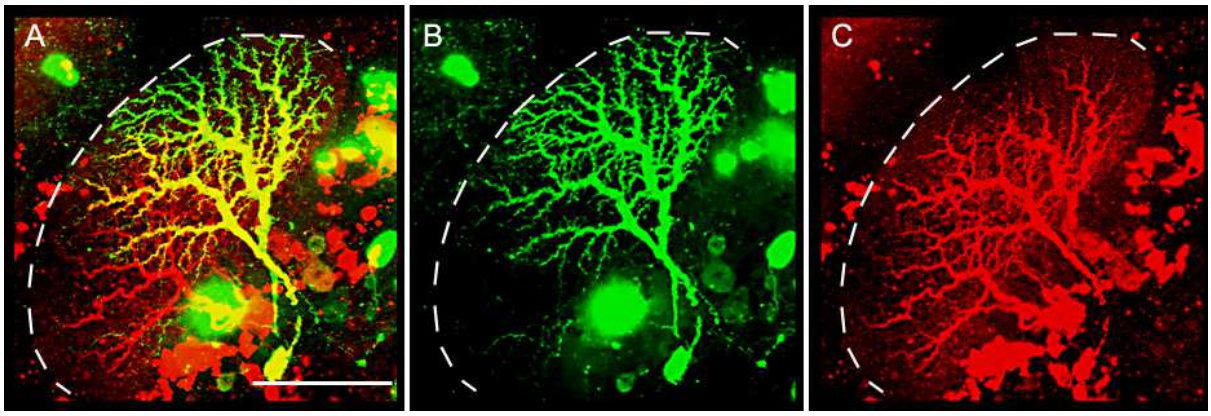

Fig. 42: HS cells with Dscam +11.31.25.1 phenotype are still electrically coupled with each other despite reduced dendritic fields.

(A) Here, HSN was filled by a sharp electrode with neurobiotin (red) in UAS-mCD8::GFP; G73-Gal4/ Dscam +11.31.25.1 flies. (B) GFP labeled HSN and HSE neurons are illustrated in green. Here, HSE possesses a decreased dendritic field and HSN. (C) Neurobiotin was spreading into neighboring HS cells indicating that the cells are still electrically coupled with each other. The dendritic field of neurobiotin labeled HSS also seems be impaired in the observed fly. The dotted line depicts the distal lobula plate border. Confocal image stacks were taken with a z-increment of 0.2 µm, a 63X objective and minimized pinhole. Composite images were generated by collapsing ~100 images. Scale bar 50µm.

So far, the analysis was focused on HS cell dendrites. In the next step, the influences of Dscam overexpression on the axonal terminal were observed. Previous studies showed differences in localization of Dscam isoforms with transmembrane domain 1 (TM1) or transmembrane domain 2 (TM2). It has been suggested that TM2-containing isoforms were distributed along the entire cell surface, while TM1-containing isoforms are largely excluded from axons (Zhan et al. 2004). In this study, two isoforms with different TM-domains, Dscam +7.6.19.2 with TM2 and Dscam +11.31.25.1 with TM1, were identified to elicit a strong dendritic misprojection phenotype. For a closer observation of the different elicited phenotypes, DB331-Gal4

was used as driver line. There, the axonal terminals were easily traceable down to the central brain region. In control flies, the axons of HS and VS cells terminate in two separate destination areas in the central complex: The VS cell axons were located slightly above the esophagus and HS cell axons ventral to the esophagus. In DB331-Gal4, a third axonbundle from yet unidentified cells was descending from the lobula plate terminating dorsal to the esophagus.

Dscam +7.6.19.2 did not change the pathway finding of HS or VS cell axons (DB331-Gal4/ +; UAS-mCD8::GFP/ +; Dscam +7.6.19.2/ +). Flies were observed in adult stages so that nothing was known about the developmental outgrowth itself. Nevertheless, the axon bundles appeared to reach their destination areas in the central complex without showing altered projection pathways. However, the axonal terminals seemed to fasciculate and did not ramify as strongly as in wildtype cells (Fig. 43). In contrast to Dscam +7.6.19.2, misexpression of Dscam +11.31.25.1 was severely disrupting the axonal projection pathways (DB331-Gal4/ +; UAS-mCD8::GFP/ +; Dscam +11.31.25.1/ +). Especially in the HS cell, the axon bundle revealed a great number of single fibers separating from the main axonbundle prior to their destination area (Fig. 43 arrowhead). Compared to control flies (DB331-Gal4/ +; UAS-mCD8::GFP/ CyO), the axons seemed to fail in pathway finding and their terminal branching complexity seemed to be reduced (Fig. 43 asterisks).

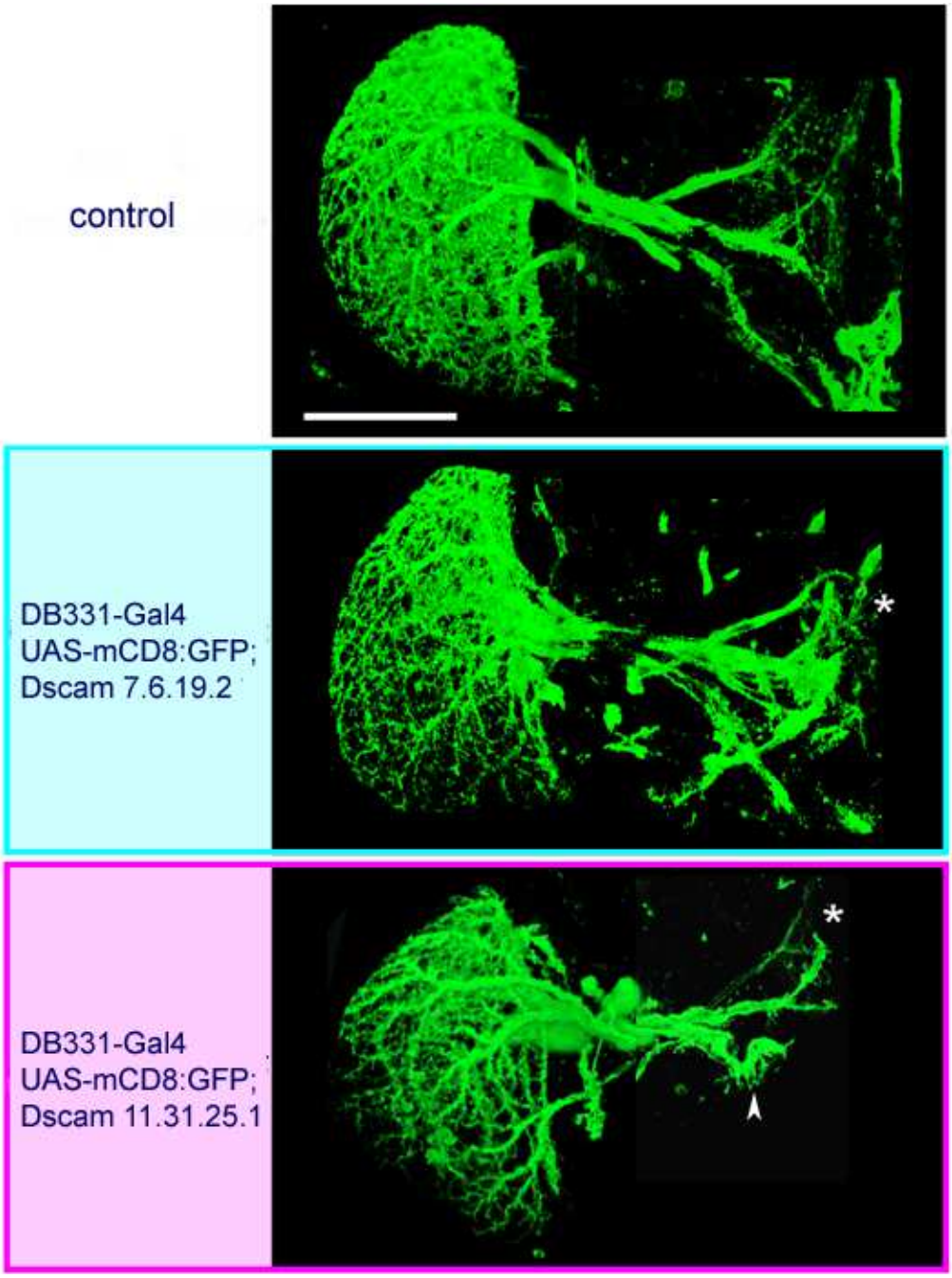

Fig. 43: Dscam misexpression disrupts axonal branching pattern of HS as well as VS cells.
The figure shows the entire cell morphology of LPTCs labeled with GFP (green) (DB331-Gal4;UAS-mCD8::GFP). The mutant phenotype in the dendritic area of Dscam +7.6.19.2 and +11.31.25.1 samples seems to be continued at the axonal terminals. Both Dscam overexpression isoforms elicit a decrease of complexity within the axonal terminal branching pattern (asterisks) whereas in +11.31.25.1 additionally, a strong error in the projection itself occurs (arrowhead). In this case, the axonbundle of HS cells does not only target the wrong area but also ramifies prior to its destination area. Confocal image stacks were taken with a z-increment of 0.2 µm, a 63X objective and minimized pinhole. Composite images were generated by collapsing ~150. Scale bar 50µm.

5.2 Further investigations on the function of LPTCs and their role in flight control: A series of genetic tools

For a better understanding of single LPTCs and their functionality within their environment, several molecular constructs were generated. One approach was to creat constructs that enable to learn more about the molecular and electrophysiological properties of single LPTCs. The second approach was selectively disconnect single LPTCs from each other by RicinA ablation. This should provide a yet unknown insight into the cell-autonomous mechanisms of single LPTCs during development. The third focus lied on the development of a new tracer strategy that uses VSV for labelling single neurons in flies.

5.2.1 Shedding light on the presynaptic input elements of LPTCs

LPTCs receive presynaptic inhibitory input from GABAergic neurons. However, these neurons have yet to be identified. Here, I tried to generate Gal4 driver lines under the control of vesicular GABA transporter (vGat) promoter, which would be the first step towards analyzing the neuronal circuitry. In the publication ?by Enell et al. (2007), the genomic region encoding for the vGat gene was identified as being located on the 2nd chromosome (Fig. 44) in *Drosophila melanogaster*. Therefore, the corresponding promoter region should be located upstream to the gene site. Looking at the genomic assembly upstream of that sequence, it was possible to identify a potential 700 bp region upstream of the gene region, an intron area between the Sox-box and the vGat gene, where the promoter could be present.

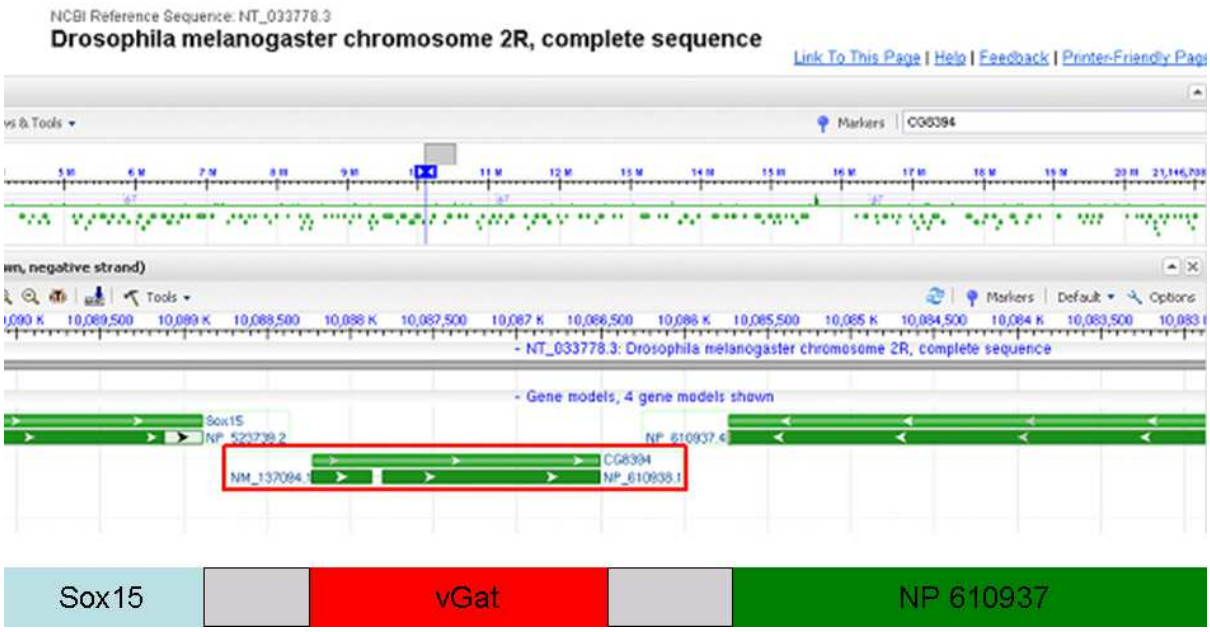

Fig. 44: Identification of the vGat promoter region.

The screenshot from the NCBI search result shows the genomic location of the vGat gene in *Drosophila melanogaster*. The gene is located at the second right (2R) chromosome at CG8394 (red box). The scheme beneath depicts surrounding regions of the vGat gene. Upstream of the vGat gene is an intron sequence of about 700 bp (grey box) before the Sox box (blue box) encoding region starts. Downstream to the gene another intron sequence is followed by the genomic region encoding for NP 610937(green box). Data obtained from NCBI.

Firstly, the 700 bp intron region was cloned into the pChs-Gal4 vector at the KpnI/SacII restriction sites (Fig. 44) (gift from Heisenberg M.). The fragment was amplified within the genome of a wildtype fly using primers flanked with an additional KpnI restriction site at the N-terminus and an additional SacII restriction site at the C-terminus via PCR. The positive transgenic flies were crossed with UAS-mCD8::GFP. Unfortunately, the offspring generation did not show any expression pattern for this construct (Fig. 45). As many promoters do not work without corresponding enhancers, a 4 kb fragment upstream of the vGat gene site was extracted in the next approach. This time, it was possible to observe a strong and wide GFP expression within the salivary glands in early larval stages under the fluorescent microscope. However, during development the strength of GFP expression decreased dramatically. Confocal images were taken from adult brains after immunolabeling with anti-GFP antibody. The images revealed a very faint remaining expression within the cell bodies but no neuronal processes were visible. The decrease in GFP expression

during development points to a homeostatically regulated gene expression that might be due to some influences of Sox box enhancers.

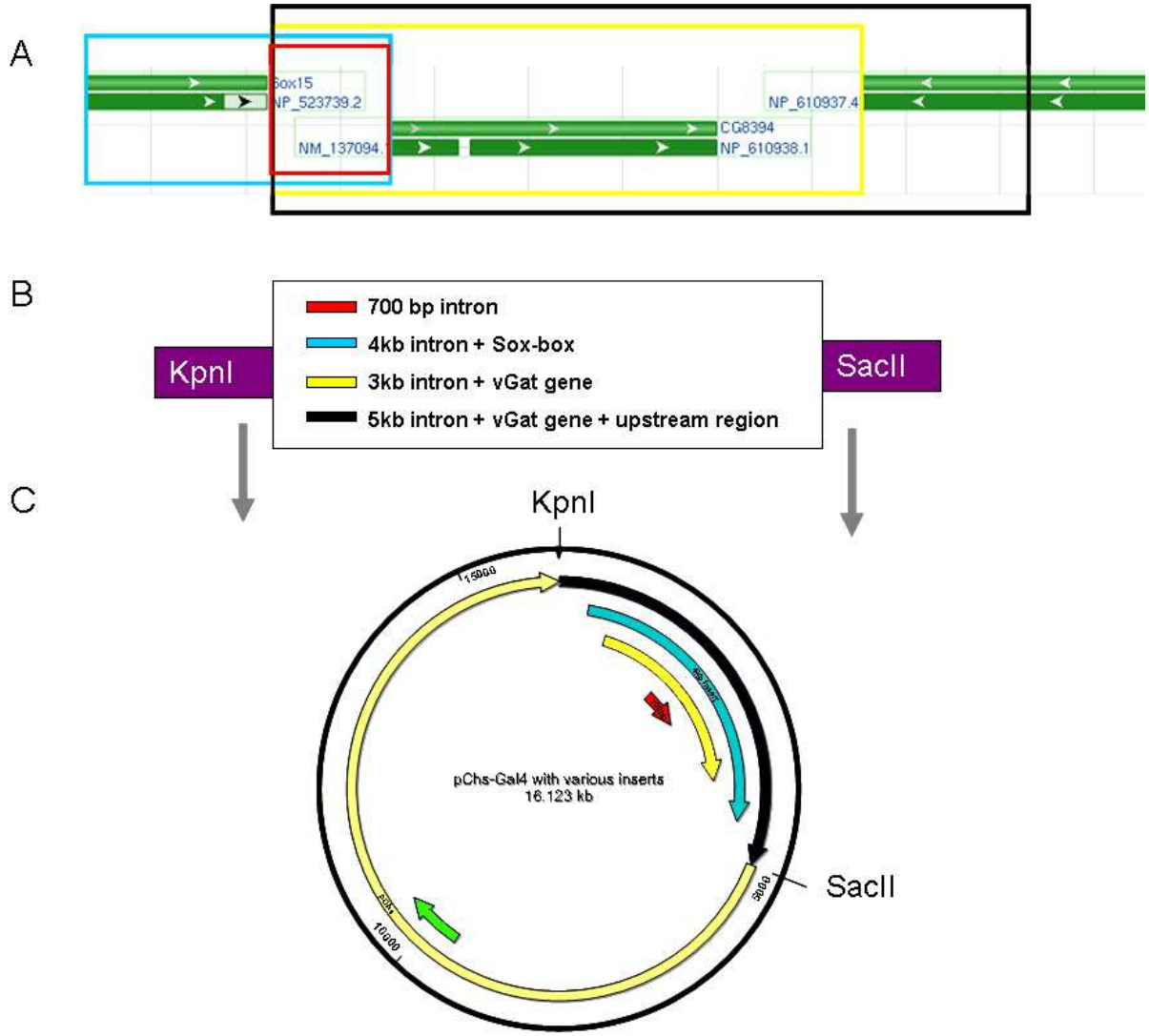

Fig. 45: Screen of vGat promoter and enhancer regions.

(A) Different genome fractions were selected at the surrounding locations of the vGat gene: 1. 700 bp intron region (red box) between the Sox box gene region and upstream of vGat; 2. a 4 kb fragment upstream of vGat (blue box) including a part of the Sox box gene; 3. 3 kb (yellow box) fragment including the intron sequence, the vGat gene sequence, and the intron upstream of vGat; 4. 5 kb fragment (black box) including the region of the yellow box and a small part of the gene downstream of vGat. All fragments were amplified within the wildtype *Drosophila* genome (B) and inserted at KpnI/SacII restriction sites of the pChs-Gal4 vector (light yellow). The pChs vector possesses an Ampicillin resistance sequence (green).

However, the dim expression could also be enhanced by a different fluorescent marker or the expression of several copies of the driver line. Therefore, a different marker was used for revealing the expression pattern. Here, cytosolic GFP showed much higher expression strength than the previously used mCD8::GFP marker. Furthermore, in combination with immunolabeling it was possible to detect neuronal processes (Fig. 46). Although, the expression strength was thereby enhanced, it was still not bright enough for potential single-cell analysis. Based on these results, a new set of experiments were started, this time targeting sequences downstream of the intron part.

As enhancers were not exclusively located upstream of the gene sequence but also downstream and even within the gene coding region itself, a 3kb fragment including the whole vGat gene and a 5kb fragment including the sequence of the following gene and a further intron region were cloned into the Gal4 vector.

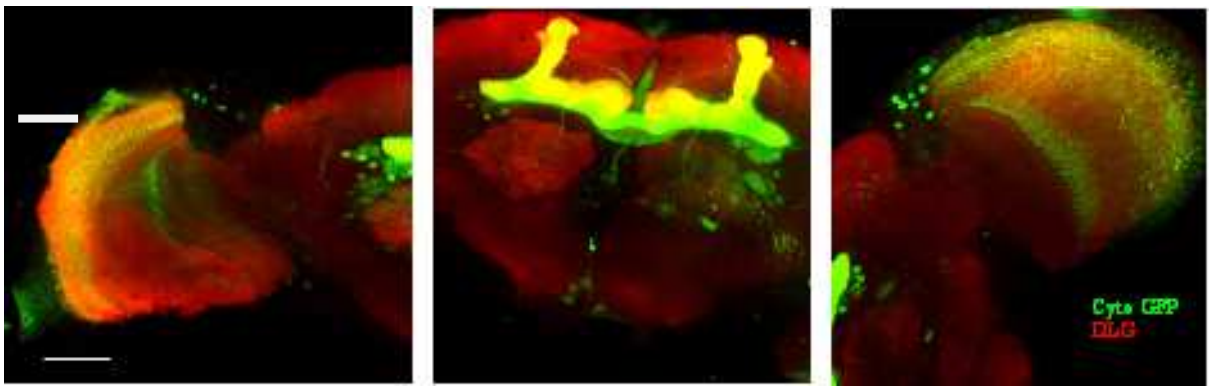

Fig. 46: Expression pattern driven with vGat-Gal4 4kb fragment reveals neurons in the optical lobe as well as in the central brain.

The expression of vGat 4kb-Gal4 driven pattern is restricted to small neuronal subpopulations in the optical lobes (left and right) and the central brain (middle). As a marker protein, cytosolic GFP was used and for background staining anti disc-large was applied. Confocal image stacks were taken with a z-increment of 0.2 µm, a 20X objective and minimized pinhole. Composite images were generated by collapsing ~100 images. Scale bar 50 µm.

The vGat-Gal4 3 kb flies did not drive GFP expression in any cells whereas vGat-Gal4 5 kb transgenes showed a strong GFP expression in the guts during larval stages. However consistently, in adult flies only very weak GFP was detected in neurons of the central brain, optical lobes, and ventral ganglia (Fig. 47). Here, the

results revealed the enhancers of the vGat promoter were neither present within the gene sequence nor downstream of the subsequent intron area.

The conclusion therefore was that the only vGat enhancer region detected throughout this series of DNA extraction was the one in the vGat-Gal4 4kb construct upstream of the vGat gene.

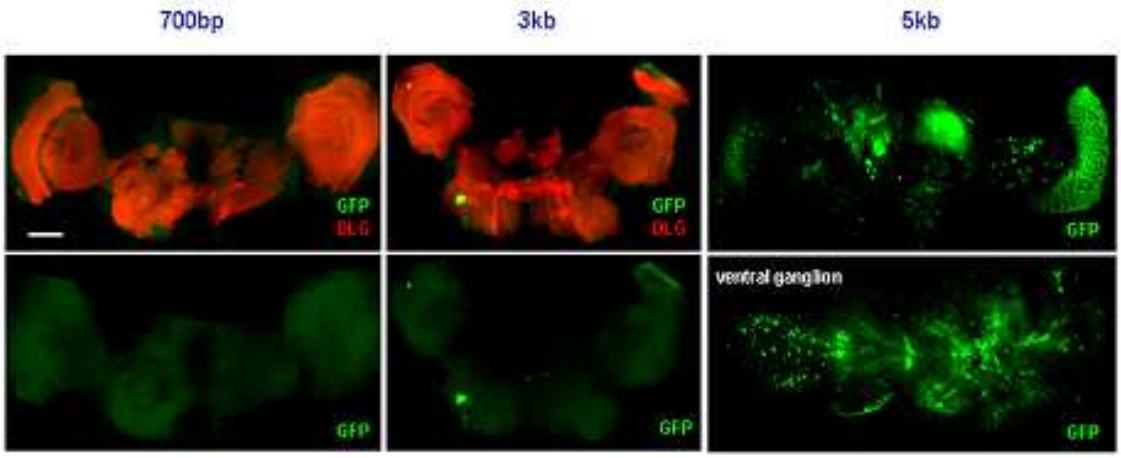

Fig. 47: Systematic dissection of the genomic regions around the vGat promoter region and anatomical analysis of various vGat-Gal4 transgenic flies.

In this picture, the different expression patterns of three vGat-Gal4 constructs are illustrated. For neuronal labeling mCD8::GFP was used (green). The first 700bp intron sequence upstream of the vGat-gene sequence does not give any expression pattern within transgenic flies. Furthermore, transgenic flies with downstream fragments (3kb and 5kb) of the vGat gene region do not give any reasonable, strong expression pattern. In the 3kb construct, only single cells are labeled. In the 5kb construct, a diffuse pattern within the central brain as well as the ventral ganglion appears. Confocal image stacks were taken with a z-increment of 0.5 µm, a 40X objective and minimized pinhole. Composite images were generated by collapsing ~100 images. Scale bar 50 µm

5.2.2 UAS->Stop>TN-XXL: refined expression of a genetic encoded calcium indicator

TN-XXL represents an efficient tool for the analysis of activities in neurons. However, using this indicator under the control of the UAS system requires Gal4 driver lines with a highly restricted expression pattern in order to be able to recognize the cell region from which the recording was made. I tried to confront this problem by generating a construct with a FRT (Flippase Recognition Target) flanked Stop sequence for spatial restriction of TN-XXL expression. The Stop sequence will prohibit translation of the downstream-located TN-XXL sequence. Here, the Flippase recombination enzyme can induce site-directed recombination of FRT sites leading to removal of the Stop sequence. In addition, Flippase expression in transgenic flies carrying heatshock Flippase (hs-FLP) is restricted during heatshock treatment. Therefore, the combination of FRT/FLP system and Stop cassette should enable a restriction of TN-XXL in small subgroups of neurons. Here, I combined classical cloning tools with the gateway cloning system (Fig. 48) for isolating the DNA construct.

Transgenic flies were tested with DB331-Gal4;hs-Flp/CyO impaired with heatshock treatment that was induced at various developmental stages starting 48 hours after egg deposition until late 3rd instar larval stage. Therefore, the resulting number of TN-XXL highlighted LPTCs varied from cell clones to the complete number of LPTCs covered by the DB331 expression pattern (Fig. 49). This indicated that the construct was enabling restrictive expression in the way it was intended, i.e. the Stop cassette was able to prohibit completely the transcription of TN-XXL, and furthermore, it can be efficiently flipped out by heatshock-induced Flipase activity. The confocal images were taken directly after dissection and without fixation or further immunostaining in order to determine the absolute strength of TN-XXL expression within these neurons.

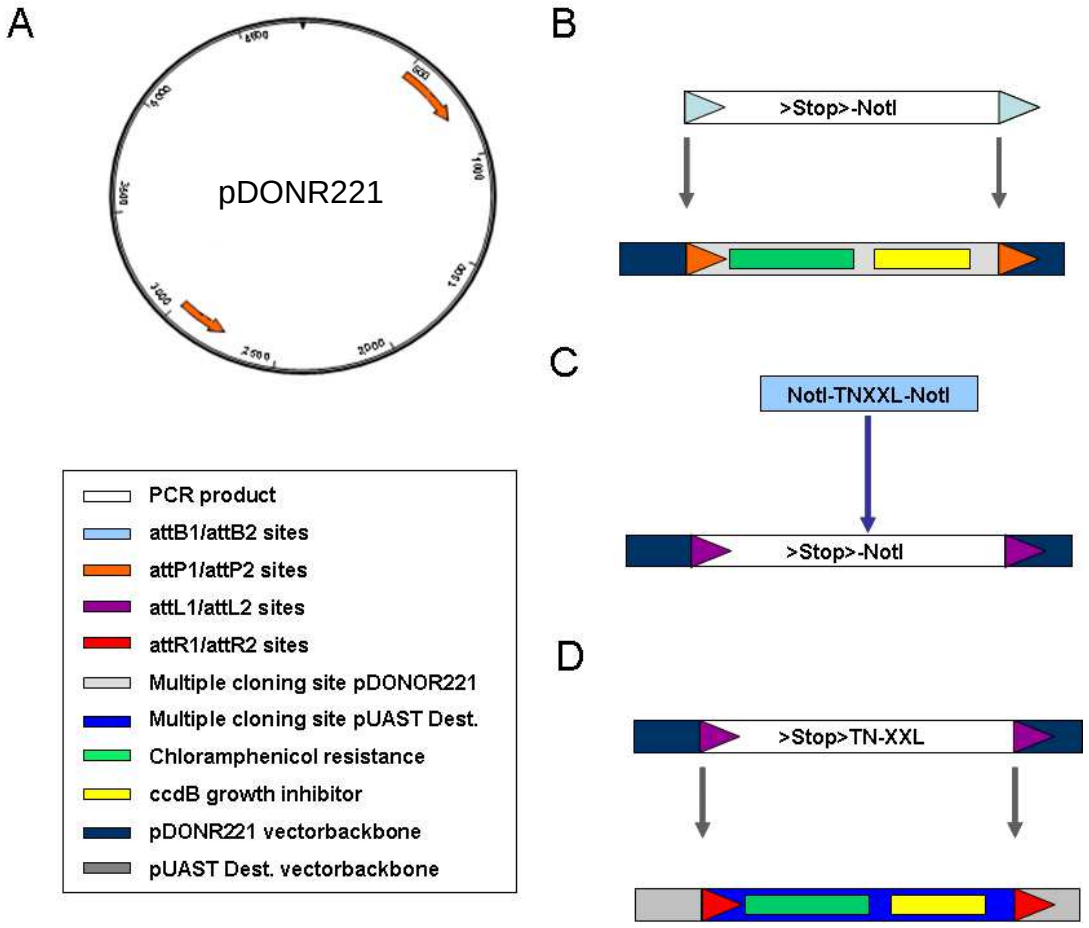

Fig. 48: Molecular approach to generate UAS->Stop>TN-XXL flies.

The scheme shows the cloning strategy for generating the UAS>Stop>TN-XXL vector. Using common cloning strategies did not work in the past. Gateway Cloning Technology' was therefore used primarily here. The pDONR221 (from invitrogen) is depicted in (A). Mainly all cloning steps were performed within this vector, as the size is much smaller than the pUAST destination vector. First, the FRT-flanked Stop sequence (>Stop>) with an additional NotI restriction site at the C-terminus was recombined into the pDONR vectors (B) via BP reaction. Subsequently, TN-XXL was inserted through the NotI restriction site (C). Finally, the completed insert was recombined into the pUAST vector via LR reaction.

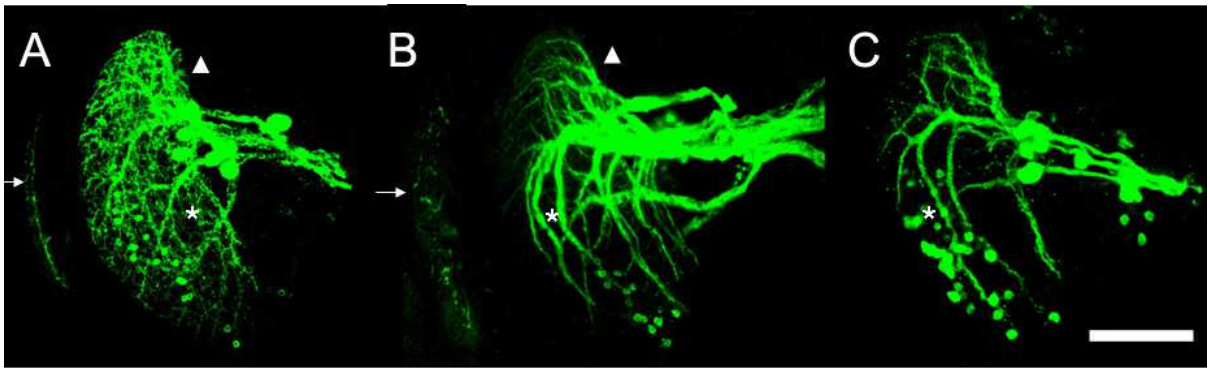

Fig. 49: Heatshock-induced expression pattern in DB331-Gal4,hsFlp;UAS>Stop>TN-XXL.
UAS>Stop>TN-XXL flies were crossed with DB331-Gal4,hs-Flp flies; 2nd and 3rd instar larvae were given heatshock treatment for 2 hours. The TN-XXL expression in green was observable within 24 hours under fluorescent stereomicroscope. Adult brains were dissected for detailed analysis. Compared to control flies (A) with mCD8::GFP expression, a decreased number of LPTCs and general reduction of the expression pattern was observed (B). Depending on the timing of heatshock treatment, different sets of neurons were labeled by TN-XXL. The first TN-XXL sample (left) shows expression in the medulla (arrow) as well as VS (asterisk) and HS cells (triangle) whereas the second sample (right) expresses TN-XXL only in VS cells (asterisk). All mages show the optical lobes in full projection. Confocal image stacks were taken with a z-increment of 0.2 µm, a 63X objective and minimized pinhole. Composite images were generated by collapsing ~100 images. Scale bar 50 µm

Here, it has been demonstrated that the generated UAS>Stop>TN-XXL transgenic flies were indeed working for inducing TN-XXL transcription restrictively in subsets of LPTCs. In order to target specific LPTCs, refinement of the heatshock protocol was needed. Nevertheless, the strength of the expressed TN-XXL was high enough to take high-resolution images via confocal microscope without further antibody treatment and therefore might enable tracing calcium changes within single cells via 2-Photon microscope.

5.2.3 Genetic ablation of LPTCs by expression of RicinA.

Transgenic flies of the stock: UAS>Stop>RicinA (from Luo.L) were used for cell ablation. RicinA is a ribosome-inactivating molecule that should lead to cell lethality. Thus, its expression needed to be controlled and targeted to specific neurons to prevent the fly from dying. Previous experiments have shown that leaky-expression of RicinA from a UAS-RicinA transgene was sufficient to kill. In order to enable the use of RicinA, a translation Stop cassette flanked by FRT sites was introduced. This allows triggering the expression of RicinA both temporal and spatial by using Gal4/UAS system in combination with the FRT/hs-FLP system.

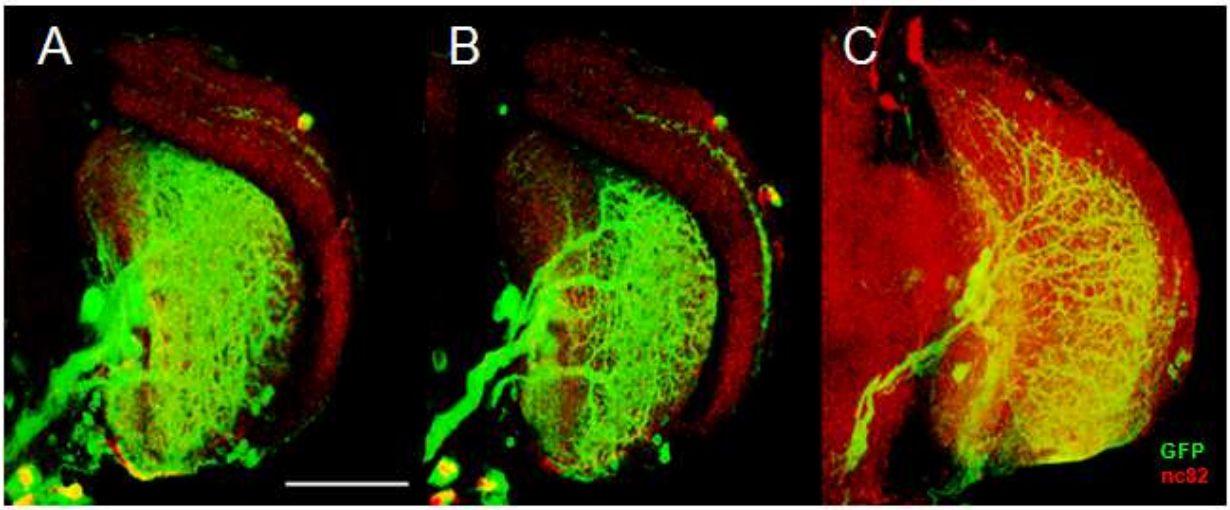

Fig. 50: The expression pattern of DB331-Gal4.

Maximum projection view of the expression pattern driven by DB331-Gal4 and coexpression of UAS-mCD8::GFP as marker gene (A). The pattern includes all 3 HS (B) and 6 VS neurons present in the optical lobe in *Drosophila.* In addition, some lobula plate intrinsic neurons are included (C). Confocal image stacks were taken with a z-increment of 0.5 µm, a 63X objective and minimized pinhole. Composite images were generated by collapsing ~ 60 images. Scale bar 50 µm.

My aim was to establish a protocol for the specific ablation of LPTCs. By eliminating subsets of LPTCs from the motion detection circuitry, it might be possible to study their function in controlling optomotor behavior of the fly. Here, DB331-Gal4 was chosen to drive expression of UAS>Stop>RicinA in 6VS and 3HS cells (Fig. 50). Furthermore, mCD8::GFP was co-expressed as marker to label all surviving neurons.

The remaining expression was then compared with wildtype expression. The exact genetic backgrounds of the used stocks were depicted in Fig. 51.

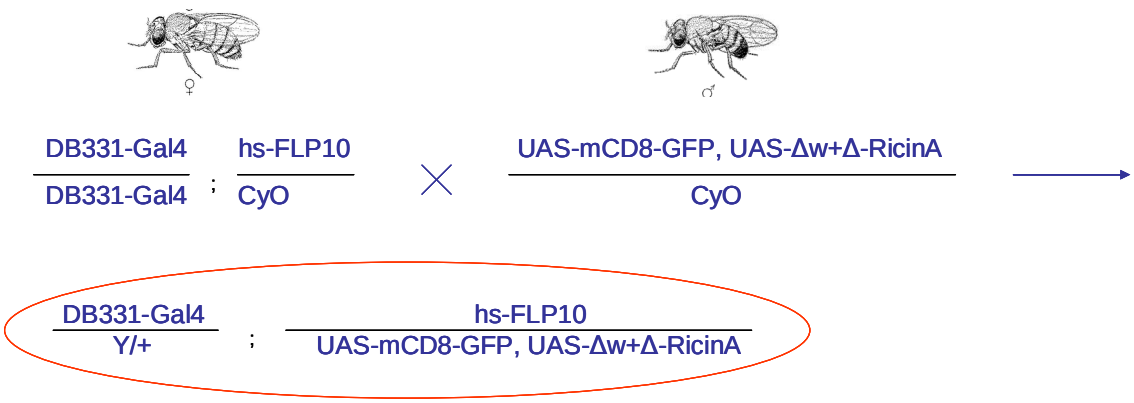

Fig. 51: Crossing scheme for heatshock-induced ablation of LPTCs in *Drosophila.*

Female virgin flies of the stock: DB331-Gal4; hs-Flp/CyO are crossed to male flies of the following stock: UAS>Stop>RicinA, UAS-mCD8::GFP/CyO. The female offspring with following genetic background: DB331/+; hs-Flp/UAS-mCD8::GFP, UAS>Stop>RicinA were selected for further heat shock treatment.

Due to the early onset of the used Gal4 line, it was possible to observe GFP expression in all larval stages. Hence, the probability was high that the expression time of the dirver line coincides with the developmental onset of LPTC progenitor cells. Therefore, in the next step, I determined the exact time point when the progenitor cells of LPTCs occurred during development. In this experiment, flies of the stock DB331-Gal4; UAS-mCD8::GFP were analyzed via confocal imaging at different developmental stages. This analysis determined the late 3rd instar larval stage to be the best time for RicinA induction in DB331.

During this developmental stage, LPTC cell bodies were detectable for the first time, while in the white pupal stage the rudimentary branches already had appeared (Fig. 52). The branches of HS cells were particularly identifiable at the later stage. However, the number of cell bodies at late 3rd instar stage was less than the number of LPTCs present in the adult stage, leading to the assumption that there was a successive development of different LPTCs.

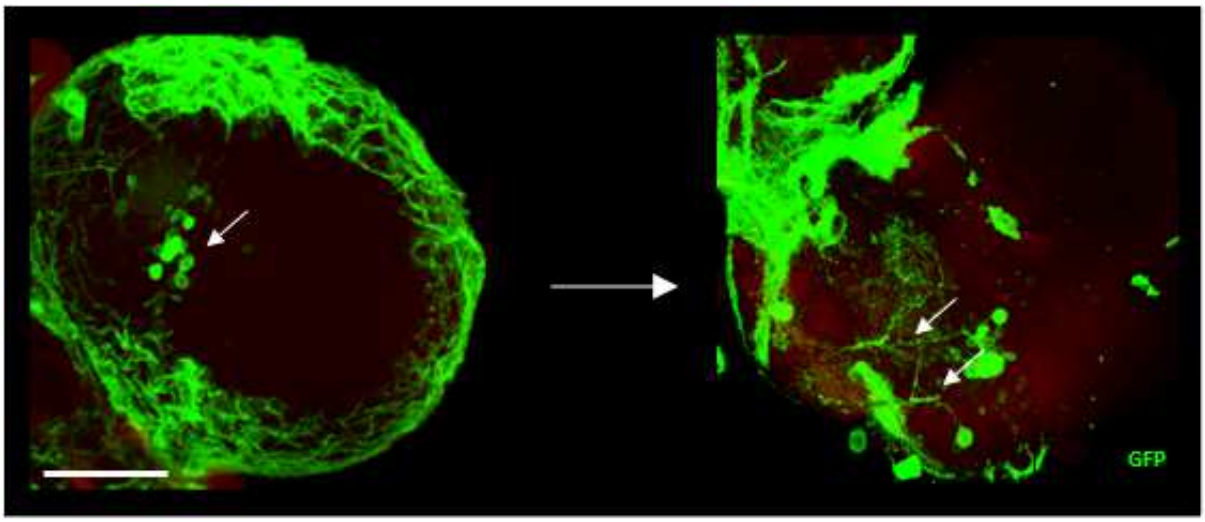

Fig. 52: In the DB331-Gal4 driven expression pattern, LPTCs are first detectable at late 3rd instar larval stage.

Flies from the stock DB331-Gal4; UAS-mCD8::GFP are screened for LPTCs at several developmental stages. In late 3rd instar larval stage, the cell bodies of LPTCs are visible for the first time (left image). Later, in the white pupa stage, first rudimentary outgrowing neurites are visible (right image). Neuritis of outgrowing HS cells are depicted in the right image (double arrows). Confocal image stacks were taken with a z-increment of 0.2 µm, a 63X objective and minimized pinhole. Composite images were generated by collapsing ~ 60images. Scale bar 50 µm

In the next step, an appropriate heatshock protocol was established to ablate restrictively LPTCs based on previous developmental study (Fig. 52). Depending on the developmental stage and heat shock duration, it should be possible to control the number of ablated LPTCs. Heatshock treatment was also applied in later pupal stages and in adult flies, resulting in inefficient ablation of LPTCs. These experiments suggested that the flip-out does not work in post-mitotic cells.

However, the ablation efficiency rate rose to 100 % when heatshock was induced at late 3rd instar stage. After one to two hours of heatshock treatment, larvae were taken out of the tubes and transferred into a vial containing fresh medium. Until the adult stage, the flies were kept at room temperature. For analysis of the ablation efficiency in flies that were treated in late instar larval stage, confocal images were taken in adult stages and the numbers of remaining LPTCs counted for each optical lobe. Here, the efficiency of cell ablation was extremely high. There were no flies with less than 50% loss of LPTCs in the expression pattern. Mostly 3-4 remaining LPTCs were detectable. Furthermore, in 30% of all observed optical lobes, no LPTCs were left at all (Fig. 53).

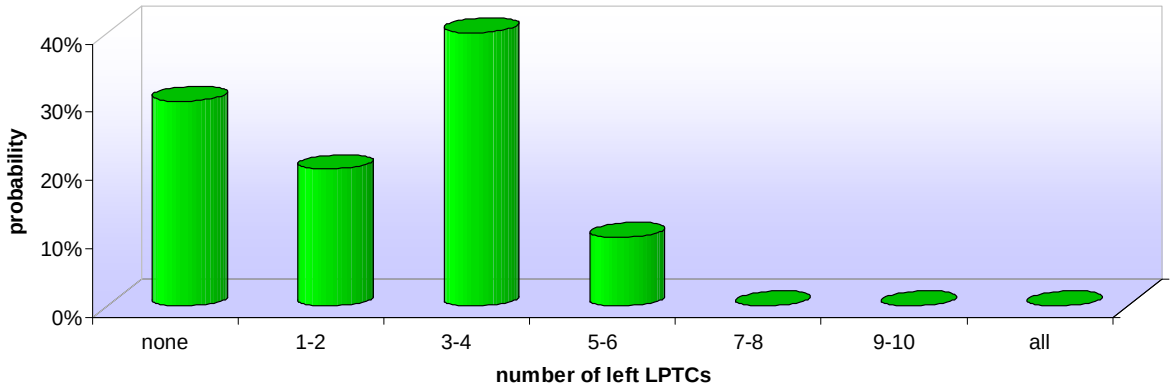

Fig. 53: Ablation efficiency of RicinA by heat shock induction in 3rd instar larvae.
The scheme depicts the statistical distribution of the number of ablated LPTCs. In the examined flies, more than 40% of the examined flies showed a reduction of LPTCs down to 3-4 remaining LPTCs, around 20% possessed 1 or 2 and around 10% 5 or 6 remaining LPTCs. Around 30% had a total loss of LPTCs. None of the flies possessed more than 7 remaining LPTCs.

Depending on the exact developmental stage when heatshock was given, which can vary between single late 3rd instar larvae up to 24 hours, the number of remaining LPTCs in each lobe (Fig. 54 A-C) was also very variable. Within a single fly, it was possible to observe different expression patterns in both hemispheres (Fig. 54 D).
At first sight, remaining LPTCs did not reveal any obvious anatomical differences in terms of dendritic shape or neuronal size compared to wildtype morphological structures. Nevertheless, in order to prove this assumption, a cell vitality test was performed. Here, Propidium iodide (PI from Invitrogen) was used as a fluorescent, intercalating agent for DNA staining. In viable cells, PI cannot pass the cell membrane whereas, in dead cells or non-vital cells, the protein synthesis is interrupted and therefore PI is able to pass through the porous membrane.
Adult brains were first dissected and then immediately incubated in PI solution (1:3000) for 1 minute without fixation. After several washing steps with PBS, confocal images were taken. PI was thereby excited with a 488 nm argon-ion laser light and detected by a 562-588 nm band pass filter. In the following step, a screen for PI positive LPTCs was done. In all tested brains, no overlap of PI with GFP positive LPTCs was observable, showing that the remaining neurons were not affected by RicinA expression (Fig. 55) in neighboring neurons.

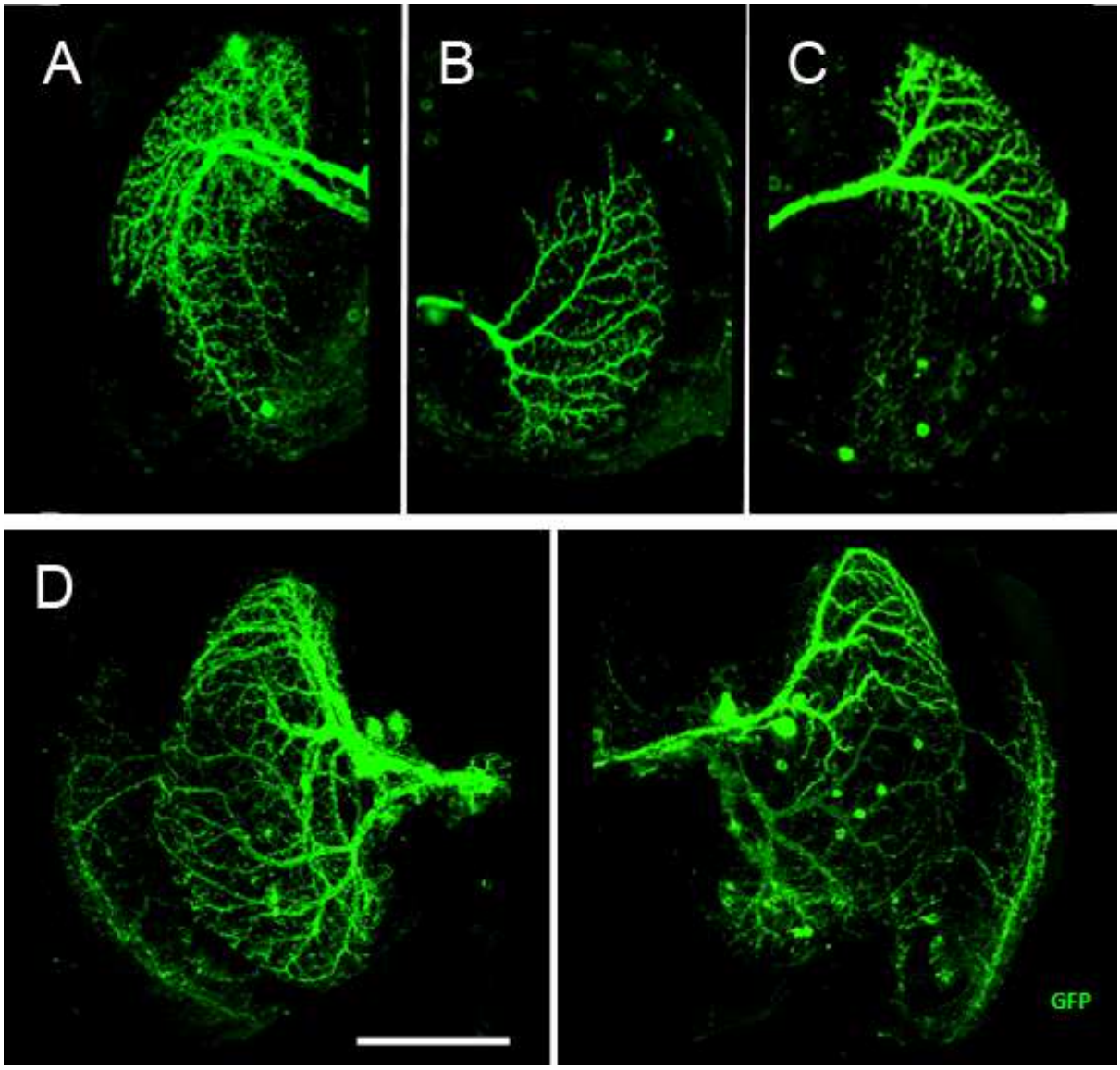

Fig. 54: Comparison of the DB331 expression pattern after RicnA induction in late third instar larval stage.

The images demonstrate the efficiency of RicinA ablation in LPTCs with the developed heatshock protocol. Depending on the cell type, progenitor cell or non-mitotic cell, in which RicinA is initially induced, the number of surviving LPTCs decreases to a single LPTC. In (A) only a small subset (VS1, VS2 and HSN) has remained whereas in (B) and (C) only HSS and HSN respectively escaped ablation. At first sight, the dendritic branching pattern does not obviously differ from those in control flies. The neurons are displayed in the relative position within the brain, i.e. left and right hemispheres are not oriented in the same direction. In (D) the differences in cell ablation efficiency within a single RicinA fly are illustrated. Here, both optical lobes within one specimen are shown. The left hemisphere possesses less remaining LPTCs than the right one. Confocal image stacks were taken with a z-increment of 0.2 µm, a 63X objective and minimized pinhole. Composite images were generated by collapsing ~ 60 images. Scale bar 50 µm.

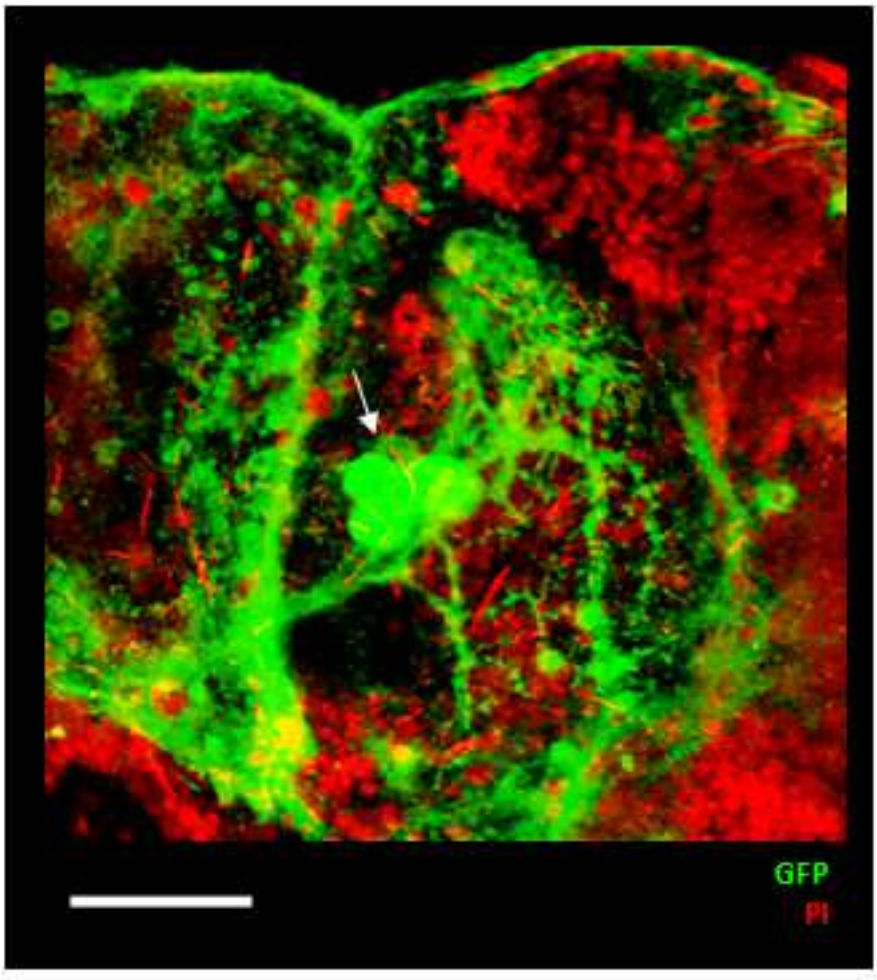

Fig. 55: Cell vitality test with Propidium Iodide reveals that remaining LPTCs are not affected from leaky RicinA expression.

No Propidium Iodide (red) could be detected could be detected in any of the tested animals (n=7) within GFP labeled LPTCs (green). This suggests that cells are vital. Confocal image stacks were taken with a z-increment of 0.2 µm, a 63X objective and minimized pinhole. Composite images were generated by collapsing ~ 60 images. Scale bar 50 µm

The timed ablation of neurons by RicinA expression represents a powerful tool for ablation of subgroups of cells without interfering with cell vitality of neighboring neurons. Here, a very narrow timeframe of 24 hours was defined in which heatshock treatment leads to effective ablation of LPTCs. Furthermore, it was possible to unravel some surprising developmental mechanisms in anatomy of LPTCs leading to the conclusion that single LPTCs formation of dendritic branching patterns does not depend on neighboring LPTCs. This method combined with the elaborated heatshock protocol makes it possible to understand the function and importance of individual LPTCs for optomotor response in future behavior experiments.

5.2.4 Transsynaptic retrograde labeling of neurons with Vesicular Stomatitis Virus in *Drosophila*

Recent studies have demonstrated the manifold ways in which viruses for the transsynaptic retrograde labeling can be used to highlight cell morphology as well to identify presynaptic connected cells (Wickersham et al. 2007). However, the use of viral abilities has only been demonstrated in the mammalian model system. The aim of this study was to establish this labelling method in *Drosophila melanogaster.* The experiments were carried out in collaboration with Alexander Ghanem and Klaus Conzelmann who provided all viral stocks for following experiments.

5.2.4.1 Pseudotyped VSVs infect efficiently Drosophila cells in culture

As viral systems for the infection of neurons have not been established in *Drosophila*, the initial starting point of the project was to take the same virus that has been used in the mammalian system. However, feeding experiments of fly larvae with Rabies Viruses (RV) containing media demonstrated that they were not penetrating *Drosophila* tissue at all. We therefore continued to screen for a virus that was able to infect insect cells. It was known from previous studies that the Vesicular Stomatitis Virus (VSV) was capable of infecting and reproducing in S2 Schneider cell cultures (Moffat, KG. 2002). Here, this experiment was repeated whereby a massive infection of S2 cells by VSVeGFP viruses could be observed (Fig. 56). This virus strain was derived from the wildtype VSV strain. Within the VSV genome, an additional mRNA sequence encoding for enhanced GFP (eGFP) was inserted subsequently to the gene encoding the Glycoprotein (G-protein). A further recombinant virus strain was generated based on VSVeGFP in which the genomic G-protein sequence was deleted (DG) in order to trap the virus within the initial infected host cell (VSV DG eGFP). As the G-Protein was also absent within the initial VSV DG eGFP, the virus needed to be pseudotyped with its own G-Protein in order to be able to infect any host cells. Pseudotyping was the procedure where the virus was uniquely provided with a Glycoprotein in *trans* via host cells from which the virus was harvested. However, as these deletion viruses do not genetically encode for the G-protein themselves they were not able to spread to neighboring cells. This allowed the infection efficiency of VSVs to be determined and furthermore, based on this deletion,

mutant pseudotyping with either the own G-protein, VSV-G, or other coating proteins like Rabies Virus G- and Matrixproteins (M-protein) could be implemented. In order to pseudotype VSV DG deletion viruses, the virus was first pseudotyped with its own G-protein and afterward within the host cells the corresponding Rabies proteins were provided in *trans*. One key point here was that VSVs were reported to spread through diffusion- The aim aim was therefore to transfer the ability of the Rabies virus to spread transsynaptically to VSV. The spreading behavior was characterized through the G-protein that differs between virus species. However, the M-protein was also speculated to play a role.

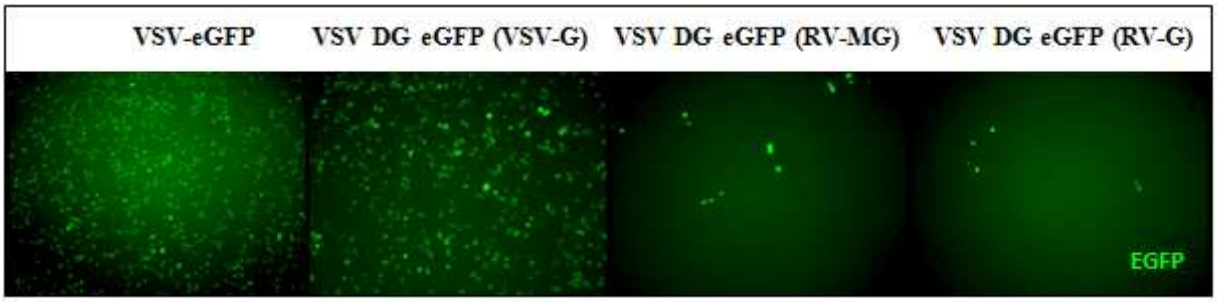

Fig. 56: Infectivity of VSVeGFP and different pseudotyped VSV strains of *Drosophila* S2 cells.
The image shows S2 cells infected with different genetically manipulated VSV strains. Infection (green) is detected under fluorescence stereomicroscope. Here, the number of infected cells does not give any conclusive results about infection efficiency, as different concentrations of the virus stocks were applied. All tested strains infect and replicate within S2 cells. The wildtype VSV strain with eGFP insertion is the only strain which can potentially "spread" to neighboring cells. The other strains possess a deletion (D) of the genomic Glycoprotein (G-protein) site and therefore are not able to process the budding step. However, through pseudotyping with either their own G-Protein or foreign G-Proteins like RV-G (Rabies Virus Glycoprotein), these deletion viruses are able to spread. All transfected cultures are positive for virus infection. Data was kindly provided by Alexander Ghanem.

Therefore, we also tested VSVDG deletion strains which were pseudotyped with different Rabies Virus components and, indeed, both pseudotyped VSV strains, one with Rabies Virus G and M protein (VSV DG eGFP (RV-MG)) and the other only with G-protein (VSV DG eGFP (RV-G)) were able to infect S2 cells. However, the infection rate could not be compared between different VSV strains that were used, as the virus concentrations applied with the solution differed. Though the experiments with S2 cells provide initial evidence that VSV viruses might be used to infect *Drosophila* S2 cells, it was fully unclear whether the virus would enable retrograde

tracing. The main reason was that S2 cells were derived from late embryo stages non-neuronal cells and therefore do not possess synapses. In the next step, we applied the virus stock to intact fly brains.

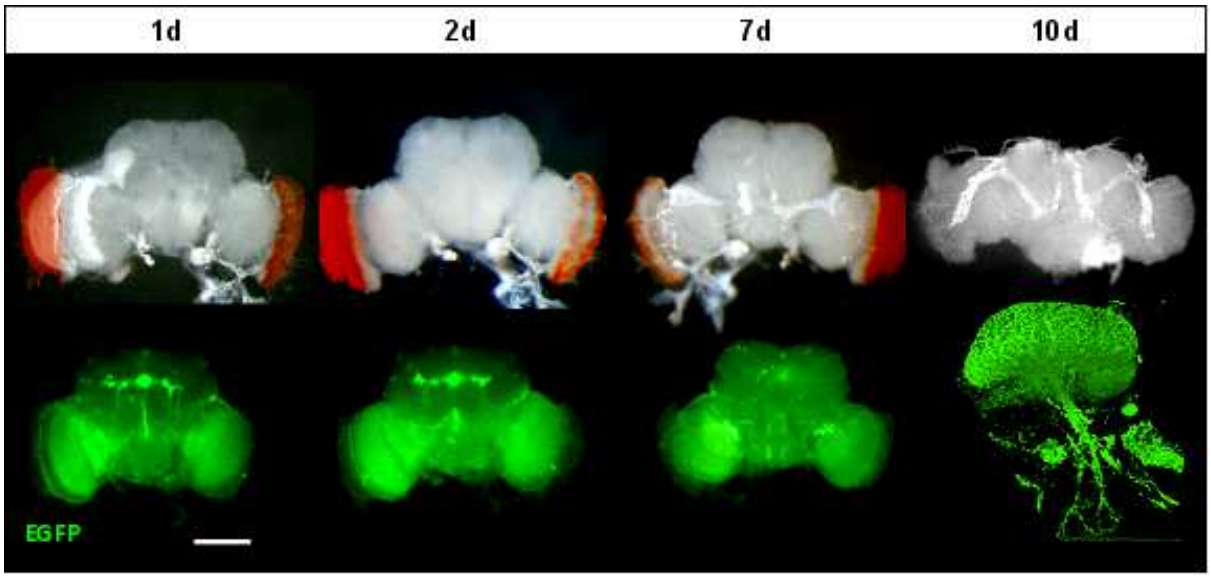

Fig. 57: *Drosophila* brains can be cultured ex vivo for more than 10 days.
In the first row, wildtype brains are successively observed during a total incubation time of 10 days. The brains do not undergo any visible morphological changes or degradation during incubation time besides minimal flattening of the entire brain. For closer observation of the vitality, brains taken from the stock DB331-Gal4; UAS-mCD8::GFP are kept in culture (second row). Flies out of that stock possess a strong GFP expression pattern, which is observable under fluorescence microscope. After 10 days, the GFP expression level is still maintained. In addition, at day 7, confocal images were taken of the entire LPTCs in the optical lobe, thereby revealing intact morphology in both dendritic and axonal parts within these neurons (second row, right). Stereomicroscope images were taken with a Leica M205 FA and full apochromatic zoom. Confocal image stacks was taken with a z-increment of 0.5 µm, a 63X objective and minimized pinhole. Composite images were generated by collapsing ~ 60 images. Scale bar 25 µm and 50 µm respectively

In a recent publication from Ayaz et al. 2008, a protocol for culturing whole *Drosophila* brains was presented. In order to test whether this system would also work for viral infection, brains from adult wildtype flies as well as from the stock DB331-Gal4; mCD8::GFP were dissected and taken into culture. Anatomical observations of those brains throughout an incubation time of 10 days revealed no substantial change in the general appearance of the brain. Only a minor flattening of the brain was observable. No decrease in the GFP expression level was found (Fig.

57). Furthermore, to underline these findings confocal images were taken from DB331-Gal4; mCD8::GFP brains after 7 days of incubation. The LPTCs showed no differences in their anatomy. Even after 10 days' incubation, the brains appeared to be intact.

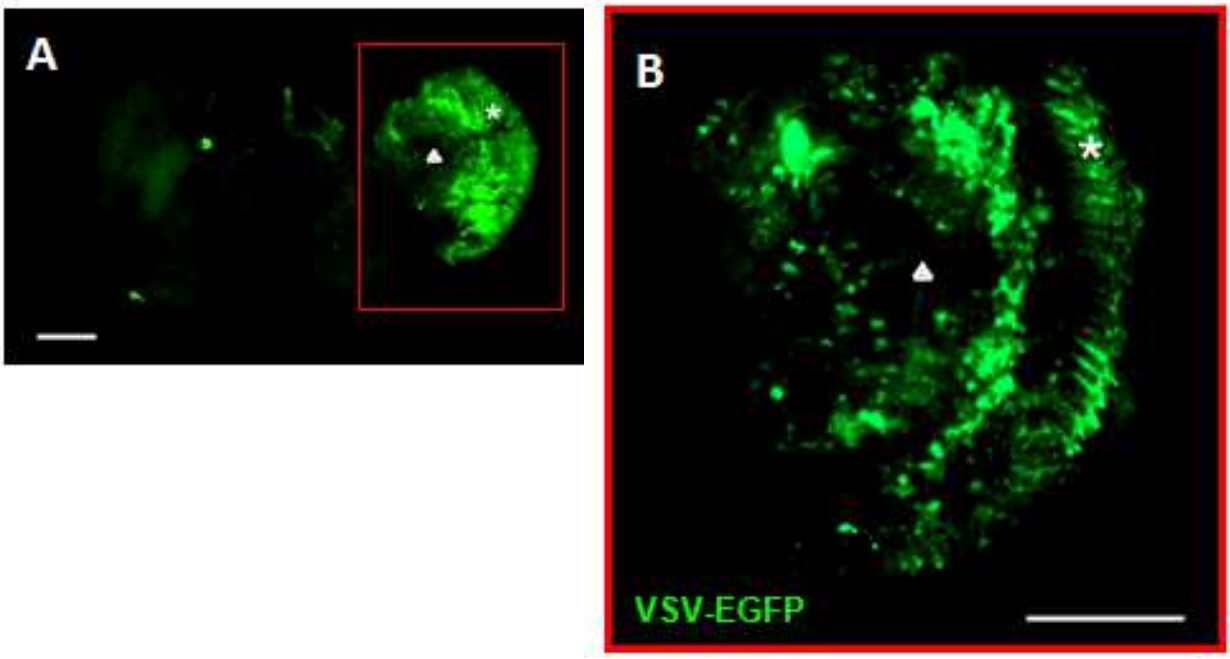

Fig. 58: VSV-eGFP infects neurons in cultured *Drosophila* brains.
An entire fly brain is shown in (A). Infection of VSV-eGFP (green) is most prominent in the right optical lobe. There are further single cells and small cell populations GFP labeled though the virus within the central brain that are labeled by GFP expression from the virus. The brain is incubated for 4 days with virus solution at 25℃. A close up at the infected optical lobe (40X objective) reveals labeling of neurons but also glia cells in the medulla (asterisk) and the lobula complex (triangle) which are distinguishable through their characteristic morphology. Brains were only fixed but not additionally immunolabeled. Confocal image stacks were taken with a z-increment of 0.2 µm, a 10X objective and 40X objective with minimized pinhole. Composite images were generated by collapsing ~ 60images. Scale bar 50 µm

As the replication of VSV takes only several hours at 37℃, the established culture was well suited for observing viral spread. In a next step, 1 µl of a solution containing VSVeGFP was applied to wildtype brains in culture. After 3 days, brains were fixed and confocal images were immediately taken without additional immunolabeling of GFP. Massive infection of the brains by VSVeGFP was detected (Fig. 58). Broad patches of GFP positive infected cells could be mainly observed. The infection

process of the deletion virus VSV DG eGFP (VSV-G) was also tested in brain culture. Consistent with previous studies, only single cells were infected and labeled (Fig. 59). After another two days, maximum infectivity was reached, i.e. no further neurons appeared GFP labeled, and confocal images were taken. Here, even the processes of single cells could be tracked due to decreased density of marked cells.

Taken together, by comparing the observations made with VSV eGFP and VSV DG eGFP (VSV-G), it can be assumed that spreading occurred in the first case (Fig. 59). However, the patches did not in any way show that the virus was spreading within the brain whether through diffusion or throughout synaptic connections. Nevertheless, the cell types were both distinguishable, neurons and glia cells were equally infected leading to the question as to which cell type the virus preferred.

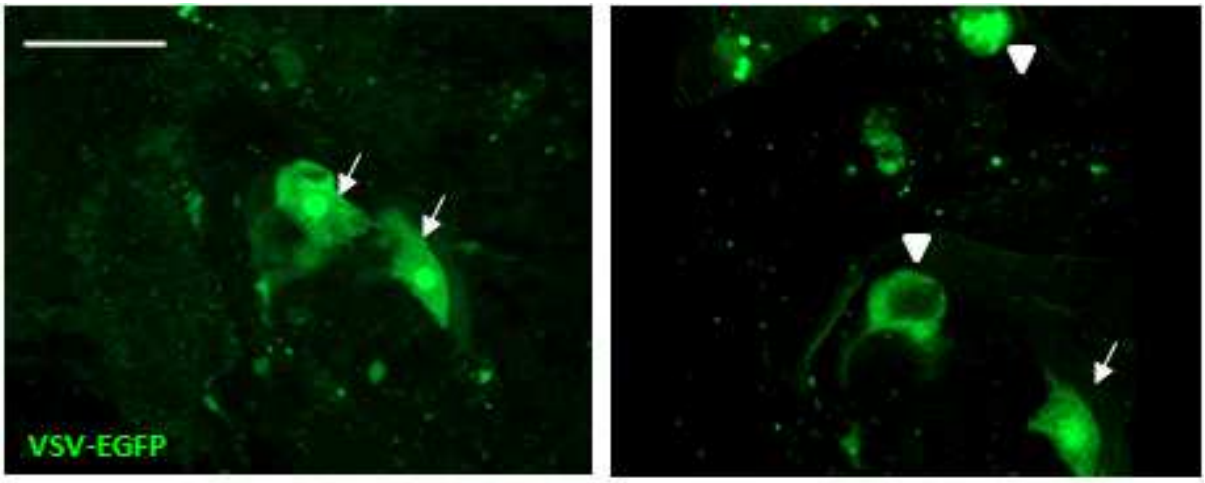

Fig. 59: VSV DG eGFP deletion viruses are trapped within initially infected host cells.

After 2 days' incubation time of the fly brains with VSV DG eGFP solution at 25℃, single infected neurons (triangle) as well as glia cells (double arrow) are GFP labeled (green) through the virus. Longer incubation time does not reveal any spreading of the virus throughout the initially infected cell. The brains were only fixed without additional immunolabeling. Confocal image stacks were taken with a z-increment of 0.5 µm, a 63X objective and minimized pinhole. Composite images were generated by collapsing ~ 20 images. Scale bar 25 µm.

The same procedure was carried out with VSV DG eGFP RV (GM) and this time a general increase in the number of infected cells was observed accompanied by a pattern of GFP-positive cell patches. This finding suggests that pseudotyping VSV G-protein deletion viruses with Rabies G- and M-protein enables VSV to spread beyond the initial infected cell (Fig. 60). However, it is still unclear whether the combined

expression of both proteins was needed for viral spread. These results lead to the assumption that recombinant VSV strains allow labeling of *Drosophila* cells by infection, replication, and spreading of the virus.

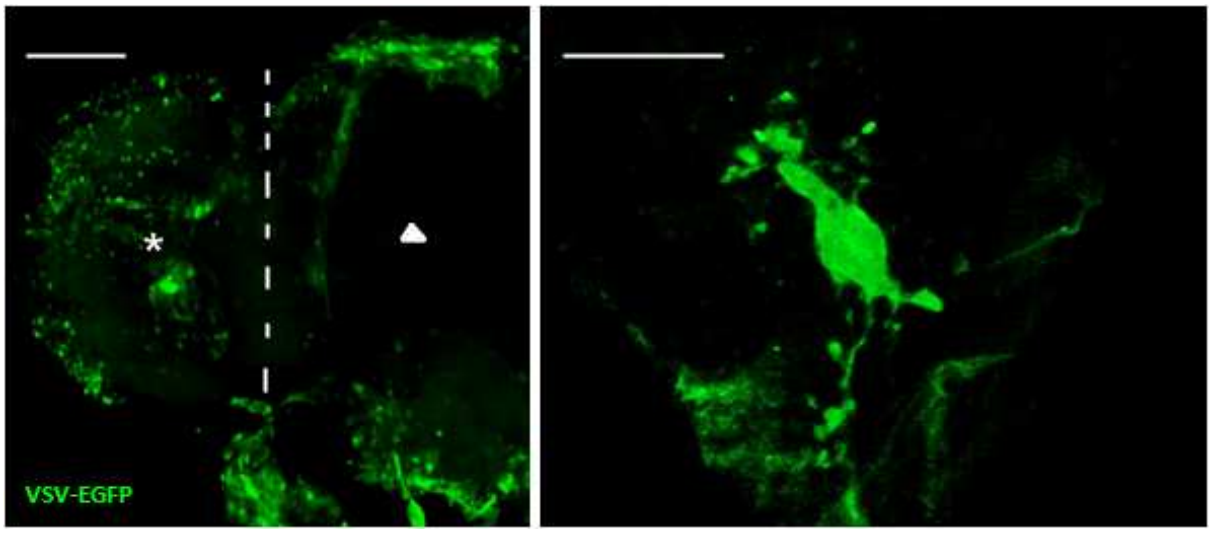

Fig. 60: VSV DG eGFP pseudotyped RV (GM) infects cultured *Drosophila* brains.
Deletion VSVs pseudotyped with rabies Matrix and Glycoprotein are able to infect *Drosophila* brains in culture. Three days after infection the first infected neurons are GFP labeled (green). In the left image, the left side of the fly brain is shown where VSV-positive cells are visible in the optical lobe (asterisk, left side of the dashed line) and the central brain (triangle, right side of the dashed line). The left image shows a close-up of a VSV labeled glia cell where the processes are labeled. Confocal image stacks were taken with a z-increment of 0.5 µm, 63X objective and minimized pinhole. Composite images were generated by collapsing ~ 60 images. Scale bar 50 µm and 25 µm, respectively.

5.2.4.2 TVA/EnvA system for specific targeting of neurons

Given that VSV might be useable for viral tracing of neuronal circuits, the next aim was to target the virus to neurons of interest. Therefore, an established two-component system was chosen called TVA/EnvA system. One component, the TVA receptor was expressed by the host cell. Transgenic flies encoding the TVA sequence under control of the UAS promoter were generated. The construct was designed in such a way that dsRed was additionally translated as a marker protein however, independently from the TVA sequence. This was enabled through a linker called “2A like” which controls ribosome activity (Tang, W. 2009, Szymczak, AL. 2004) (Fig. 61) and leads to separation at protein synthesis level by causing a ribosomal

skip mechanism. The expression of UAS-TVA-2Alike-dsRed flies was tested by crossing them with DB331-Gal4. Already in early larval stages, dsRed expression was detectable under the fluorescence strereomicroscope. Expression strength was constant throughout the entire development (Fig. 62). Confocal images of fixed adult brains confirmed the expression of dsRed within the neurons of interest. Here, the main branches were strongly labeled whereas higher order branches were merely visible due to the cytoplasmic localization of the marker protein. This observation points to a separated translation of dsRed and TVA translation through the 2Alike sequence.

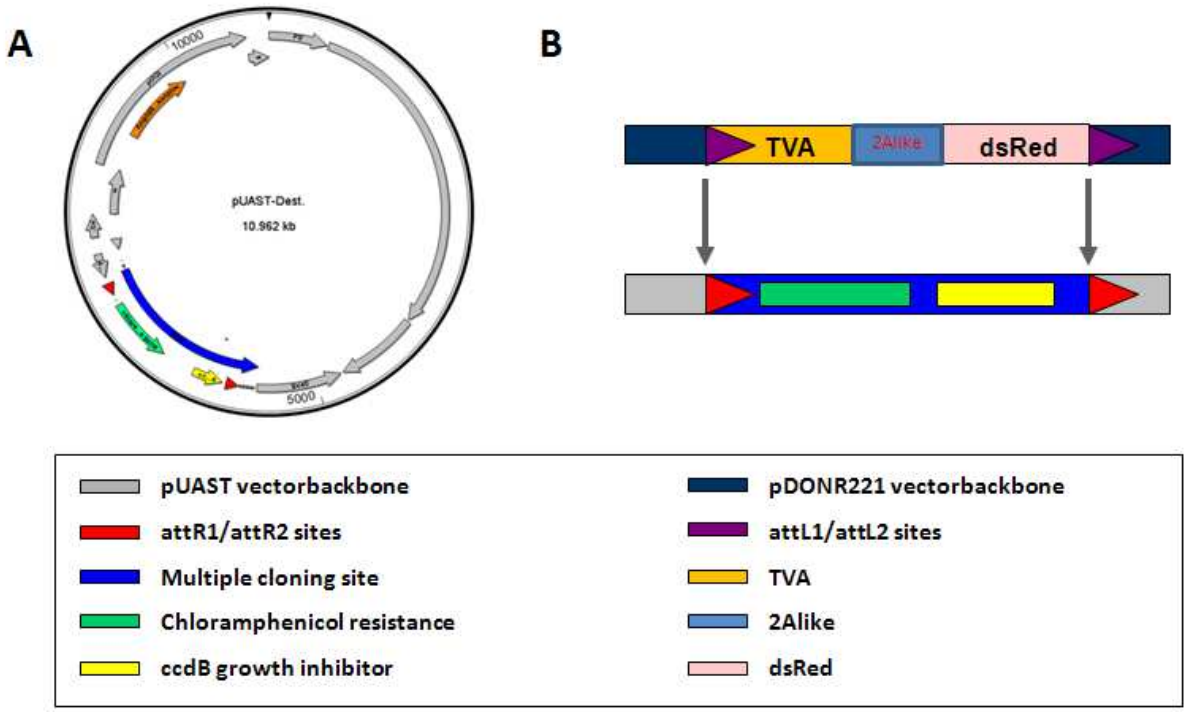

Fig. 61: TVA-2Alike-dsRed integration into the pUAST vector.

The sequence of the TVA-2Alike-dsRed construct is integrated into the pUAST-vector through the gateway cloning system. The pUAST destination vector depicted in (A) possesses attR1/attR2 recombination sites which allow the integration of the TVA-2Alike-dsRed sequence that is flanked with attL1/attL2 recombination sites via enzymatic reaction (B). Original construct was kindly provided by Alexander Ghanem.

In parallel, VSV DG eGFP was pseudotyped with EnvA (VSV DG eGFP (EnvA)) forming the complementary partner to the UAS-TVA-2Alike-dsRed flies. For expressing TVA in LPTCs, we chose DB331-Gal4 as driver line. For testing whether this system really ensures infection specificity, brains dissected from adult TVA expressing flies were taken into culture and together incubated with VSV DG eGFP (EnvA) solution at 29℃. The temperature was increa sed in order to speed up the infection process. 24 hours later first neurons were labeled by viral infection and could be detected under fluorescence microscope. Moreover, some of the labeled neurons could be identified as vertical sensitive (VS) neurons belonging to the group of LPTCs (Fig. 63).

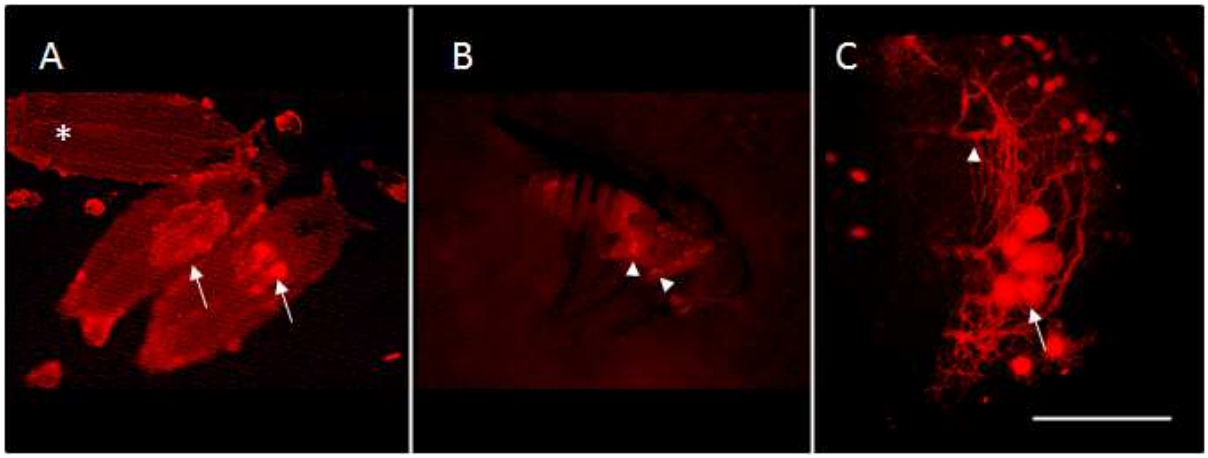

Fig. 62: Expression pattern of DB331-Gal4; UAS-TVA-2Alike flies

Expression of dsRed is observed under the fluorescence sterecmicroscope during larval stages (not shown) and throughout the entire development. (A: arrows). This is also true for adult flies (B). A strong expression level of dsRed was observable. Confocal images reveal the localization of dsRed within the entire cell structure like soma (arrow) and dendritic ramifications (triangle). Here, images were taken immediately after fixation. The confocal stack was taken with a z-increment of 0.5 µm, a 63X objective and minimized pinhole. Composite images were generated by collapsing ~ 30 images. Scale bar 50 µm.

Up to this stage, all experiments were performed in vitro in brain cultures. However, to allow labeling of presynaptic neurons and to preserve anatomical structures as well as health of infected neurons in long-term experiments, the virus needed to be applied to living animals. Furthermore, the incubation time of the virus can be expanded to the lifetime of the flies and thereby could be combined with electrophysiology as well as behavior assays in future experiments. Therefore,

recombinant VSVs were injected directly into the head of *Drosophila.* Here, VSV DG eGFP (EnvA) should have high target specificity towards TVA expressing neurons.

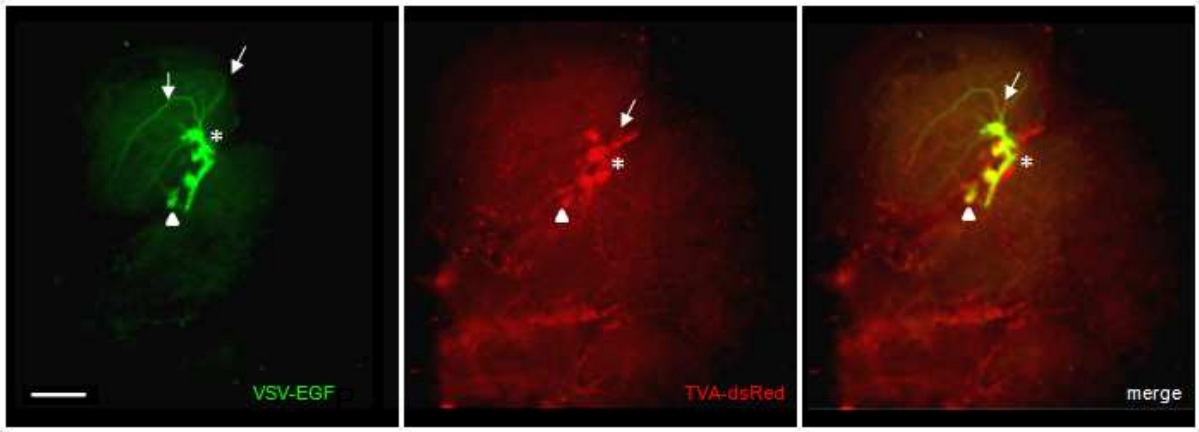

Fig. 63: Targeted virus infection of LPTCs through the TVA/EnvA system.
The image of one-half of a brain reveals that the TVA/EnvA system is working in flies and allows a specific targeting of the virus to LPTCs. Here, several neurons in the lobula plate (asterisk) are GFP labeled (triangle, arrows) through virus infection and even anatomically identifiable as vertical sensitive (VS) cells (arrows), whereas the dsRed expression shows the endogenous expression pattern of DB331-Gal4. However, the dsRed labeling is very weak compared to GFP expression. Nevertheless, GFP localization coincides with dsRed labeled cells revealing the efficiency of that system. Single image was taken from fluorescence microscope. Scale bar 50 µm.

In the first application, a fluorescent dye, Alexa Fluor 488 (Invitrogen), was used instead of a transparent virus solution for determining the pressure with which the solution should be applied via the microinjector (Fig. 64 B, C). A minimum invasive procedure was thereby developed which allowed flies only to be anesthetized with carbon dioxide but not fixed during injection (s.Methods). The filled capillary was inserted into the back of the head close to the lobula plate (Fig. 64 A). Pressure was adjusted so that the volume of the injected solution (< 1µl) would only spread throughout the head but not the entire animal (Fig. 64 C). An increase in the injected solution volume was leading to death of the fly.

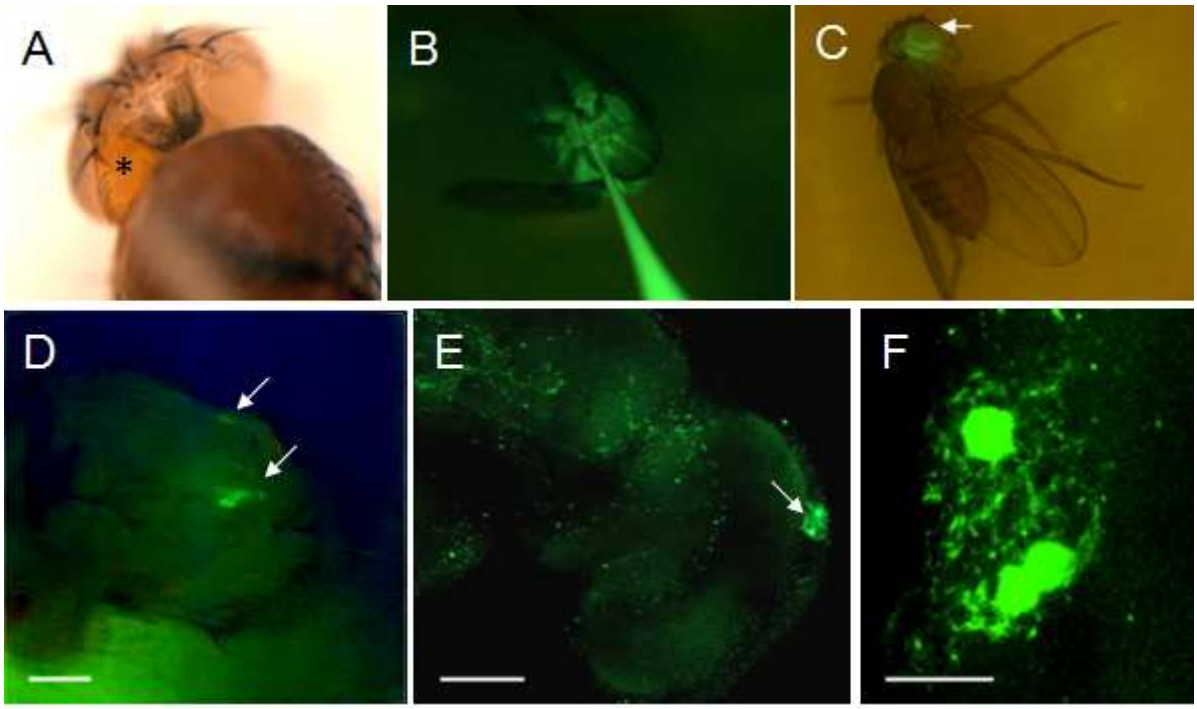

Fig. 64: Injection of virus solution into living flies results in GFP labeling of infected cells.
The injection procedure is shown with Alexa Fluor 488 under fluorescence microscope (A-C). Flies are anesthetized with carbon dioxide. The head of the fly is positioned with brushes and forceps so that the back of the head is exposed (A) and the loaded capillary can be inserted close to the lobula plate (A) (asterisk). Afterwards, a < 1µl is injected into the head via microinjector, leading to a concentration of around 100 viruses per injection (B). Spreading of the virus throughout the hemolymph was determined under fluorescence microscope combined with bright field light (C). The same pressure is taken for injecting VSV DG eGFP (envA) solution into TVA expressing adult flies (DB331-Gal4/UAS-TVA -2Alike-dsRed). 24 hours post injection, adult flies are decapitated, and brains dissected. Already, under fluorescence microscope, green-labeled cells equivalent to virus infection are observed (D) (arrows). Confocal images reveal an infection of a large number of cells within the optical lobe as well as the central brain (E). A close up image of infected glia cells in the Medulla region (arrow) demonstrates the detailed anatomical structure of those cells (F). Scale bars 50 µm (D/E) and 25 µm (F).

Injection of VSV DG eGFP (envA) solution into the back of the head of DB331-Gal4; UAS-TVA-2Alike-dsRed adult flies showed that VSV was infecting a large number of cells (Fig. 64 E) and furthermore, that infected flies were surviving this procedure. Therefore, the next step was to generate transgenic flies that would produce viral G-protein that would allow monosynaptic spreading. Therefore, six independent transgenic fly lines were generated encoding for G-proteins from different virus species (Fig. 65).

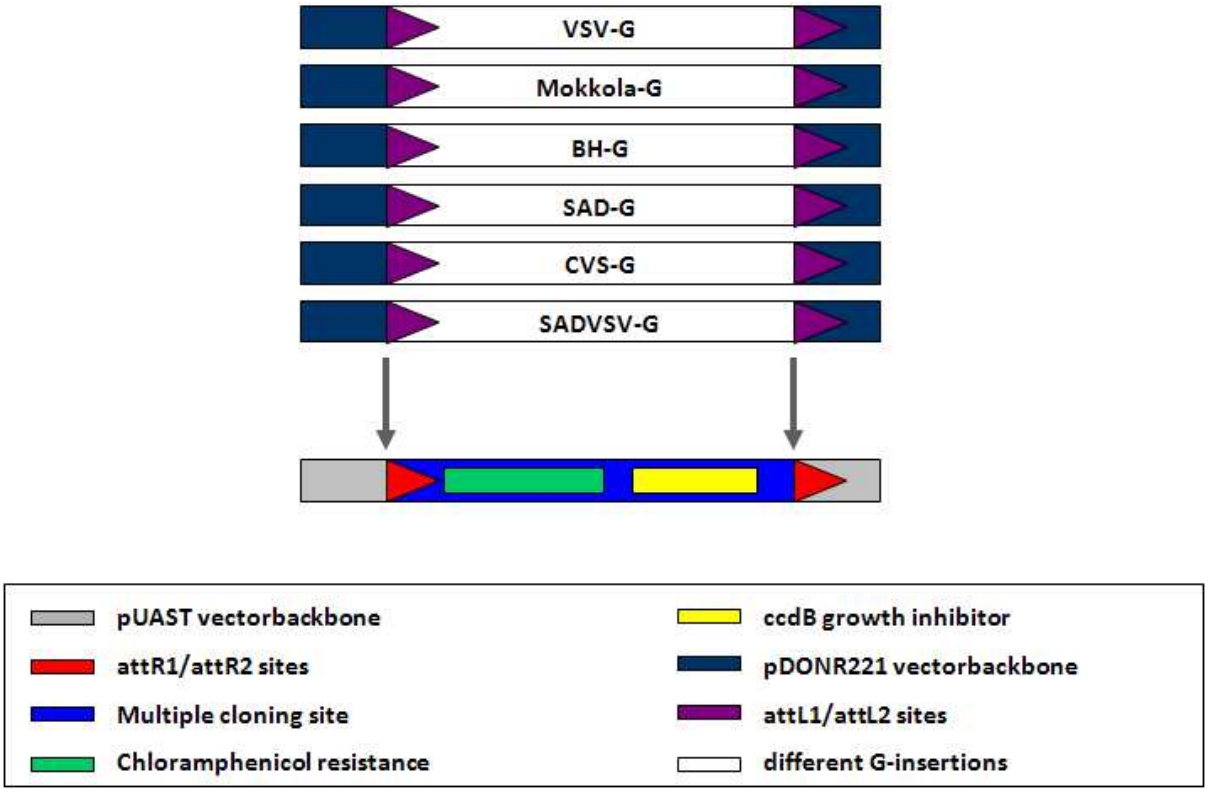

Fig. 65: Integration of viral Glycoproteins into the pUAST vector.

The sequences of the G-protein constructs are integrated into the pUAST-vectors through the gateway cloning system. The pUAST destination vector possesses attR1/attR2 recombination sites, which allows the integration of the TVA-2Alike-dsRed sequence that is flanked with attL1/attL2 recombination sites through an enzyme-mediated process (s.methods). Original constructs were kindly provided by Alexander Ghanem.

The G-proteins were put under control of the UAS promoter, thus the expression could be combined with that of the TVA receptor. First experiments made in brain culture did not lead to a conclusive result. In addition, immunolabeling of rabies virus-G revealed non-specific localization or binding of the antibody (Fig. 66). However, previous studies have shown that ubiquitin-driven expression of pCVS-G vector in S2 cells showed positive protein synthesis in Western Blot (not shown), thereby revealing that *Drosophila* cells were able to create viral Glycoproteins. Nevertheless, studies that are more conclusive are needed for testing the expression level of G-proteins as well as functional aspects.

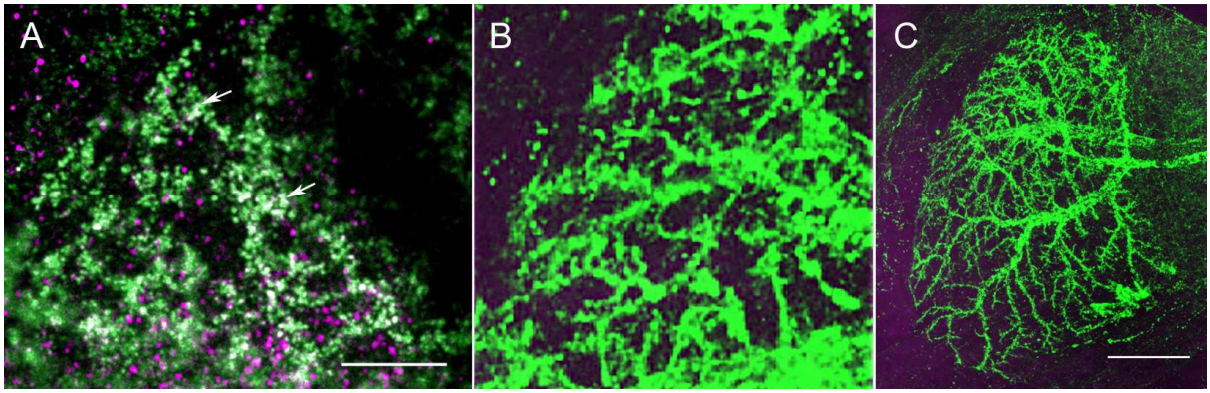

Fig. 66: Immunolabeling against rabies virus Glycoprotein reveals localization at the membrane surface of HS cells.

Here, the UAS-CVS-G construct was expressed under control of G73-Gal4. This driver line includes HSN and HSE as well as some columnar neurons. For cell labeling, mCD8::GFP (green) was used as a marker. CVS-G was detected by immunolabeling with an antibody specifically targeted against rabies virus Glycoprotein (magenta).In (A) a close up section of the HSN dendritic area is depicted in green showing some colocalization (arrows) with expressed virus G-protein in magenta but much more non-specific localization of the antibody. Close up image of HSN dendrites (B) as well as overview image of the entire lobula plate (C) do not show any CVS-G detection in control flies, hence determine antibody specificity. The confocal stack was taken with a z-increment of 0.2 µm, a 63X objective and minimized pinhole. Composite image (B+C) was generated by collapsing ~ 120images. Scale bar 10 µm (A+B), 25µm (C).

Here, the first steps towards a new method of labeling neuronal circuitries. Besides the identification of virus species that infect and reproduce in *Drosophila melanogaster*, a proof was provided that specific targeting to the neurons of interest can be achieved through the EnvA/TVA system. So far the method should be applicable in living animals and was therefore only temporally restricted through the lifetime of the specimen itself. The complementation with G-protein expressing flies has been started and needs to be tested for synaptic specificity.

6 Discussion

6.1 Manipulation of the endogenous Dscam code in HS cells elicits different anatomical phenotypes

In this study, we were able to provide strong evidence that HS cells possess an endogenous Dscam code. Immunostaining against the Dscam intracellular domain has revealed colocalization of the antibody with the GFP labeled HS cells. Furthermore, all Dscam null HS cells showed a strong self-crossing phenotype, which is due to the loss of any self-avoidance mechanism among sister dendrites. In addition, an increase in the number of higher-order branches was observable in Dscam null cells generated by site-directed recombination, whereas the dendritic fields remained unaltered. This Dscam null phenotype was highly reproducible and thus Flipase activity might have been strong enough to induce recombination in the entire expression pattern. In contrast to this, the attempt to create Dscam loss of function cells by deleting Exon 6 and gene silencing with RNAi turned out to be inaccurate. Although self-crossing events occurred in both cases as in Dscam null flies, the phenotypes were in general different from case to case and very inconsistent. This might be due to incomplete flip-out of the Exon 6 and incomplete silencing that could lead to either mosaic cells with and without Dscam code or cells with Dscam deficiency. The opposing phenotypes of Dscam null and Dscam deficiency cells are explained by the stochastic yet biased expression mechanism of Dscam isoforms in neurons. It has been shown that neurons largely express a nonspecific set of isoforms but some isoforms are needed for correct targeting and self-avoidance. Given the complexity of the *Dscam* locus, it is reasonable to expect that different roles for diversity will be observed in different cell populations or even different processes of a cell (Matthews et al. 2007). Deleting a subset of isoforms could therefore lead to errors in several developmental processes of HS cells, thereby eliciting other and more variable phenotypes than Dscam null is doing.

Besides the dendritic ramifications in the lobula plate, the axonal terminals were also seriously impaired in pathway finding and ramification: They were innervating wrong areas in the central brain and their endings were fasciculating, forming clumps. Taken together, these observations support the model that HS cell self-avoidance, but not heteroneuronal tiling, may depend on Dscam. This is in line with previous

studies in the mouse retina in which DSCAM has been shown to mediate isoneuronal self-avoidance for arborization and heteroneuronal self-avoidance within specific cell types to prevent fasciculation and to preserve mosaic spacing of the mouse retina (Fuerst, PG. 2007). Furthermore, from a genetic mosaic screen, it has been found that a lethal mutation in *Dscam* specifically perturbs segregation of axonal branches in the mushroom bodies (Wang et al. 2002).

Reduction of Dscam diversity by excision of Exon 2 led to variable phenotypes in the dendritic branching pattern of HS cells. Self-crossing events as well as decrease in the dendritic field were observable. The branching defects let us assume that, in HS cells, more than 1584 Dscam isoforms are needed for establishing wildtype branching pattern. Indeed, from mathematical modeling studies as well as from other Dscam deficiency studies, it is concluded that thousands of isoforms are essential to provide neurons with a robust discrimination mechanism to distinguish between self and non-self during self-avoidance (Hattori et al. 2009).

The Dscam single isoform overexpression screen demonstrated a high variability in strength between each elicited phenotype. In two cases, Dscam +7.6.19.2 and +11.31.25.1, overexpression resulted in a strong anatomical alteration of HS cells. In +7.6.19.2 flies, the cells showed a strong decrease in higher-order branches in the dendritic regions with thinner main branches, whereas the axonal region appeared unaltered. Furthermore, in some cases the dendritic fields appeared to be smaller. The phenotype elicited by Dscam +11.31.25.1 tended to be similar, with a significant reduction of the dendritic fields especially in the distal area of the lobula plate, but the remaining branches appeared thicker compared to wildtype ones. In addition, the axonal terminals were also impaired. Both phenotypes possessed different penetrance rates, which also depended on the used driver lines: DB331-Gal4, G73-Gal4, or GR104-Gal4. Nevertheless, the characteristics of the phenotype itself were consistent; i.e. Dscam +11.31.25.1 consequently elicited the same phenotypes in HS cell dendrites. In the *Drosophila* olfactory system, this uniqueness of overexpression phenotype has been described before as well as the variability of penetrance that might be due to the variability of the transgene expression level (Spletter et al. 2007, Zhu et al. 2006).

Reconstruction of Dscam +11.31.25.1 cells revealed a strong reduction of spanning fields as well as overlapping areas between HSN and HSE. Furthermore, increased cell increment along with an enlargement of the entire lobula plate hull area suggests

Dscam-mediated heteroneural repulsion between HS cells and most probably columnar neurons as well as other LPTC subgroups. So far, it is known that Dscam promotes isoform-specific binding, and interactions between identical Dscam proteins seem to promote contact-dependent repulsion (Hughes et al. 2007). However, it is unclear whether interaction of the same Dscam isoform is able to elicit such a strong overall phenotype.

The general reduction of higher order branches in the dendritic areas of HS cells was confirmed by immunostaining with α-Btx conjugated Alexa Fluor that suggests a decrease in density of nAchR in the observed lobula plate section. Furthermore, the receptor density seemed to be locally enhanced in +11.31.25.1 HS cells. This might point to a local agglomeration of synaptic input elements where presynaptic structures might follow their target structures despite their dislocation. Supporting this idea, the anatomical study of Dscam+11.31.25.1 driven by GR104-Gal4 showed that T4 and T5 cells were majorly mistargeting in the lobula plate region. Studies done by Zhu et al. (2006) have provided evidence in the olfactory system that positional shift of projection neuron dendrites causes a corresponding shift of its partner olfactory receptor neurons axons, thus maintaining the connection specificity. In HS cells, such a pre- and post-synaptic matching mechanism independent of precise dendritic positioning could be present. However, as quantification of the staining was not feasible and T4/T5 neurons are only shown to costratify in the LPTC layers without proof of synaptic connectivity, the conclusions are very speculative.

A general open question is why Dscam +11.31.25.1 elicits a strong phenotype in the dendritic region of HS cells but not in the axonal terminals as this isoform possesses the transmembrane domain 2 which has been shown to be enriched in axons. In contrast to this, isoforms carrying the transmembrane domain 1 are supposed to be restricted in dendrites (Yang et al. 2008).

MARCM experiments with Dscam +11.31.25.1 demonstrated that overexpression in single cells do not elicit altered morphology. In addition, neurobiotin injection in Dscam null flies revealed that wildtype cells, which were closely located to Dscam null neurons, also showed self-crossing phenotype despite their intact Dscam code. However, in case of MARCM, differences in expression levels intrinsic to the method are present and could decrease the penetrance rate. Nevertheless, the cell labeling result strongly suggests a non-cell-autonomous effect of Dscam +11.31.25.1. This conclusion also underlines previous findings in which *Dscam* mutant axons have

been shown to alter the projections of wild-type axons within the same mushroom body (Wang et al. 2002).

Furthermore, we were able to determine a time point during the development of HS cells after which Dscam +11.31.25.1 induction did not elicit the phenotype anymore. The strength of Dscam +11.31.25.1 phenotype decreased gradually towards that time point. One explanation could be that Dscams are only needed during neurite outgrowth, but not in the mature neuron. Once the destination areas are innervated, the neuronal pattern is not changeable by Dscams anymore. Supporting this idea, previous developmental studies in the mushroom body have postulated that Dscams might be widely used to mediate various growth cone behaviors (Wang et al. 2002).

Neurobiotin injection into HS cells displaying Dscam +11.31.25.1 phenotype revealed an intact electrical coupling despite reduced dendritic fields, which supports the hypothesis that heteroneuronal tiling does not depend on Dscams.

Taken together, we have provided strong evidence that Dscam1 is required for appropriate patterning in HS neurons. We further investigated which functional consequences altered anatomy has on the functional role of HS cells.

6.2 Electrophysiology analysis displays strong correlations between morphological changes and response properties of HS cells

The entire electrophysiology study was performed by Bettina Schnell. Complementary to this, the anatomical structures of recorded cells were also examined due to the variability in penetrance of Dscam overexpression. In this study, two major aspects have been observed: contrast dependency and receptive field of single HS cells.

Our studies revealed a strong reduction in the frontal receptive field of HS cells in Dscam +11.31.25.1 flies correlating with observed morphological changes. The smaller receptive fields were caused by the lack of dendritic trees in the distal areas, which correspond to the frontal visual field of the fly. In addition, in the proximal areas, the responses were slightly increased which supports the finding of receptor accumulation at the remaining branches. Contralateral responses were also slightly decreased. In the contrast dependency assay, cell performance was generally weaker than that of wildtype cells, reaching a lower saturation plateau. This phenomenon of gain control mechanism in EMDs has been examined in detail. It has

been postulated that the exact value of saturation in large-field motion detectors like HS cells is set by the activation ratio of their excitatory and inhibitory input elements. The reversal potentials and conductance of EMDs, as well as the absolute numbers of activated pairs (proportional to the pattern size), determine that value (Borst, A. 1995). Therefore, with a decreased cell size the total number of input elements also decreased and with that the dendritic membrane potential as well as the saturation plateau. The observed impact of the response to contralateral stimuli might be assigned to the misdirecting of axonal terminals. In *Calliphora*, contralateral projecting H-cells have been described as providing information from the frontal visual field at the contralateral side (Haag and Borst 2001, 2008)

Changing gear, we now focus on Dscam +7.6.19.2. Here, electrophysiological recordings revealed that in a few cases HS cells did not respond to ipsilateral stimulation at all whereas response to contralateral stimulation was unaltered. These results revealed a strong decrease or else loss of presynaptic columnar input to the HS cell dendrites, while information flow from contralateral projecting neurons was still maintained. Contrast dependence of those cells was similar to Dscam +11.31.25.1 HS cells showing weaker but not total loss of response to whole-field stimuli. By mere anatomical study, these functional errors were not predictable as the main branches were still present in Dscam +7.6.19.2 cells. Nevertheless, in general, we were able to determine a correlation between fluctuations in phenotypical penetrance and variations in individual cell performance; i.e., the stronger the elicited phenotype, the more the function of the cell was impaired.

In this study, we were able to prove that Dscams are essential for guidance and functional branching of HS cell neurites. Furthermore, gain-of-function studies have elucidated for the first time the physiological significance of a precise branching pattern in HS cells. These results encouraged us to have a further look at the optomotor responses of Dscam overexpression flies.

6.3 Behavioral analysis reveals strong correlations between morphological changes and optomotor response deficits

This behavior study was carried out by Väinö Haikala. Complementary to this, the anatomical structures of HS cells were examined subsequently after the performance.

In this study, the yaw responses to three different stimuli were observed: elevation, contrast and azimuth dependency.

This study revealed that overall there was a strong decrease of about 40% in optomotor response along all tested elevations compared to control flies. By presenting the moving stimulus at different heights, different parts of the visual field along the dorso-ventral axis were covered and hence the optomotor responses could be partially shown to be elicited by HSN, HSE or HSS due to their distinct receptive fields. However, detailed analysis suggests that there was indeed a direct coherence between HS cell anatomy and optomotor response; e.g., flies showing a strong Dscam +11.31.25.1 phenotype in HSN and HSE performed worse upon stimuli presented at northern and equatorial elevations than flies in which only HSN is mainly impaired. These observations underline the idea that HS cells are involved in the yaw torque response in flies (Pflugfelder and Heisenberg 1995).

In line with the previous assay, the responses determined at the contrast dependency assay showed a significant decrease in response of about 50% for all tested contrast levels. This result is similar to the obtained physiology data and assumes that the same EMDs with altered gain control, which provide input to HS cells, might be also part of the optomotor pathway in the fly. Recently, the first premotor descending neurons connected to LPTCs have been identified in *Calliphora* (Haag et al. 2007; Wertz et al. 2009).

The azimuth assay only showed a constant slight decrease of about 30% in response strength starting at 120° azimuth. Unfortunately, there had been a gap of 30° at the frontal visual field, which would correspond to the distal receptive field missing in Dscam+11.31.25.1 HS cells. The optomotor responses had therefore not been obtained from that area. Nevertheless, the results provide strong evidence that HS cells are strongly involved in optomotor response.

Taken together the findings, we were able to carry out a unique study on the function of Dscam1 in HS cells. Anatomical results were greatly complemented by reconstruction analysis and physiology as well as behavior studies. The results show that Dscams are necessary for correct pattern formation and target finding. Moreover, the anatomy of HS cells is pivotal for its function of motion detection and strongly affects the optomotor response of the fly.

6.4 Genetic tools for the manipulation and recording of neuronal function

We generated several transgenic lines with the goal of directly monitoring or manipulating input activity. Genetically encoded calcium indicators have great potential for the recording of neuronal activity (Hires et al. 2008). We used a FRT flanked 'Stop' cassette for controlling translation activation of TN-XXL with Flipase activity and induced labeling only in small cell populations. In initial experiments, the generated UAS>Stop>TN-XXL transgenics allowed expression of the indicator to be restricted to only a few cells within the pattern of DB331. This allows unambiguous identification of the neurons from which activity is measured (Hou et al. 2009). However, we still need to test whether the expression level and affinity of the indicator is sufficient in live imaging experiments.

The other approach we made for dissecting the input elements was to identify the neurons of the inhibitory pathway. We tried to do so by generating vGat-Gal4 flies. The vesicular GABA transporter is highly concentrated at the nerve endings of all GABAergic neurons. It mediates accumulation of the transmitter into synaptic vesicles. It is known that LPTCs receive inhibitory inputs from GABAergic neurons (Raghu et al. 2007). In trying to isolate the promoter region together with its enhancers, we were able to extract promising regions. We finally obtained one transgenic fly strain, vGat4kb-Gal4, giving expression in a subset of probably GABAergic neurons. Difficulties in generating driver lines covering the entire endogenous expression pattern have been reported before. In most cases, one promoter region can give different expression patterns depending on the flanking enhancer regions (Schwyter et al. 1995). Another approach could be to make a knock-in construct; i.e., to preserve the given intron exon structure by replacing the vGat gene region through the Gal4 coding sequence (Champtiaux and Changeux 2004; Horn and Handler. 2005; Huang et al. 2009) in the *Drosophila* genome. In addition, we had to face the problem that the expression of marker genes was not strong enough to identify individual neurons. We will need to enhance the expression level with a UAS-Gal4 loop or change the construct itself with an additional Kozak consensus sequence. The strength of the Kozak sequence controls the amount of protein synthesized from a given mRNA (Kozak 2002).

For manipulating the excitatory input system of LPTCs, we expressed α-Btx that binds and modulates nAchRs (Chen and Patrick 1997), the major excitatory input elements on their dendrites (Raghu et al. 2009). Experiments done with lynx-1, a

novel member of the same gene family, have shown that it is highly expressed in the Mammalian CNS, where it modulates nAChR activity. Lynx-1 enhances desensitization of nAchR, increases Ach-evoked currents, and protects against brain degeneration exacerbated by nicotine. As α-Btx needs to bind directly to nAChR in order to block channel activity, the protein must be in close proximity to the receptor. Therefore, the toxin was not directly fused to the membrane but had a linker sequence that allowed the toxin to act more flexibly. In addition, the secretory signal of lynx-1 was used to transport the toxin next to the receptors (Holford et al. 2009). Transgenic flies expressing membrane-bound α-Btx fused to EGFP revealed an inhomogeneous dotted distribution along the membrane surface of the entire cell and soma. Preliminary electrophysiological recordings were carried out by Bettina Schnell. For recording macroscopic currents in HS cells, a monocular large field stimulus moving in PD and ND direction was presented in the visual field of transgenic flies. The results revealed that HS cells coexpressing α-Btx-EGFP were showing a twice-augmented response to ipsi- and contralaterally provided PD stimuli compared to wildtype flies. However, this enhancement is only observable at 100% pattern contrast. Responses at 20% contrast level are unaltered. The results are surprising as we expected a decreased response to PD stimuli as the toxin should block the entire channel activity. However, the opposite effect is elicited which is more similar to the effects which have been reported to be typical for lynx-1, namely a more homogeneous distribution of current amplitudes, with a shift to large-current amplitude (Ibanez-Tallon et al. 2002). It has been reported that Ach evoked macroscopic currents were enhanced by 30%-40% in *in vitro* assays (Miwa et al. 1999). Coincident with the shift, an enhancement of desensitization occurs (Miwa et al. 2006). Hence, the stronger response to PD stimuli at 100% contrast might be elicited through binding of α-Btx to nAchR and resulting conformation changes instead of blockage of the receptors. At 20% contrast level, the concentration of the transmitter Acetylcholine might be too low for eliciting the toxin effect. It has been reported that, in the case of lynx1, the evoked effects only occur if the natural agonist is also present; thus lynx1 functions as an allosteric modulator of nAchR in vivo (Miwa et al. 2006). This is most probably also, how α-Btx modulates the function of the main excitatory input pathway in the observed transgenic flies. Furthermore, it has been reported that mutant flies without Dalpha7 nAChRs still revealed direction selectivity of VS and HS cells; and remaining nAChRs were labeled by α-Btx,

pointing to a robust cellular implementation of dendritic processing that warrants direction selectivity (Raghu et al. 2009).

To summarize, we were able to generate UAS- α-Btx-EGFP flies which can be used modulate nAchR activity in specific neurons including LPTCs in *Drosophila*. The toxin has unexpectedly displayed similar effects like lynx1. It can therefore, be used to modify the function of ion channels like nAchRs in LPTCs. However, which underlying mechanisms are elicited by binding of α-Btx has yet to be unraveled.

6.5 Ablation of LPTCs with RicinA gives insights into developmental processes

The UAS>Stop>RicinA construct works very effectively for cell ablation. After induction of RicinA, LPTCs that are normally included in the DB331 expression pattern were missing and no remaining cell fragments were observable. Furthermore, cell vitality testing with propidium iodide demonstrated intact membranes of remaining GFP labeled LPTCs. This result is in line with previous experiences with temperature sensitive RicinA constructs (Moffat et al. 1996) in which RicinA expression was shown to be restricted to those cells in which it was induced. Therefore, the expression of RicinA under control of the Stop cassette is not leaky; i.e., does not affect neighboring cells without RicinA expression. Nevertheless, for successful and targeted cell ablation, a clearly defined time point of RicinA induction is essential. Beside the developmental time point, the duration of heatshock is a crucial factor in restricting the ablation pattern (Gomez and Alcorta 2008). Therefore, this time point had to be experimentally defined for each individual Gal4 line. In case of the DB331-Gal4 line, the time frame turned out to be the late 3rd instar which is a well-defined and recognizable stage when all larvae are attached to the walls of the vials. This protocol was extremely useful as in all flies LPTCs could be ablated. For avoiding or decreasing the number of ablated neurons other than LPTCs, heatshock induction at later stages might provide a solution. However, experiments in later pupa stages turned out to induce RicinA very inefficiently in LPTCs. One reasonable explanation could be developmental conditions protecting against heat influences like the pupa shell or the adult cuticula, which is more protective than larval skin and, therefore, might prohibit heatshock-induced Flipase activity in later stages. Another explanation could be molecular mechanisms like DNA condensations that build a

barrier against Flipase activity (Oudman 1991, Vermeulen and Loeschcke 2007, Overgaard and Sorensen 2008). Another theory for the lack of cell ablation in later stages could be a decrease in the number of mitotic dividing cells (Wu and Luo 2006). These results suggest that Flipase does not work in adult flies in which neurons are already differentiated.

To our surprise, there was not only a difference in the RicinA-induced ablation pattern between different flies but also within the optical lobes of one single fly. Both optical lobes possess different numbers and types of remaining LPTCs. As inhomogeneous heatshock treatment can be excluded as the reason for the difference between both optical lobes, this result hints to a time difference in the developments of LPTC precursor cells in both lobes. Different patterns of remaining LPTCs in the two optic lobes offer the advantage of testing two scenarios but also decrease the probability of having the same set of remaining LPTCs in both hemispheres. This might complicate the interpretation of behavioral experiments beside the variety of factors like motivation, flight experience, etc., of tested flies. Furthermore, assuming that LPTCs would play a key role in optomotor behavior of the fly, then unbalanced ablation in both optic lobes would elicit a total misbalance in optic flow perception in both hemispheres. Considering network connectivity between both optical lobes that has been shown to exist but has not yet been identified (Schnell et al. 2010), disequilibrium might cause an unpredictable change in optomotor response. Nevertheless, experiments with laser ablation of single HS and VS precursor cells at an early larval stage in *Musca* have demonstrated that these animals show reduced response to large-field regressive ND stimuli whereas the response to progressive PD stimuli is only slightly affected. In addition, object response to a single stripe hardly differs from wildtype (Geiger and Nässel 1981, 1983). Due to the ablation differences in both optical lobes, responses must be measured monocularly in order to prove whether specific alterations in optomotor behavior can be correlated with the loss of specific LPTCs. In any case, it is necessary to analyze anatomically which LPTCs are missing, after each behavioral experiment.

In addition, our study also shed light on the development of LPTCs. Remaining cells preserved normal dendrite branching patterns even in the absence of other LPTCs included in the expression pattern of DB331. Consistent with the observations made with RicinA, previous ablation studies of R7 photoreceptors have shown that the loss of cells does not interfere with outgrowth and target finding of neighbored

photoreceptor cells. However, the photoreceptors differentiate in a defined sequence where R7 is the last to be formed (Tomlinson 1988). Hence, it is unclear whether LPTCs either develop cell-autonomously or are guided through other RicinA unaffected neurons or molecular guidance cues. Columnar neurons presynaptic to LPTCs could still be intact in RicinA flies and thus guide outgrowing axonal and dendritic processes of remaining LPTCs to their target areas. On the other hand, mechanisms such as gradient cues could make single LPTCs independent of neighboring cells. It is well known that, during early development, gradients form guidance cues for embryonic development (Nüsslein-Volhard and Wieschaus 1980) and for axonal targeting like in the case of the robo/slit interaction (Kidd et al. 1999). The independent development of LPTCs is not surprising as motion detection is of vital importance for the fly and thus has to build upon mechanisms making this system less susceptible to perturbations.

Preliminary optomotor studies with RicinA flies were done in collaboration with Steven Fry. In a wing-beat analyzer, the yaw torque of tethered flies was monitored and subsequently the anatomy of remaining LPTCs analyzed. However, more than 50% of all tested flies were not flying or only flew briefly. Others seemed to be blind and did not show any escape behavior when held in the hand. This observation presumably results from loss of all LPTCs but can also have another reason such as loss of motor neurons in the ventral ganglion. As the entire expression pattern of DB331 has never been completely studied, both scenarios are possible. Furthermore, we could not distinguish between a lack of motivation and the inability to fly. One means of proving the functionality of motor neurons is a walking paradigm instead of tethered flight (Strauss and Heisenberg 1993). However, from previous studies, it has been reported that many factors including flight experience, habituation to the torque and general environmental factors influence the flight performance of flies (Hesselberg, T. 2009). By excluding flies with general gait impairment, all variations in the optomotor response can then be attributed to an altered motion detection system.

6.6 Vesicular Stomatitis Virus used in *Drosophila* as a neuronal tracer

Drosophila melanogaster is a model organism with a broad spectrum of established genetic tools. Yet a method is lacking which allows identification of presynaptic

neurons besides EM studies (Van Haeften and Wouterlood 2000). The unique advantages of viral tracers have been demonstrated in studies done in mammalian organisms like *mus musculus* (Card 1998, Wickersham et al. 2007). However, transferring this method to another organism that does not even belong to the same phylum was a great challenge. Usually, viruses are specific to certain replication machineries in the cells of their host animals. However, in our case, when we tried to infect *Drosophila melanogaster* with attenuated rabies viruses, the host specificity of the virus prohibited infection of cells. Our goal was to use EGFP encoding viruses for labeling and identifying columnar neurons that are presynaptically connected to LPTCs and, in long term, revealing all neurons involved in the motion detection network. This network has largely not been unraveled (Fischbach and Dittrich 1989, Bausenwein and Fischbach 1992) in flies but is essential for understanding the cellular mechanisms underlying motion detection. There has only been speculation about the role of T4/T5 cells, which are supposed to synapse onto LPTCs. In a single EM study, synaptic connectivity was reported to exist between these groups of neurons (Strausfeld and Lee 1991). However, since then there has not been any further proof for that kind of interaction. In this thesis, we tried to establish a new method for tracing presynaptic neurons. We showed for the first time that VSV viruses were not only able to infect S2 cells (van den Pol, AN. 2009) but also various other cell types in isolated *Drosophila* brain cultures (Ayaz et al. 2008). With the cultured brains, we showed that VSV could infect and replicate within *Drosophila* neurons ex vivo. Furthermore, our model organism also provides the replication system of VSV viruses. This conclusion we drew from the infection studies in brain culture where we monitored viral spread during several days of incubation (Klingen et al. 2008) and observed the replication behavior of deletion viruses and pseudotyped viruses ex vivo. These results are fundamental for future experiments as infectiousness, fertility, and vitality of the virus are necessary for successful targeting (De Clercq et al. 1973, Aderka et al. 1985, Granstedt et al. 2010, Lancaster and Pfeiffer 2010). As reported before in vertebrates, VSVdG does not spread beyond its primarily infected *Drosophila* host cell. This ability to predict and guide the targeting behavior of VSV viruses through genetic manipulations is an essential source for using them as tracer viruses in future experiments. Moreover, we revealed that the in vitro brain culture was an easy and efficient way to test those factors for different viruses before applying promising candidates to living animals. This method will allow

an easy but also safe way to make a preliminary screen of viruses for future experiments.

In our brain culture experiments, we observed preferential infection of glia cells. Considering the native spreading behavior of VSV viruses through diffusion (Haseltine et al. 2008), this observation might be because excised brains were still covered by glia cells (Awasaki et al. 2008). As we wanted to keep the brains as intact as possible, we did not remove the glial neurolemma (Demerec 1994) and tried to preserve all air sacs and tracheas. Most probably, this was the reason for the high ratio of glia to neuron infection rate.

All labeled cells revealed a high level of fluorescence after infection. Therefore, a high viral replication rate was present in the cells. In most cases, even small cellular structures like synaptic endings were completely invaded by virus particles. The resulting detailed resolution shown in confocal images is comparable to reported results (Granstedt et al.. 2009). This is the most important criteria as presynaptic cells can only be identified based on their unique branching patterns. Additionally, for specific targeting and retrograde spreading of VSV, we used the EnvA/TVA system (Balliet et al. 1999, Wickersham et al. 2007) within flies. Transgenic flies, which express the Rabies Virus G-protein and TVA receptors under the control of the UAS promoter, ensure the infection and spreading specificity. The G-protein should enable an exclusively retrograde transportation of the virus, once the target neuron is infected. However, it was unclear whether the M-protein is also needed. The TVA-EnvA system should exclusively target the virus with EnvA shell to cells exposing TVA receptors on their membrane surface. The fly line UAS-TVA-2Alike-dsRed was successfully generated. The expression of TVA receptors was verified through the dsRed marker that is independently translated from the TVA due to the 2Alike sequence. This linker has been shown to allow both constructs TVA and dsRed to provide two major advantages. First, TVA and dsRed are translated with equal efficiency as ribosomes quit after TVA-mRNA translation and start translating the dsRed-mRNA independently from previous translated sequence. From other translation regulators like the IRES (internal ribosome entry sites) sequence, an uneven translation level of both components has been revealed as problematic (Gilberst et al. 2010). The second important issue is, dsRed is not directly tagged to the TVA receptor and hence does not interfere with it. However, it is unknown whether the cytoplasmic domain possesses any functional role in virus targeting.

Nevertheless, we demonstrated for the first time that the EnvA/TVA system is working in *Drosophila melanogaster* both in vitro and possibly with in vivo assays as well. The in vivo assay still needs to be refined but is providing the basis for the next step, the monosynaptic retrograde spread. In previous studies, the time frame starting from infection of the host cell by rabies virus until spreading to the presynaptic neurons was reported to be around 3-4 days at 37℃ in mammalian slice culture (Ugolini 2010). However, for insects the optimum environmental temperature is 25℃ that would result in an incubation time of 10-14 days. This time period is much too long for recording any spreading behavior in brain cultures. Therefore, we needed to establish an in vivo assay. The preliminary injection protocol was tested successfully but needs to be refined. Furthermore, all generated transgenic glycoprotein expressing flies need to be tested. We are still way apart from our goals but we made the first step towards a revolutionary technique in *Drosophila* enabling specific targeting of single neurons in living animals. Nevertheless, with the first part of the technique, the UAS-TVA-2Alike-dsRed flies, we opened up the possibility (using the virus as gene carrier) of studying the function of single neurons with TN-XXL, silencing single neurons with RicinA or inducing neuronal activity with the split Gal4 technique.

7 References

Aderka D, Novick D, Hahn T, Fischer DG, Wallach D.
Increase of vulnerability to lymphotoxin in cells infected by vesicular stomatitis virus and its further augmentation by interferon.
Cell Immunol. 1985 May;92(2):218-25.

Awasaki T, Lai SL, Ito K, Lee T.
Organization and postembryonic development of glial cells in the adult central brain of Drosophila.
J Neurosci. 2008 Dec 17;28(51):13742-53.

Ayaz D, Leyssen M, Koch M, Yan J, Srahna M, Sheeba V, Fogle KJ, Holmes TC, Hassan BA.
Axonal injury and regeneration in the adult brain of Drosophila.
J Neurosci. 2008 Jun 4;28(23):6010-21.

Balliet JW, Berson J, D'Cruz CM, Huang J, Crane J, Gilbert JM, Bates P.
Production and characterization of a soluble, active form of Tva, the subgroup A avian sarcoma and leukosis virus receptor.
J Virol. 1999 Apr;73(4):3054-61.

Basler K, Hafen E.
Dynamics of Drosophila eye development and temporal requirements of sevenless expression.
Development. 1989 Dec;107(4):723-31.

Bausenwein B, Wolf R, Heisenberg M.
Genetic dissection of optomotor behavior in Drosophila melanogaster. Studies on wild-type and the mutant optomotor-blind H31.
J Neurogenet. 1986 Mar;3(2):87-109. Erratum in: J Neurogenet 1986 Aug;3(4):247.

Bausenwein B, Buchner E, Heisenberg M.
Identification of H1 visual interneuron in Drosophila by [3H]2-deoxyglucose uptake during stationary flight.
Brain Res. 1990 Feb 12;509(1):134-6.

Bausenwein B, Dittrich AP, Fischbach KF.
The optic lobe of Drosophila melanogaster. II. Sorting of retinotopic pathways in the medulla.
Cell Tissue Res. 1992 Jan;267(1):17-28.

Bausenwein B, Fischbach KF.
Activity labeling patterns in the medulla of Drosophila melanogaster caused by motion stimuli.
Cell Tissue Res. 1992 Oct;270(1):25-35.

Benzer S.
Genetic dissection of behavior.
Sci Am. 1973 Dec;229(6):24-37.

Blair SS.
Genetic mosaic techniques for studying Drosophila development.
Development. 2003 Nov;130(21):5065-72.

Bohm RA, Welch WP, Goodnight LK, Cox LW, Henry LG, Gunter TC, Bao H, Zhang B.
A genetic mosaic approach for neural circuit mapping in Drosophila.
Proc Natl Acad Sci U S A. 2010 Sep 14;107(37):16378-83. Epub 2010 Sep 1.

Borst A, Haag J.
Neural networks in the cockpit of the fly.
J Comp Physiol A Neuroethol Sens Neural Behav Physiol. 2002 Jul;188(6):419-37. Epub 2002 Jun 7. Review

Brand AH, Perrimon N.
Targeted gene expression as a means of altering cell fates and generating dominant phenotypes.
Development. 1993 Jun;118(2):401-15.

Brunner A, Wolf R, Pflugfelder GO, Poeck B, Heisenberg M.
Mutations in the proximal region of the optomotor-blind locus of Drosophila melanogaster reveal a gradient of neuroanatomical and behavioral phenotypes.
J Neurogenet. 1992 Feb;8(1):43-55.

Card JP.
Exploring brain circuitry with neurotropic viruses: new horizons in neuroanatomy.
Anat Rec. 1998 Dec;253(6):176-85.

Champtiaux N, Changeux JP.
Knockout and knockin mice to investigate the role of nicotinic receptors in the central nervous system.
Prog Brain Res. 2004;145:235-51. Review.

Chen BE, Kondo M, Garnier A, Watson FL, Püettmann-Holgado R, Lamar DR, Schmucker D.
The molecular diversity of Dscam is functionally required for neuronal wiring specificity in Drosophila.
Cell. 2006 May 5;125(3):607-20.

Chen D, Patrick JW.
The alpha-bungarotoxin-binding nicotinic acetylcholine receptor from rat brain contains only the alpha7 subunit.
J Biol Chem. 1997 Sep 19;272(38):24024-9.

Conzelmann KK.
NONSEGMENTED NEGATIVE-STRAND RNA VIRUSES: Genetics and Manipulation of Viral Genomes.
Annu Rev Genet. 1998;32:123-62.

Cummings RD and Etzler ME.
Chapter 28 R-type lectins.
Essentials of Glycobiology. 2nd edition.
Varki A, Cummings RD, Esko JD, et al.
Cold Spring Harbor (NY): Cold Spring Harbor Laboratory Press; 2009.

Cuntz H, Forstner F, Borst A, Häusser M.
One rule to grow them all: a general theory of neuronal branching and its practical application.
PLoS Comput Biol. 2010 Aug 5;6(8). pii: e1000877.

De Clercq E, Stewart WE 2nd, De Somer P.
Increased toxicity of double-stranded ribonucleic acid in virus-infected animals.
Infect Immun. 1973 Feb;7(2):167-72.

Demerec M.
Biology of Drosophila.

Dickinson MH, Lehmann FO, Götz KG.
The active control of wing rotation by Drosophila.
J Exp Biol. 1993 Sep;182:173-89.

Dobzhansky T.
Genetics 23: 28-64, 1938

Dvorak. D.R., Bishop, L.G., Eckert, M.E.
On the identification of movement detectors in the fly optic lobe.
J. comp. Physiol. 1975 100, 5 25

Enell L, Hamasaka Y, Kolodziejczyk A, Nässel DR.
gamma-Aminobutyric acid (GABA) signaling components in Drosophila: immunocytochemical localization of GABA(B) receptors in relation to the GABA(A) receptor subunit RDL and a vesicular GABA transporter.
J Comp Neurol. 2007 Nov 1;505(1):18-31.

Etessami R, Conzelmann KK, Marion R, Tsiang H, Ceccaldi PE.
Neuronal expression of foreign genes with recombinant rabies virus variants
Rev Neurol (Paris). 2000 Mar;156(3):236-41.

Farrow K, Borst A, Haag J.
Sharing receptive fields with your neighbors: tuning the vertical system cells to wide field motion.
J Neurosci. 2005 Apr 13;25(15):3985-93.

Farrow K, Haag J, Borst A.
Nonlinear, binocular interactions underlying flow field selectivity of a motion-sensitive neuron.
Nat Neurosci. 2006 Oct;9(10):1312-20. Epub 2006 Sep 10.

Fischbach KF.
Neural cell types surviving congenital sensory deprivation in the optic lobes of Drosophila melanogaster.
Dev Biol. 1983 Jan;95(1):1-18. Review.

Fischbach KF. und Dittrich A.P.M.
The Optic Lobe of Drosophila melanogaster. Part I: A Golgi Analysis of Wild-Type Structure.
Cell Tissue Res. 1989;258, 441-475

Fuerst PG, Koizumi A, Masland RH, Burgess RW.
Neurite arborization and mosaic spacing in the mouse retina require DSCAM.
Nature. 2008 Jan 24;451(7177):470-4.

Geiger G, Nässel DR.
Visual orientation behavior of flies after selective laser beam ablation of interneurones.
Nature. 1981 Oct 1;293(5831):398-9.

Gomez-Diaz C, Alcorta E.
Quantitative analysis of antennal mosaic generation in Drosophila melanogaster by the MARCM system.
Genesis. 2008 Jun;46(6):283-8.

Götz KG.
Optomoter studies of the visual system of several eye mutants of the fruit fly Drosophila
Kybernetik. 1964 Jun;2(2):77-92.

Götz KG.
Flight control in Drosophila by visual perception of motion.
Kybernetik. 1968 Jun;4(6):199-208.

Götz KG
Course-control, metabolism and wing interference during ultralong tethered flight in Drosophila melanogaster.
J Exp Biol. 1987 Oct;128: 35-48

Granstedt AE, Szpara ML, Kuhn B, Wang SS, Enquist LW.
Fluorescence-based monitoring of in vivo neural activity using a circuit-tracing pseudorabies virus.
PLoS One. 2009 Sep 9;4(9):e6923.

Granstedt AE, Kuhn B, Wang SS, Enquist LW.
Calcium imaging of neuronal circuits in vivo using a circuit-tracing pseudorabies virus.
Cold Spring Harb Protoc. 2010 Apr;2010(4):pdb.prot5410.

Graveley BR.
Mutually exclusive splicing of the insect Dscam pre-mRNA directed by competing intronic RNA secondary structures.
Cell. 2005 Oct 7;123(1):65-73.

Grotewiel MS, Beck CD, Wu KH, Zhu XR, Davis RL.
Integrin-mediated short-term memory in Drosophila.
Nature. 1998 Jan 29;391(6666):455-60.

Haag J, Borst A.
Recurrent network interactions underlying flow-field selectivity of visual interneurons.
J Neurosci. 2001 Aug 1;21(15):5685-92.

Haag J, Borst A.
Dendro-dendritic interactions between motion-sensitive large-field neurons in the fly.
J Neurosci. 2002 Apr 15;22(8):3227-33.

Haag J, Borst A.
Electrical coupling of lobula plate tangential cells to a heterolateral motion-sensitive neuron in the fly.
J Neurosci. 2008 Dec 31;28(53):14435-42.

Haag J, Denk W, Borst A.
Fly motion vision is based on Reichardt detectors regardless of the signal-to-noise ratio.
Proc Natl Acad Sci U S A. 2004 Nov 16;101(46):16333-8. Epub 2004 Nov 8.

Haag J, Wertz A, Borst A.
Integration of lobula plate output signals by DNOVS1, an identified premotor descending neuron.
J Neurosci. 2007 Feb 21;27(8):1992-2000.

Hardie RC, Raghu P
Visual transduction in Drosophila.
Nature. 2001 Sep 13;413(6852):186-93.

Haseltine EL, Lam V, Yin J, Rawlings JB.
Image-guided modeling of virus growth and spread.
Bull Math Biol. 2008 Aug;70(6):1730-48. Epub 2008 Apr 25.

Hattori D, Demir E, Kim HW, Viragh E, Zipursky SL, Dickson BJ.
Dscam diversity is essential for neuronal wiring and self-recognition.
Nature. 2007 Sep 13;449(7159):223-7.

Hattori D, Millard SS, Wojtowicz WM, Zipursky SL.
Dscam-mediated cell recognition regulates neural circuit formation.
Annu Rev Cell Dev Biol. 2008;24:597-620.

Hattori D, Chen Y, Matthews BJ, Salwinski L, Sabatti C, Grueber WB, Zipursky SL.
Robust discrimination between self and non-self neurites requires thousands of Dscam1 isoforms.
Nature. 2009 Oct 1;461(7264):644-8.

Hausen K, Wehrhahn C.
Neural circuits mediating visual flight control in flies. I. Quantitative comparison of neural and behavioral response characteristics.
J Neurosci. 1989 Nov;9(11):3828-36.

Hausen K.
Functional characterization and anatomical identification of motion sensitive neurons in the lobula plate of the blowfly Calliphora erythrocephala.
Z. Naturforsch.C31 629–633

Heisenberg M, Wonneberger R, Wolf R.
Optomotor-blindH31—aDrosophila mutant of the lobula plate giant neurons
J. comp. Physiol.124, 287-296 (1978)

Heisenberg M, Borst A, Wagner S, Byers D.
Drosophila mushroom body mutants are deficient in olfactory learning.
J Neurogenet. 1985 Feb;2(1):1-30.

R. Hengstenberg, K. Hausen und B. Hengstenberg
The number and structure of giant vertical cells (VS) in the lobula plate of the blowfly Calliphora erythrocephala
Journal of Comparative Physiology A: Neuroethology, Sensory, Neural, and Behavioral Physiology; Volume 149, Number 2, 163-177

Hesselberg T, Lehmann FO.
The role of experience in flight behavior of Drosophila.
J Exp Biol. 2009 Oct;212(Pt 20):3377-86.

Hires SA, Tian L, Looger LL.
Reporting neural activity with genetically encoded calcium indicators.
Brain Cell Biol. 2008 Aug;36(1-4):69-86. Epub 2008 Oct 22.

Holford M, Auer S, Laqua M, Ibañez-Tallon I.
Manipulating neuronal circuits with endogenous and recombinant cell-surface tethered modulators.
Front Mol Neurosci. 2009;2:21. Epub 2009 Oct 30.

Horn C, Handler AM.
Site-specific genomic targeting in Drosophila.
Proc Natl Acad Sci U S A. 2005 Aug 30;102(35):12483-8. Epub 2005 Aug 22.

Hou BH, Takanaga H, Griesbeck O, Frommer WB.
Osmotic induction of calcium accumulation in human embryonic kidney cells detected with a high sensitivity FRET calcium sensor.
Cold Spring Harb Protoc. 2010 Apr;2010(4):pdb.prot5410.

Howerth EW, Stallknecht DE, Dorminy M, Pisell T, Clarke GR.
Experimental vesicular stomatitis in swine: effects of route of inoculation and steroid treatment.
J Vet Diagn Invest. 1997 Apr;9(2):136-42.

Huang J, Zhou W, Dong W, Watson AM, Hong Y.
From the Cover: Directed, efficient, and versatile modifications of the Drosophila genome by genomic engineering.
Proc Natl Acad Sci U S A. 2009 May 19;106(20):8284-9. Epub 2009 May 8.

Hughes ME, Bortnick R, Tsubouchi A, Bäumer P, Kondo M, Uemura T, Schmucker D.
Homophilic Dscam interactions control complex dendrite morphogenesis.
Neuron. 2007 May 3;54(3):417-27.

Ibañez-Tallon I, Miwa JM, Wang HL, Adams NC, Crabtree GW, Sine SM, Heintz N.
Novel modulation of neuronal nicotinic acetylcholine receptors by association with the endogenous prototoxin lynx1.
Neuron. 2002 Mar 14;33(6):893-903.

Joesch M, Plett J, Borst A, Reiff DF.
Response properties of motion-sensitive visual interneurons in the lobula plate of Drosophila melanogaster.
Curr Biol. 2008 Mar 11;18(5):368-74.

Joesch M, Schnell B, Raghu SV, Reiff DF, Borst A.
ON and OFF pathways in Drosophila motion vision.
Nature. 2010 Nov 11;468(7321):300-4.

Kidd T, Bland KS, Goodman CS.
Slit is the midline repellent for the robo receptor in Drosophila.
Cell. 1999 Mar 19;96(6):785-94.

Klingen Y, Conzelmann KK, Finke S.
Double-labeled rabies virus: live tracking of enveloped virus transport.
J Virol. 2008 Jan;82(1):237-45. Epub 2007 Oct 10.

Kozak M.
Pushing the limits of the scanning mechanism for initiation of translation.
Gene. 2002 Oct 16;299(1-2):1-34.

Kunes S, Steller H.
Ablation of Drosophila photoreceptor cells by conditional expression of a toxin gene.
Genes Dev. 1991 Jun;5(6):970-83.

Lancaster KZ, Pfeiffer JK.
Limited trafficking of a neurotropic virus through inefficient retrograde axonal transport and the type I interferon response.
PLoS Pathog. 2010 Mar 5;6(3):e1000791.

Lee T, Luo L.
Mosaic analysis with a repressible cell marker (MARCM) for Drosophila neural development.
Trends Neurosci. 2001 May;24(5):251-4.

Llewellyn ZN, Salman MD, Pauszek S, Rodriguez LL.
Growth and molecular evolution of vesicular stomatitis serotype New Jersey in cells derived from its natural insect-host: evidence for natural adaptation.
Virus Res. 2002 Oct;89(1):65-73.

Luan H, Peabody NC, Vinson CR, White BH.
Refined spatial manipulation of neuronal function by combinatorial restriction of transgene expression.
Neuron. 2006 Nov 9;52(3):425-36.

Lue NF, Chasman DI, Buchman AR, Kornberg RD.
Interaction of GAL4 and GAL80 gene regulatory proteins in vitro.
Mol Cell Biol. 1987 Oct;7(10):3446-51.

Ly A, Nikolaev A, Suresh G, Zheng Y, Tessier-Lavigne M, Stein E.
DSCAM is a netrin receptor that collaborates with DCC in mediating turning responses to netrin-1.
Cell. 2008 Jun 27;133(7):1241-54.

Mank M, Santos AF, Direnberger S, Mrsic-Flogel TD, Hofer SB, Stein V, Hendel T, Reiff DF, Levelt C, Borst A, Bonhoeffer T, Hübener M, Griesbeck O.
A genetically encoded calcium indicator for chronic in vivo two-photon imaging.
Nat Methods. 2008 Sep;5(9):805-11.

Matthews BJ, Kim ME, Flanagan JJ, Hattori D, Clemens JC, Zipursky SL, Grueber WB.
Dendrite self-avoidance is controlled by Dscam.
Cell. 2007 May 4;129(3):593-604.

Mebatsion T, Konig M, Conzelmann KK.
Budding of rabies virus particles in the absence of the spike glycoprotein.
Cell. 1996 Mar 22;84(6):941-51.

Meigen JW.
Volume 6 of his substantial treatise on the Diptera of Europe
Wiley. 1830.

Meijers R, Puettmann-Holgado R, Skiniotis G, Liu JH, Walz T, Wang JH, Schmucker D.
Structural basis of Dscam isoform specificity.
Nature. 2007 Sep 27;449(7161):487-91. Epub 2007 Aug 26.

Merriam JC, Lyon HS, Char DH.
Toxicity of a monoclonal F(ab')2:ricin A conjugate for retinoblastoma in vitro.
Cancer Res. 1984 Aug;44(8):3178-83.

Miwa JM, Ibanez-Tallon I, Crabtree GW, Sánchez R, Sali A, Role LW, Heintz N.
lynx1, an Endogenous Toxin-like Modulator of Nicotinic Acetylcholine Receptors in the Mammalian CNS
Neuron. 1999 May;23(1):105-14.

Miwa JM, Stevens TR, King SL, Caldarone BJ, Ibanez-Tallon I, Xiao C, Fitzsimonds RM, Pavlides C, Lester HA, Picciotto MR, Heintz N.
The prototoxin lynx1 acts on nicotinic acetylcholine receptors to balance neuronal activity and survival in vivo.
Neuron. 2006 Sep 7;51(5):587-600.

Moffat KG, Gould JH, Smith HK, O'Kane CJ.
Inducible cell ablation in Drosophila by cold-sensitive ricin A chain.
Development. 1992 Mar;114(3):681-7.

Morgan TH.
The Mechanism of Mendelian Heredity.
New York: Henry Holt.

Morgan TH.
Sex-limited inheritance in Drosophila.
Science. 1910 Jul 22;32(812):120-2.

Muqit MM and Feany MB
Modeling neurodegenerative diseases in Drosophila: a fruitful approach?
Nat Rev Neurosci. 2002 Mar;3(3):237-43.

Nässel DR, Geiger G, Seyan HS.
Differentiation of fly visual interneurons after laser ablation of their central targets early in development.
J Comp Neurol. 1983 Jun 1;216(4):421-8.

Neves G, Zucker J, Daly M, Chess A.
Stochastic yet biased expression of multiple Dscam splice variants by individual cells.
Nat Genet. 2004 Mar;36(3):240-6. Epub 2004 Feb 1.

Nüsslein-Volhard C, Wieschaus E.
Mutations affecting segment number and polarity in Drosophila.
Nature. 1980 Oct 30;287(5785):795-801

Oudman L.
A locus in Drosophila melanogaster affecting heat resistance.
Hereditas. 1991;114(3):285-7.

Overgaard J, Sørensen JG.
Rapid thermal adaptation during field temperature variations in Drosophila melanogaster.
Cryobiology. 2008 Apr;56(2):159-62. Epub 2008 Jan 18.

Pierantoni R.
A look into the cock-pit of the fly. The architecture of the lobular plate.
Cell Tissue Res. 1976 Aug 16;171(1):101-22.

Pflugfelder GO, Heisenberg M.
Optomotor-blind of Drosophila melanogaster: a neurogenetic approach to optic lobe development and optomotor behaviour.
Comp Biochem Physiol A Physiol. 1995 Mar;110(3):185-202. Review.
Raghu SV, Joesch M, Sigrist SJ, Borst A, Reiff DF.
Synaptic organization of lobula plate tangential cells in Drosophila: Dalpha7 cholinergic receptors.
J Neurogenet. 2009;23(1-2):200-9.

Raghu SV, Joesch M, Borst A, Reiff DF.
Synaptic organization of lobula plate tangential cells in Drosophila: gamma-aminobutyric acid receptors and chemical release sites.
J Comp Neurol. 2007 Jun 1;502(4):598-610.

Reichardt W:
Processing of optical information by the visual system of the fly.
Vision Res. 1986;26(1):113-26.

Reiff DF, Plett J, Mank M, Griesbeck O, Borst A.
Visualizing retinotopic half-wave rectified input to the motion detection circuitry of Drosophila.
Nat Neurosci. 2010 Aug;13(8):973-8. Epub 2010 Jul 11.

Schmucker D, Clemens JC, Shu H, Worby CA, Xiao J, Muda M, Dixon JE, Zipursky SL.
Drosophila Dscam is an axon guidance receptor exhibiting extraordinary molecular diversity.
Cell. 2000 Jun 9;101(6):671-84.

Schmucker D.
Molecular diversity of Dscam: recognition of molecular identity in neuronal wiring.
Nat Rev Neurosci. 2007 Dec;8(12):915-20.

Schmucker D, Chen B.
Dscam and DSCAM: complex genes in simple animals, complex animals yet simple genes.
Genes Dev. 2009 Jan 15;23(2):147-56.

Schnell B, Joesch M, Forstner F, Raghu SV, Otsuna H, Ito K, Borst A, Reiff DF.
Processing of horizontal optic flow in three visual interneurons of the Drosophila brain.
J Neurophysiol. 2010 Mar;103(3):1646-57. Epub 2010 Jan 20.

Schnitzlein WM, Reichmann ME.
Characterization of New Jersey vesicular stomatitis virus isolates from horses and black flies during the 1982 outbreak in Colorado.
Virology. 1985 Apr 30;142(2):426-31.

Schwyter DH, Huang JD, Dubnicoff T, Courey AJ.
The decapentaplegic core promoter region plays an integral role in the spatial control of transcription.
Mol Cell Biol. 1995 Jul;15(7):3960-8.

Spletter ML, Liu J, Liu J, Su H, Giniger E, Komiyama T, Quake S, Luo L.
Lola regulates Drosophila olfactory projection neuron identity and targeting specificity.
Neural Dev. 2007 Jul 16;2:14.

Spradling AC, Rubin GM.
Transposition of cloned P elements into Drosophila germ line chromosomes.
Science. 1982 Oct 22;218(4570):341-7.

Strausfeld NJ, Lee JK.
Neuronal basis for parallel visual processing in the fly.
Vis Neurosci. 1991 Jul-Aug;7(1-2):13-33.

Strauss R, Heisenberg M.
A higher control center of locomotor behavior in the Drosophila brain.
J Neurosci. 1993 May;13(5):1852-61.

Struhl G, Basler K.
Organizing activity of wingless protein in Drosophila.
Cell. 1993 Feb 26;72(4):527-40.

Szymczak AL, Workman CJ, Wang Y, Vignali KM, Dilioglou S, Vanin EF, Vignali DA.
Correction of multi-gene deficiency in vivo using a single 'self-cleaving' 2A peptide-based retroviral vector.
Nat Biotechnol. 2004 May;22(5):589-94. Epub 2004 Apr 4.

Tamamaki N, Nakamura K, Furuta T, Asamoto K, Kaneko T.
Neurons in Golgi-stain-like images revealed by GFP-adenovirus infection in vivo.
Neurosci Res. 2000 Nov;38(3):231-6.

Tang W, Ehrlich I, Wolff SB, Michalski AM, Wölfl S, Hasan MT, Lüthi A, Sprengel R.
Faithful expression of multiple proteins via 2A-peptide self-processing: a versatile and reliable method for manipulating brain circuits.
J Neurosci. 2009 Jul 8;29(27):8621-9.

Tomioka R, Rockland KS.
mproved Golgi-like visualization in retrogradely projecting neurons after EGFP-adenovirus infection in adult rat and monkey.
J Histochem Cytochem. 2006 May;54(5):539-48. Epub 2005 Dec 12.

Tomlinson A.
Cellular interactions in the developing Drosophila eye.
Development. 1988 Oct;104(2):183-93. Review.

Tully, T. and Quinn, WG.
Classical conditioning and retension in normal and mutant Drosophila melanogaster.
J Comp Physiol A. 1985 Sep;157(2):263-77.

Ugolini G.
Specificity of rabies virus as a transneuronal tracer of motor networks: transfer from hypoglossal motoneurons to connected second-order and higher order central nervous system cell groups.
J Comp Neurol. 1995 Jun 5;356(3):457-80.

Ugolini G.
Advances in viral transneuronal tracing.
J Neurosci Methods 2010 Jan 5.

Van den Pol AN, Ozduman K, Wollmann G, Ho WS, Simon I, Yao Y, Rose JK, Ghosh P.
Viral strategies for studying the brain, including a replication-restricted self-amplifying delta-G vesicular stomatis virus that rapidly expresses transgenes in brain and can generate a multicolor golgi-like expression.
J Comp Neurol. 2009 Oct 20;516(6):456-81.

Van Haeften T, Wouterlood FG.
Neuroanatomical tracing at high resolution.
J Neurosci Methods. 2000 Nov 15;103(1):107-16.

Vermeulen CJ, Loeschcke V.
Longevity and the stress response in Drosophila.
Exp Gerontol. 2007 Mar;42(3):153-9. Epub 2006 Nov 15. Review.

Wang J, Zugates CT, Liang IH, Lee CH, Lee T.
Drosophila Dscam is required for divergent segregation of sister branches and suppresses ectopic bifurcation of axons.
Neuron. 2002 Feb 14;33(4):559-71.

Warzecha AK, Borst A, Egelhaaf M.
Photo-ablation of single neurons in the fly visual system reveals neural circuit for the detection of small moving objects.
Neurosci Lett. 1992 Jul 6;141(1):119-22.

Wertz A, Borst A, Haag J.
Nonlinear integration of binocular optic flow by DNOVS2, a descending neuron of the fly.
J Neurosci. 2008 Mar 19;28(12):3131-40.

Wickersham IR, Finke S, Conzelmann KK, Callaway EM.
Retrograde neuronal tracing with a deletion-mutant rabies virus.
Nat Methods. 2007 Jan;4(1):47-9. Epub 2006 Dec 10.

Wickersham IR, Lyon DC, Barnard RJ, Mori T, Finke S, Conzelmann KK, Young JA, Callaway EM.
Monosynaptic restriction of transsynaptic tracing from single, genetically targeted neurons.
Neuron. 2007 Mar 1;53(5):639-47.

Wojtowicz WM, Flanagan JJ, Millard SS, Zipursky SL, Clemens JC.
Dscam generates axon guidance receptors that exhibit isoform-specific homophilic binding.
Cell. 2004 Sep 3;118(5):619-33.

Wojtowicz WM, Wu W, Andre I, Qian B, Baker D, Zipursky SL.
A vast repertoire of Dscam binding specificities arises from modular interactions of variable Ig domains.
Cell. 2007 Sep 21;130(6):1134-45.

Wu JS, Luo L.
A protocol for mosaic analysis with a repressible cell marker (MARCM) in Drosophila.
Nat Protoc. 2006;1(6):2583-9.

Yamakawa K, Huot YK, Haendelt MA, Hubert R, Chen XN, Lyons GE, Korenberg JR.
DSCAM: a novel member of the immunoglobulin superfamily maps in a Down syndrome region and is involved in the development of the nervous system.
Hum Mol Genet. 1998 Feb;7(2):227-37.

Yang JS, Bai JM, Lee T.
Dynein-dynactin complex is essential for dendritic restriction of TM1-containing Drosophila Dscam.
PLoS One. 2008;3(10):e3504. Epub 2008 Oct 23.

Zeidler MP, Tan C, Bellaiche Y, Cherry S, Häder S, Gayko U, Perrimon N.
Temperature-sensitive control of protein activity by conditionally splicing inteins.
Nat Biotechnol. 2004 Jul;22(7):871-6. Epub 2004 Jun 6.

Zhan XL, Clemens JC, Neves G, Hattori D, Flanagan JJ, Hummel T, Vasconcelos ML, Chess A, Zipursky SL.
Analysis of Dscam diversity in regulating axon guidance in Drosophila mushroom bodies.
Neuron. 2004 Sep 2;43(5):673-86.

Zhu H, Hummel T, Clemens JC, Berdnik D, Zipursky SL, Luo L
Dendritic patterning by Dscam and synaptic partner matching in the Drosophila antennal lobe.
Nature Neuroscience 9: 349-355.

Acknowledgement

I would like to express my gratitude to all those who enabled me to finish this thesis. I owe my deepest gratitude to Alexander Borst who enabled and allowed me to work in a unique laboratory environment where scientific questions can be approached in an amazing broad spectrum. I appreciated him very much as my doctor thesis adviser with whom I always could discuss about scientific and personal topics. He has always been guidance for me both, in research, and in social aspects. Furthermore, I thank Dierk Reiff who instructed me in all the projects I presented in this thesis. He was a great supervisor with many inspiring ideas for new experiments making his support available in a number of ways. I also would like to thank Karl Friedrich Fischbach, a friend and member of my thesis committee for giving outstanding support in all aspects. I am indebted to my many of my colleagues and collaboration partner: Väinö Haikala, Bettina Schnell, Friedrich Förstner and Alexander Ghanem for great support. They opened up new dimensions in the projects and allowed me to look beyond my own backyard. I would like to show my gratitude to Klaus Conzelmann for collaboration in the virus project and for all insights about this alien system. Furthermore, I would like to thank Shamprasad Raghu for our intense discussions about project design and experiments. He helped me a lot in interpreting results and answering questions. I also enjoyed him very much as supervisor of the vGat project. Special thanks to our technicians Christian Theile and Wolfgang Eßbauer for taking care of the fly stocks, which was fundamental work for the success of all experiments. Thanks go also to the people in P1 for providing a nice atmosphere at my working place. I am indebted to my many of my colleagues to support me and therefore, would like to thank the entire Borst group for the wonderful time that I was able to spend in this lab.

Finally yet importantly, I want to thank my parents and my fiancé. They were very patient and supportive during the entire PhD time.